DEVELOPMENT OF ENHANCED SURVEILLANCE TOOLS FOR LOW-RESOURCE

MALARIA CONTROL AND ELIMINATION

By

Carson Paige Moore

Dissertation

Submitted to the Faculty of the

Graduate School of Vanderbilt University

in partial fulfillment of the requirements

for the degree of

DOCTOR OF PHILOSOPHY

in

Chemistry

August 13, 2021

Nashville, Tennessee

Approved:

David W. Wright, Ph.D.

David E. Cliffel, Ph.D.

Timothy P. Hanusa, Ph.D.

Frederick R. Haselton, Ph.D.

"Bad things happen to good people because *things* happen all the time, and it is up to people to determine whether they are bad or good. In the same way that your heart feels and your mind thinks, you mortal beings are the instrument by which the universe cares.

If you choose to care, then the universe cares, and if you don't, then it doesn't."

-Brennan Lee Mulligan, Dimension 20

"Churches are built where saints were martyred. A bridge requires a child in its foundations if it is to hold. All great works must begin with a sacrifice."

— Grady Hendrix, Horrorstör

ACKNOWLEDGEMENTS

and joined David's lab together- the dream team has, is, and always will be you and me. To Jenna, I was so ecstatic when we went from roommates to lab mates, and have always been beyond grateful for your willingness to lend a hand, consult on science, or just complain loudly about everything over a Dunkies iced coffee. Thank you for the fantastic laughs and truly terrible drinks. To Micaella and Kelly, I hope that you continue to support each other and work seamlessly together to maintain the lab as an efficient place for meaningful and impactful work.

Throughout graduate school, I was lucky to have several other mentors who have expanded my mind and enriched my overall experience. To Dr. Danielle Kimmel, thank you so much for holding my hand during my first foray into graduate research. You've been such a great cheerleader, reading draft after draft of everything I submit, and pushing me so hard to get this degree. I can never thank you enough. To Dr. Tom Scherr, you have helped me realize so many aspects of my dreams that I never would have and you've always been there for me, even when I'm oceans (and time zones) away losing my mind alone in the Johannesburg airport. My mom and I will always be so grateful for your clutch mediation. Thank you so much for your support and mentorship, I couldn't be more stoked to become a coding Swiss Army knife as a postdoc under your careful guidance!

Of course, no Wright lab dissertation would be complete without a huge shout out and acknowledgement of Dr. Christine Markwalter, the true gold standard for measuring the success of David's graduate students. Christine, you gave me the best template for how to succeed, while also being one of the kindest and most brilliant people I've ever

met. I was so happy to have such a magnificent conference buddy, and I am eternally grateful for your guidance and tutelage.

I must also recognize my amazing international collaborators, who have mentored me and helped me realize my place in the wide world of public health. To Dr. Phil Thuma, thank you for opening the Macha Research Trust to me, and for your continued support and incredible insight. The Macha Research Trust team (Ben, Hapi, Mukuma, Japhet, Caison, Lyle, and all the other amazing researchers) was so incredible and open during my time in Macha, and I hope to see you all again soon. I'd also like to thank Dr. Govert van Dam for his pioneering work in schistosomiasis, and his enthusiastic support of my forays into the field. I am thrilled to have the opportunity to work more closely with your team in the future! To Benji, Andrea, and the rest of the amazing researchers I've met through the course of this wild ride, I'm so grateful for the opportunities that have allowed me to make lifelong friends in my field! Here's to the next Swiss mini golf tournament!

Thank you as well to Dr. Adam Kiefer and Dr. Scott Davis, who begrudgingly allowed me to tag along on the Mercer on Mission Chemistry field expedition to Ecuador in the summer of 2016, despite having already technically graduated from the University. That trip opened me up to the idea of international field work in chemistry, and showed me how much more there is to science than crunching numbers or pushing arrows. It was truly the experience that showed me what kind of career I wanted, and pushed me towards David's lab and the work I've done over the past five years. I also could never forget the quintessential piece of wisdom that Dr. Kiefer imparted on me shortly after I began my graduate school career. It is one that has hung both over my desk and in my

home since I was a first-year graduate student: "We are all imposters. It's the people who recognize it that are the most successful."

Of course, I could never have embarked on any of this without my family and friends behind me. To my wonderful partner Ed, thank you so much for putting up with the grumpy car rides, the moments of face-down-in-bed weeping over failed experiments, and the long nights in lab interspersed among the highs of successful science days and passed exams. You are my most steadfast and enthusiastic supporter and I truly don't know if I could have done this without you. I know I definitely wouldn't have laughed as much as I have over the past 5 years. As much as moving from Adelaide, Australia to Nashville, TN wasn't exactly an expected part of your life plan, from the moment you landed in BNA, I've never looked back. I'm beyond excited for many, many more moments looking forward with you and I love you to the end of the earth and back.

To mom, dad, Natalie, Pat, Sim, Franklin and Louis, thank you all for your constant support, love, and belief. I am so lucky to have such a strong, marvelous family around me, and I can't wait for us all to be together again. Mom especially, thank you for always picking up the phone or the FaceTime to help me maintain my plants, my mental health, and my flow of ideas. You've always kept me on track, helped me see that my goals are achievable, and gave me that little push even when I was sure I didn't need it (you were right, of course). One indelible constant in my life has been your marvelous example of a powerful woman in science kicking ass at every turn, and I've been honored to follow at least partly in your footsteps.

It's been said that if you average your closest friends, you'll come up with a relatively good facsimile of your own personality. If that's the case, I must be incredibly

.

TABLE OF CONTENTS

Chapter

LIST OF TABLES

LIST OF FIGURES

LIST OF ABBREVIATIONS AND SYMBOLS

Word	Abbreviation
Analysis of variance	ANOVA
Affordable, sensitive, specific, user-friendly, rapid and robust, equipment-free, and deliverable to end users	ASSURED
BioLayer interferometry	BLI
Bovine serum albumin	BSA
Community health workers	CHWs
Citrate phosphate dextrose	CPD
Deoxyribonucleic acid	DNA
Ethylenediaminetetraacetic acid	EDTA
Enzyme-linked immunosorbent assay	ELISA
Foundation for Innovative New Diagnostics	FIND
His_6-biotin-enriched anti-PLDH antibody	HisAb
High-income countries	HIC
Human immunodeficiency virus	HIV
Horseradish peroxidase	HRPx
Histidine-rich protein 2	HRP2
Inductively coupled plasma optical emission spectroscopy	ICP-OES
Iminodiacetic acid	IDA
Immobilized metal affinity chromatography	IMAC
Coordination stability constant	K_s
Lateral flow assay	LFA
Lateral flow reader	LFR

Low- and middle-income countries	LMICs
Limit of detection	LOD
Mobile health	mHealth
Macha Research Trust	MRT
Network readiness index	NRI
Nitrilotriacetic acid	NTA
Phosphate buffered saline	PBS
Phosphate buffered saline with 0.1% Tween 20	PBST
Plasmodium falciparum	*Pf*
Plasmodium lactate dehydrogenase	*P*LDH
Rapid diagnostic test	RDT
Ribonucleic acid	RNA
Receiver operating characteristic	ROC
Strategic Advisory Group of Experts on In Vitro Diagnostics	SAGE-IVD
Severe acute respiratory syndrome coronavirus 2	SARS-CoV-2
Standard deviation	SD
Scanning electron microscopy-energy dispersive x-ray spectroscopy	SEM-EDS
Short message service	SMS
Tuberculosis	TB
World Health Organization	WHO

CHAPTER 1

INTRODUCTION[1]

Diseases of Poverty Affect Public Health in Low-Resource Settings

One of the most pressing issues facing the global community is the disparity in health between high-income countries (HICs) and low- and middle-income countries (LMICs). Less than 50% of the world's population was able to access critical healthcare services in 2017. This trend is evidenced by the increased life expectancy in HICs, where individuals on average are expected to live 18.1 years longer than those in LMICs.[1] Many of the illnesses observed in LMICs are both preventable and treatable, and their current prevalence is linked inextricably to the presence of overwhelming poverty in these areas.[2] It is estimated that 45% of the disease burden in LMICs can be attributed to diseases of poverty, with tuberculosis (TB), malaria, and human immunodeficiency virus (HIV) accounting for 18% of the total burden (Table 1.1).

---

[1] Portions of this chapter have been previously published as:
Scherr, T., Moore, C., *et al.* Evaluating Network Readiness for mHealth Interventions Using the Beacon Mobile Phone App: Application Development and Validation Study. *JMIR mHealth uHealth.,* **8(7)**, e18413, (2020). Reproduced and adapted with permission under the Creative Commons 4.0 open-access license (http://creativecommons.org/licenses/by/4.0/).

Table 1.1. Percentages of deaths due to diseases of poverty. (Adapted from Ref. 2)

"Poverty-related" disease	High-income countries (%)	Low-mortality, low-income countries (%)	High-mortality low-income countries (%)
Infectious and parasitic diseases	2.1	24.8	34.1
Respiratory infections	3.7	8.0	9.9
Perinatal and maternal conditions	0.4	6.8	8.4
Nutritional deficiencies	0.0	1.1	1.3
Tropical diseases	0.0	0.3	0.5
Total	6.2	40.7	54.1

The issues of intense poverty, including healthcare-related poverty, and limited healthcare access are inseparably linked worldwide. In 2001, the World Health Organization (WHO) Commission on Macroeconomics and Health proposed that in a 14 year time span, 10.5 million lives in LMICs could be saved annually if access to interventions designed to prevent and treat disease was increased.[3] However, while there was a 20% relative increase in healthcare coverage during the proposed time, a 2017 report found that sub-Saharan Africa and Southern Asia still lagged significantly behind the rest of the world in terms of access. Additionally, the WHO and World Bank have come up against a "missing data problem". This issue is most prevalent in LMICs that do not have healthcare data available at the national or regional level, and which may also

lack the critical components necessary for broader analysis of the contributing issues. These gaps then create an unknowable gulf of data regarding healthcare-related disparities and the true burden of disease in these countries.[4]

Malaria as a Public Health Crisis

In modern terms, malaria has become known as one of the "big three" diseases of poverty, alongside TB and HIV, and continues to affect the developing world at a drastically higher rate compared to HICs (Figure 1.1).[5,6] Malaria is projected to cost African nations a combined $12 billion USD per year in terms of lost production, but this estimate is conservative, as it neglects to incorporate the additional costs of treatment for infected individuals, lives lost, and long-term disability due to malaria infection.[7] This staggering cost for LMICs further exacerbates the stress experienced by the healthcare systems in these countries.
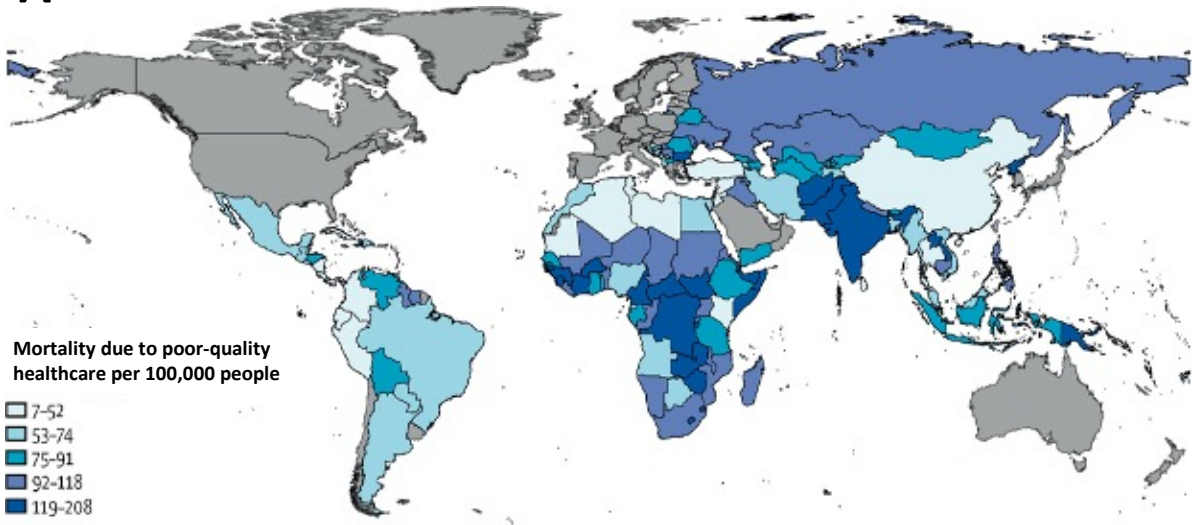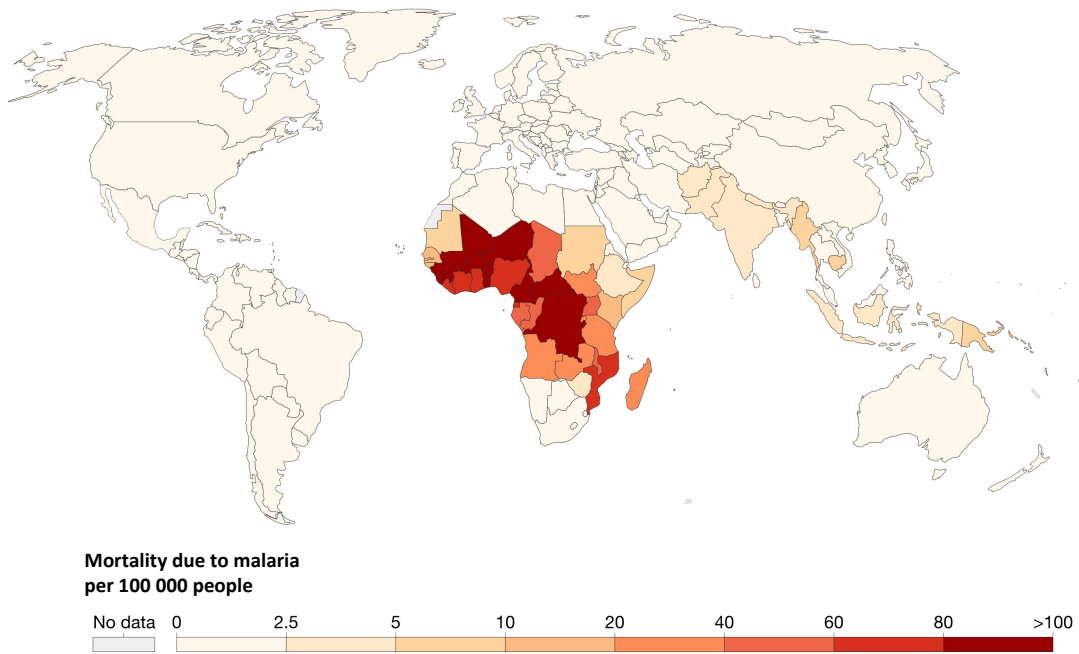
Figure 1.1. (A) Map of mortality due to poor-quality healthcare worldwide in 2018 and (B) map of global mortality due to malaria in 2017. Adapted under the Creative Commons BY 4.0 License (https://creativecommons.org/licenses/by/4.0/deed.en_US) from Refs. 5 and 6.

In addition to the stark economic costs of malaria, in 2019, there were an estimated 229,000,000 cases of malaria worldwide, with 409,000 deaths attributed to the disease.[8] Approximately 94%, or 215,000,000, of the reported cases occurred in Africa, with the remaining cases occurring in Southeast Asia, India, and South and Central America. This represents a staggering reversal in the fight against malaria, as the overall number of global incident cases per year has increased by approximately 17,000,000 since 2015 while the number of incident cases in Africa specifically has increased by 24,000,000 (4%) in that time frame.[9] This indicates that while many of the previously endemic regions continue to make progress, malaria control and elimination efforts are plateauing in heavily-affected LMICs.

Like many of the other diseases of poverty, malaria is broadly preventable, treatable, and diagnosable. Current preventative measures for malaria include: interior residual insecticide sprays (IRSs), insecticide-treated bed nets (ITNs), antimalarial chemoprophylaxis, and the preliminary malaria vaccine.[10,11] These interventions, especially IRSs and ITNs, have been shown to be successful in driving down malaria-related mortality, predominantly in vulnerable groups such as children under the age of 5, pregnant women, and immunocompromised individuals.[12,13] However, in some cases the cost of maintenance for these interventions and limited general access to preventatives for people of low socioeconomic status precluded broader use, thus reducing the efficacy overall.[10] Currently, the best available treatment for malaria is artemisinin-combination therapy, which is recommended only in cases that have been diagnosed positive in an effort to prevent artemisinin resistance.[14] Previous antimalarial drugs, such as chloroquine and oral artemisinin-based monotherapy, were used and

overused in many areas of the world, leading to subsequent multidrug resistance in the parasite.[14–16]

However, despite the vast array of existing preventative measures and treatments, malaria continues to plague LMICs. The WHO has noted the fragility of the malaria care pipeline specifically surrounding endemic settings, estimating that a 25% disruption in current malaria treatment in sub-Saharan Africa could result in over 45,000 additional deaths per year.[8] This vulnerability is also seen in the diagnostic access framework. In response to the ongoing COVID-19 pandemic, many diagnostic manufacturers have reallocated funds from malaria rapid test production towards production of rapid SARS-CoV-2 tests, particularly as the financial incentives to produce COVID-19 rapid tests rise.[8,17–19] Dr. Catharina Boehme, CEO of the Foundation for Innovative New Diagnostics (FIND) and a member of the WHO Strategic Advisory Group of Experts on In Vitro Diagnostics (SAGE IVD) reported that the profit margin on malaria rapid tests is approximately 18¢ per test, as opposed to up to $10 (USD) per test for COVID-19 production.[18] As a result of this decrease in production of rapid diagnostic tests (RDTs), many field- and community-based healthcare workers are left without the tests needed to accurately diagnose malaria, and are expected to revert to presumptive clinical diagnosis. This in turn could potentially lead to a spike in malaria-related mortality, poor antimalarial drug control, and an increase in antimalarial resistant parasite strains, as diagnosis is a critical first step in the cascade of care for malaria.[17] In order to strengthen the malaria care landscape, interventions must consider the use-cases and user-bases of the people most at risk.

Appropriate Diagnostics Address Disparities in Healthcare Infrastructure

Much of the difficulty in increasing access and surveillance is due to the vastly varied healthcare services available to the populace of LMICs. Within LMICs, the healthcare systems tend to be fragmented and vary widely, ranging from modern hospitals and laboratories with state-of-the-art equipment to roadside stalls offering medicines alongside gasoline and other necessities.[20] To encapsulate this, it is widely accepted that LMIC healthcare infrastructure can be considered as a pyramid. In this pyramid, the most well-equipped, high-functioning medical laboratories with specialized staff and equipment are the least accessible. Conversely, the most accessible are primary or community care settings with significantly less infrastructure, few if any trained personnel, and broad, decentralized methods of patient care (Figure 1.2).[21]
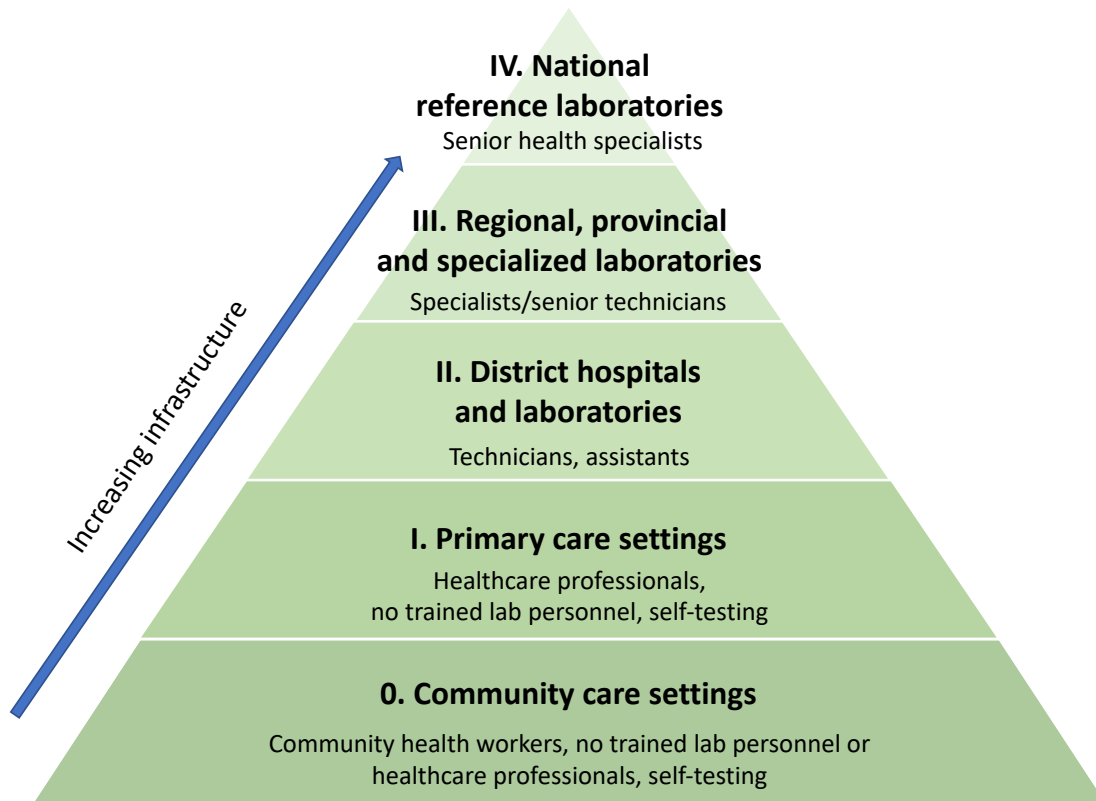
Figure 1.2. Levels of healthcare infrastructure and the personnel and resources commonly available at each level. (Adapted from Refs. 21 and 24)

These primary and community healthcare settings are less likely to have consistent electricity, running water, and appropriate data collection or dissemination tools compared to their high-infrastructure counterparts. Further, individuals seeking Level IV facilities or care often encounter insurmountable geographical and financial barriers.[22]

In the quest for global healthcare accessibility and utility, many key stakeholders are implementing tools to better overcome these significant hurdles. One substantial tool is the ASSURED diagnostic criteria, developed by the WHO. Originally designed to determine whether diagnostic tests for sexually transmitted infections were accurately meeting the needs of disease control campaigns, the ASSURED guidelines focus on the development of: affordable, sensitive, specific, user-friendly, rapid and robust, equipment-

free, and <u>d</u>eliverable to the end user.[23] The implementation of ASSURED criteria for diagnostics attempts to ensure quality testing for individuals seeking healthcare at all levels of the infrastructure pyramid, with a focus on those patients seeking care at the lowest levels. While some tests have not been successfully simplified to fit the ASSURED guidelines, many campaigns against diseases of poverty, such as HIV, TB, and malaria, rely heavily on ASSURED-consistent point-of-care diagnostics.[24]

The Current Malaria Diagnostic Landscape

Diagnostics for malaria have been of interest to researchers and epidemiologists for decades as the world moves towards control, with cutting-edge research continuing to push the barriers of the scientific possibilities.[25–27] The disease is caused by infection with one or more of the five species of *Plasmodium* parasite that infect humans: *P. falciparum*, *P. vivax*, *P. ovale*, *P. malariae*, and *P. knowlesi*. However, the majority of infections globally are caused by *P. falciparum*.[28] *Plasmodium* parasites are transmitted to the bloodstream of a human host through the bite of a female *Anopheles* mosquito. Once infected, patients may develop one of three clinical outcomes: 1) asymptomatic disease, which shows no clinical indicators of infection, 2) uncomplicated disease, which includes symptoms such as fever, chills, and headaches, or 3) complicated disease, which is characterized in part by coma, vital organ failure, and death.[29] These malaria infections can be recognized by several methods: blood-smear microscopy, polymerase chain reaction (PCR), enzyme-linked immunosorbent assays (ELISAs), and rapid diagnostic tests (RDTs).[21] Each of these methods rely on different biomarkers or indicators of malaria infection, resulting in vastly varied levels of sensitivity and specificity. The most

sensitive techniques can detect positive patients with extremely low parasite burdens, and many methods can determine differences between the infecting species. However, many of these techniques also require relatively robust laboratory infrastructure, intensive training of technicians, and incur high costs, meaning that only certain procedures can be completed directly at the point of care.

PCR is one of the most sensitive and specific malaria diagnostic tools, utilizing thermocycling to vastly amplify specific strands of RNA or DNA from parasites within a sample to reach detectable levels.[30] PCR is currently used to quantitate malaria parasite burdens and to determine the infecting species[31]. Reported limits of detection for PCR assays for malaria are <5 parasites per µL of whole blood, with some studies reporting detection limits as low as 0.004 parasites per µL.[32] However, despite this incredible level of sensitivity and specificity, PCR can be costly and time-consuming. It also requires expensive, perishable reagents, trained personnel, and instrumentation that are not widely available in LMICs.[33] In addition to this economic burden, many PCR configurations require DNA- or RNA-clean workspaces, which are not conducive to any diagnosis directly at the point of care.[34] While many advances are being made, the technology has not yet advanced to a level at which PCR could be broadly applied at Level 1 or Level 0 settings.

The existing gold standard for detection of malaria at community and primary care settings (Levels 0 and 1) is blood smear microscopy. Trained microscopists provide moderately sensitive diagnosis: on average they can detect parasite burdens of 100 parasites per µL of whole blood. However, this often leaves asymptomatic patients undetected, as asymptomatic patients carry parasite burdens in the range of single-digit

parasitemias (2-10 parasites/µL of whole blood).[35–37] Additionally, the sensitivity of the technique relies entirely on the skill of the microscopist assessing the samples, and the limit of detection varies significantly from person to person. Moreover, the cost to examine an individual sample may be low, but the cost to hire, train microscopist(s), and purchase or maintain a microscope can be very high.[36]

However, many of these methods remain limited, and no new diagnostic methods have been widely introduced since the introduction of RDTs in the early 1990's.[38,39] RDTs are perhaps the most field-optimal diagnostic technology, as they are fill many of the previously outlined ASSURED criteria. RDTs can be interpreted by individuals with almost no training or experience, are low-cost, portable, and yield results quickly and easily. Thus, they are the single most commonly used tool for malaria diagnosis directly at the point of care.[36,40–42]

For malaria, RDTs often utilize a lateral flow assay (LFA) format (Figure 1.3).
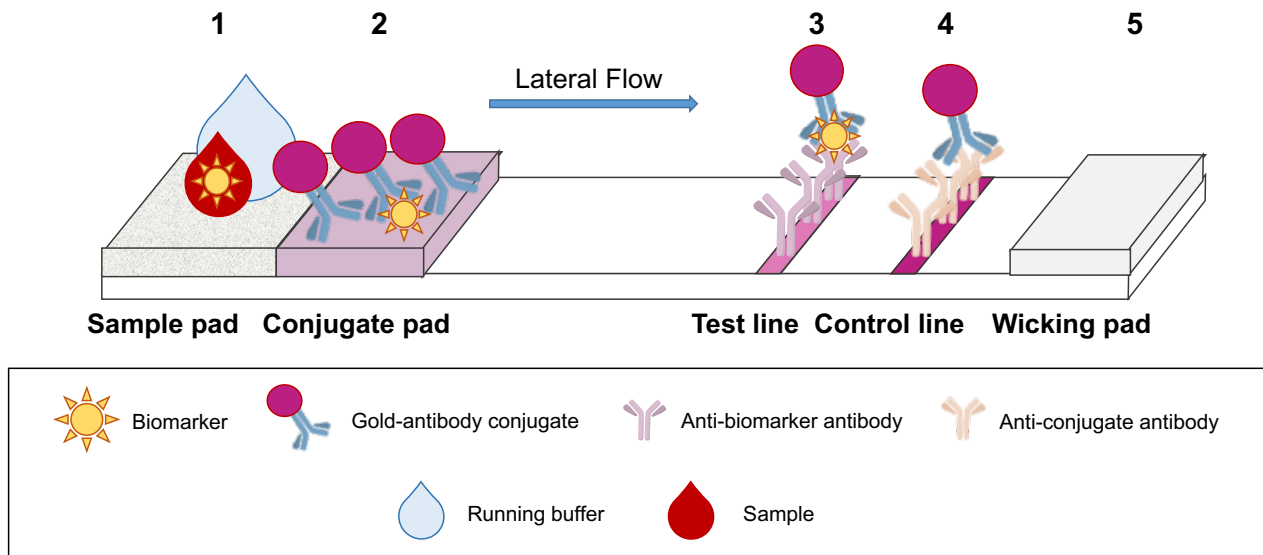
Figure 1.3. A traditional lateral flow assay. (1) Sample and running buffer are added to the paper sample pad. (2) Biomarker within a positive sample reacts with specific antibody-gold nanoparticle conjugate dried onto the conjugate pad and flows down the nitrocellulose membrane. (3) At the test line, orthogonal antibodies specific to the biomarker of interest bind the biomarker-gold conjugate complex and form a "sandwich". A visual signal is generated at this line through the aggregation of gold nanoparticles. (4) At the control line, antibodies specific to the nanoparticle conjugate bind excess conjugate and create a visual signal, indicative of a valid result. (5) Excess liquid continues down the nitrocellulose test strip and is absorbed by the wicking pad.

This format relies on antibody-antigen interactions to detect malarial biomarkers in a finger-prick blood sample.[36,43,44] Briefly, a specimen is added to the sample pad of the test, and after the addition of a running buffer, flows laterally down the test. The sample first interacts with a gold nanoparticle-antibody conjugate which specifically binds to its target biomarker. The biomarker, bound to the gold conjugate, is then captured by an antibody further down the test. The test line antibodies bind to distinct epitopes on the biomarker that are not already bound by the gold conjugate. The aggregation of gold nanoparticle-bound biomarker-antibody complex creates a visual signal at the test line. Further downstream, antibodies specific to the gold conjugate are immobilized at a control

line. Aggregation of the gold conjugate creates a second visual signal which indicates that the test has operated correctly. For more informational diagnosis, LFAs can be multiplexed for detection of more than one biomarker by increasing the number of test lines.

When evaluating RDT sensitivity, the WHO recommends that commercially available RDTs be able to detect parasite burdens of at least 200 parasites/μL.[45] While this limit of detection is useful for finding symptomatic patients with high parasite burdens, this poor sensitivity currently prevents RDTs from being used to detect asymptomatic patients and symptomatic patients with subpatent infections, that is, patients who are infected with undetectable parasite burdens. Recent studies have indicated that increasing current RDT sensitivity 100-fold will increase the percentage of patients detected from 55% to 95%, capturing a significant percentage of both symptomatic and asymptomatic patients.[37]

Mobile Technology to Supplement Malaria Diagnosis and Reporting

In addition to the need for sensitive and specific diagnostic tools that can be deployed directly at the point of need, there is a significant demand for follow-through on broad-scale surveillance, particularly in LMICs. This relationship was summarized succinctly in 1883 by Lord Kelvin: "when you cannot measure it, when you cannot express it in numbers, your knowledge is of a meagre and unsatisfactory kind".[46] The WHO states that strong surveillance requires "high levels of access to care and case detection, *and* complete reporting of health information by all sectors".[47] In 2017, nearly 22% of African countries indicated that their public health centers were reporting incomplete data

regarding malaria.[47] Thus, at that time, over 1 in 5 African nations, the areas most affected by malaria, were ineffective when reporting data to the organizations responsible for implementing critical interventions. However, the period between 2016 and 2019 has been marked by the strengthening of health reporting systems in endemic countries, due in large part to the implementation of digital aggregated data systems and computerized direct data entry programs.[8]

This focus on digital interventions has led to a spike in the uptake of mobile health (mHealth) tools. mHealth approaches originally became popular in HICs, as a method for increasing convenience for patients and providers with near real-time performance.[48–50] Thus, as mobile phone uptake began to surge worldwide, the global expansion of mHealth followed closely. The overall ubiquity of mobile devices in LMICs increased significantly between 2000 and 2019 and is expected to continue expanding.[51,52] In Africa specifically, the average number of mobile phone subscriptions per 100 people increased from 3 to 85 over that same period.[51] In some LMICs, the number of mobile subscriptions per person is higher than many developed countries (Figure 1.4), as many individuals in LMICs may own subscriptions for one or more mobile service providers at a time to account for lapses in service.[53] Further, these subscriptions are broadly utilized, as 87% of broadband connections in LMICs are known to be performed on a mobile device.[54] With the natural expansion of mobile connectivity, mHealth is a prime option to drive down healthcare costs, minimize barriers to facilitating care, and provide more useful surveillance data.[55–57]
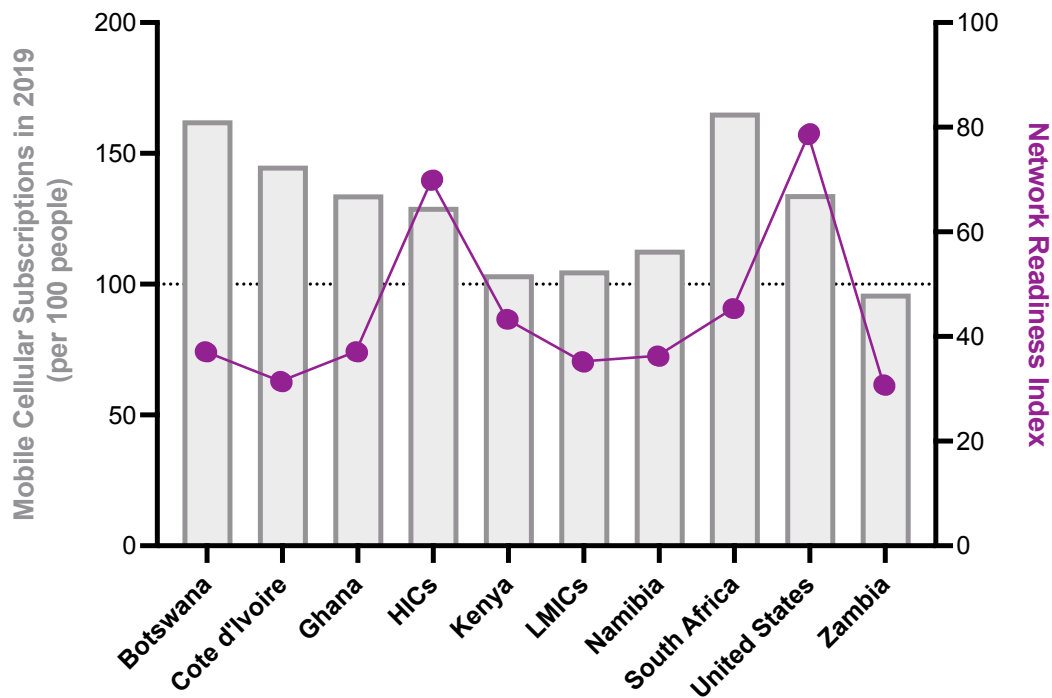
Figure 1.4. The number of mobile cellular subscriptions per 100 people in 2019 as reported by the World Bank and the World Economic Forum Networked Readiness Index for several African nations, the United States, LMICs, and HICs. NRI data for HICs and LMICs is represented by the median NRI of the income group. The dotted line indicates 100 unique cellular subscriptions per 100 people. Adapted under the Creative Commons BY 4.0 License (https://creativecommons.org/licenses/by/4.0/deed.en_US) from Refs. 51, 52, and 160.

In order to curtail the plateau of current malaria control and elimination movements, changes must be made to improve the quality and usability of field-based interventions: not only must field-ready diagnostics be capable of detecting all levels of disease, but the missing data problem must be addressed at the lowest levels of care. The lack of accurate testing and the significant gaps in infection data prevent global organizations like the WHO from accurately assessing the needs of populations in malaria-endemic nations.

Thus there is a possibility that the global community has vastly underestimated the true breadth of malaria infection and mortality.[58–60]

A Two-Pronged Approach to Enhanced Malaria Surveillance: Scope of This Work

In this work, a two-pronged approach using simple, affordable, enhanced RDTs and a tailored mobile health intervention is applied to improve malaria surveillance data collection and reporting directly at the point of care. This multifaceted approach focuses on the development of an inexpensive, multiplexed enhancement method for malaria RDTs and a mobile health intervention designed to increase RDT data recording and aggregation. In Chapter 2, a paper-based immobilized metal separation structure is functionalized and characterized. In Chapters 3 and 4, this paper membrane is used to enhance the sensitivity of RDTs specific for the two primary malarial biomarkers: histidine-rich protein 2 (HRP2) and *Plasmodium* lactate dehydrogenase (*P*LDH). In Chapter 5, a mobile health tool is developed for the immediate, standard analysis of RDTs in the field and validated with regard both to accuracy of analysis and effective data aggregation compared to the current gold standards.

The projects presented in this work look to solve the problems presented by disease surveillance and control in highly endemic areas, with a focus on providing tools that will be the most usable and useful to the communities and healthcare systems most significantly affected by malaria. Thus, all of the tools and interventions presented in this work have been designed to reflect the cost and infrastructure limits of their intended use-case scenarios (i.e., to address diseases of poverty directly at the point of care). These

tools have the potential to increase the accuracy and efficacy of malaria surveillance efforts, thus ending a years-long plateau of progress.

CHAPTER 2

SYNTHESIS AND CHARACTERIZATION OF IMMOBILIZED METAL AFFINITY

CELLULOSE MEMBRANES[2]

Introduction

Immobilized metal affinity chromatography (IMAC) is a highly-utilized protein separation technique originally developed in the 1970's.[61–64] IMAC uses metal chelating ligands bound to a solid support such as cellulose, agarose, or silica.[25,65] These ligands behave as Lewis bases by binding divalent transition metal ions such as copper(II), zinc(II), cobalt(II), nickel(II) or iron(II).[25,66]. These Lewis acidic metal centers have a natural affinity for electron-donating amino acids such as histidine, tryptophan, or cysteine allowing for the reversible isolation of peptides or proteins containing these residues from more complex solutions. These residues are often referred to as Porath's triangle, in recognition of their demonstrated utility during Porath's pioneering IMAC research.[66,67] Of the common residues in Porath's triangle, exposed histidine moieties have been shown to have the highest affinity for the metal ions, and IMAC has become a standard method for the separation or purification of His-tagged proteins.[68] Once isolated on the solid support, proteins can then be eluted from the metal complexes by several methods, including competition with a high affinity molecule such as imidazole or total chelation of the metal ion by a stronger chelating compound such as ethylenediaminetetraacetic acid (EDTA).[69]

---

[2] Portions of this chapter are in preparation for submission to *Journal of Chromatography B*.

Selectivity can vary greatly depending on the combination of IMAC ligand, metal ion, and solid support utilized.[70–73] Chelating ligands with different denticities, such as tridentate iminodiacetic acid (IDA) or tetradentate nitrilotriacetic acid (NTA), yield different available binding sites.[67] Traditionally, tridentate ligands coordinate to the transition metal of interest with three coordination sites, leaving three sites available on the metal for coordination to the histidine residues of the peptide or protein. Alternately, tetradentate ligands bind through four initial coordination sites to the metal, leaving two sites free to coordinate to histidine residues. The availability of binding sites for different ligands can affect both metal binding and downstream protein retention.

Metal ion choice can also significantly affect the ability of IMAC systems to bind peptides or proteins of interest. Metal-ligand complex formation is explained in part by hard/soft acid/base theory (HSAB).[74–76] Using chemical hardness as the defining metric, "hard" reactants are known to have smaller, unpolarizable, and more highly charged reactive sites, while "soft" reactants display opposite characteristics (large, more polarizable, less charged).[76] Certain soft metal ions, such as Cu(I), Cd(II), or Pb(II), display preferential binding to intermediate-to-soft sulfur atoms, whereas hard Lewis acids, including group II and III elements, preferentially chelate the harder oxygen atoms.[66] Borderline transition metals, which are the most common IMAC metals, have combined hard and soft characteristics, and can coordinate to oxygen and sulfur atoms interchangeably, as well as nitrogen atoms. Among these metals, there are varied levels of coordination capability, and the selection of a specific metal can drastically affect protein retention and recovery.

These separation techniques have naturally lent themselves to the diagnosis of malaria, through binding of histidine-rich protein 2 (HRP2), the primary biomarker of *Plasmodium falciparum*.[77] Most commercially-available malaria RDTs detect HRP2 by capturing the protein at a test line using HRP2-specific antibodies.[25,44,78] As HRP2 consists of 34% histidine residues, it is an ideal target for an IMAC-based enhancement strategy.[79,80] Additionally, HRP2 is a versatile biomarker, and has been utilized both as a standalone *P. falciparum* biomarker or in tandem with pan-malaria biomarkers such as *Plasmodium* lactate dehydrogenase (*P*LDH). The use of these biomarkers in point-of-care diagnostics will be expanded upon in Chapters 3 and 4.

The selectivity of different metals on commercially-available resin beads[72] and magnetic beads[73] have been investigated in the context of point-of-care sample preparation method for improved malaria diagnosis. These studies use the innate histidine-rich composition of HRP2 and histidine-enriched molecular recognition elements to concentrate malaria biomarkers from large volume blood samples for detection on LFAs, the most commonly used malaria RDT. A simpler, less expensive, more integrated approach is needed to reach areas that remain underserved by any traditional healthcare or laboratory infrastructure.

In this study, a paper membrane-based IMAC system has been developed and fully characterized. This system represents a preliminary yet critical advancement in simple-to-use, field-appropriate separation science, and will be utilized to isolate and enrich malaria biomarkers from lysed whole blood in Chapters 3 and 4.

Experimental

Materials

      Cellulose membranes (Whatman chromatography paper Grades 1 Chr, 2 Chr, 3 Chr, 4 Chr, 17 Chr, 3MM, and Whatman Grade 3 filter paper) were purchased from Cytiva Life Sciences (Marlborough, MA, USA). The flow properties of the Whatman cellulose membranes are described in Table 2.1. All other reagents were reagent grade, purchased from Fisher Scientific and Sigma Aldrich.

Table 2.1. Manufacturer-reported flow properties for all screened Whatman cellulose membranes. (NR= not reported)

Membrane	Membrane Type	Thickness (µm)	Reported Linear Flow Rate (mm/30 min)	Reported Gurley Air Permeability (s/100 mL/in^2)
1 Chr	Chromatography	180	130	11
2 Chr	Chromatography	180	115	20
3 Chr	Chromatography	360	130	26
4 Chr	Chromatography	210	180	3.67
3MM	Chromatography	340	130	20
17 Chr	Chromatography	920	190	9
Grade 3 FP	Filter paper	390	*NR*	26

Cellulose Membrane Functionalization

      The cellulose membrane functionalization method was adapted from Ke, et al. (Figure 2.1).[81]
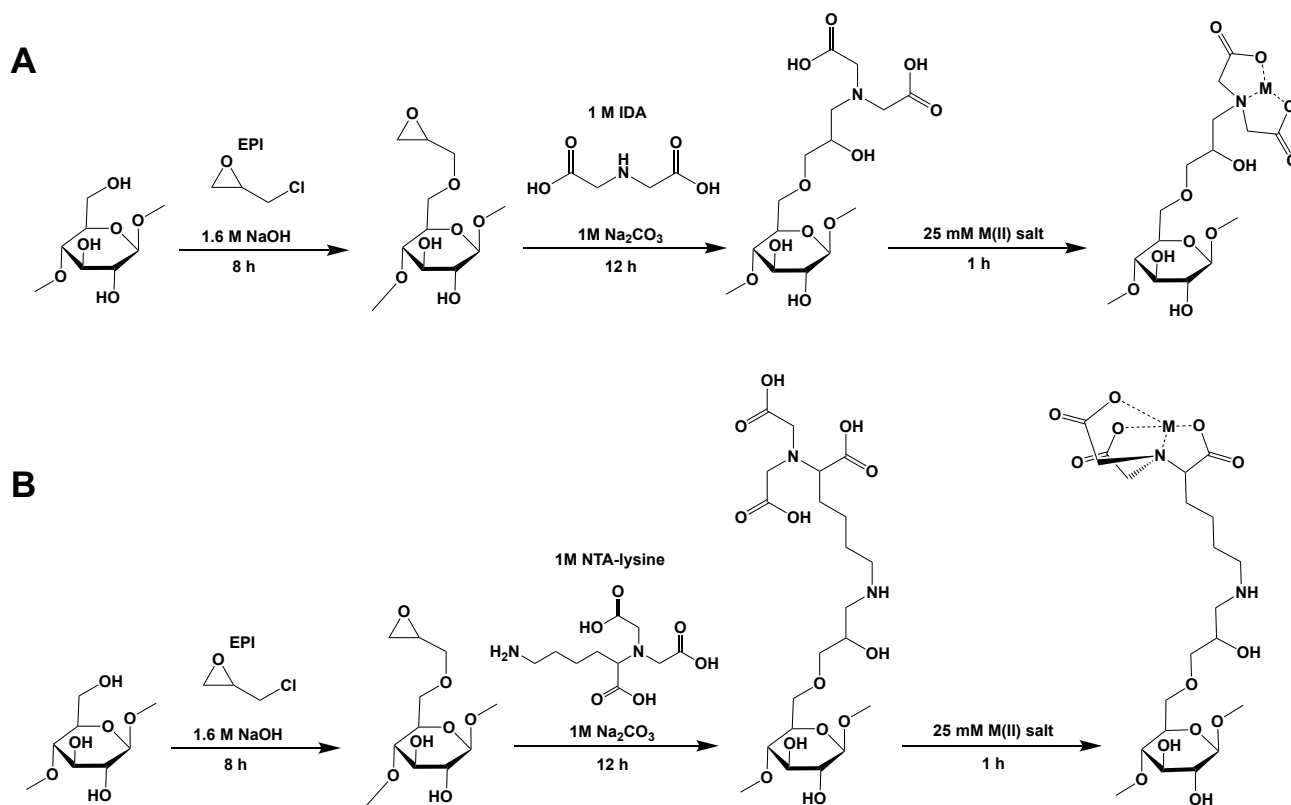
Figure 2.1. Synthesis scheme of IMAC-functionalized cellulose with (A) IDA-M(II) ligands or (B) NTA-lysine-M(II) ligands.

Briefly, a 25 cm^2 square of cellulose was submerged in a 25 mL solution of 80% 1.6 M sodium hydroxide and 20% epichlorohydrin. The membrane was incubated in solution for 8 hours, before washing 3 times with ultrapure water over vacuum filtration. The washed membrane was then incubated overnight in 25 mL of 1 M chelating ligand (iminodiacetic acid (IDA) or 2,2'-((5-amino-1-carboxypentyl) azanediyl) diacetic acid (NTA-lysine)) and 1 M sodium carbonate. The NTA-lysine derivative was synthesized in-house and used in place of pure commercial NTA in order to maximize the binding capacity of metal ions. The addition of a lysine arm to the NTA molecule prevents membrane epoxide groups binding through an NTA dentate arm during membrane functionalization. Following the overnight incubation, the membrane was again washed 3

times with ultrapure water. The membrane was then incubated in a 25 mM solution of metal sulfate for 1 hour before washing 3 times and drying at room temperature. All membranes were stored at room temperature. Before use in flowthrough experiments, functionalized membranes were cut to 144 mm^2 squares.

Membrane Flow Time Characterization

Functionalized membrane vertical flow time was investigated by pipetting 500 µL of lysed blood onto a dry 144 mm^2 square of membrane. The membrane was held in place in the sample well of a membrane holder by binder clips, and the time from addition of blood to complete flow through the membrane was measured. This measurement was then repeated for a mock elution sample. The mock elution samples were made by flowing 500 µL sample of 100 mM EDTA through the membrane following the addition of the lysed blood. The time from addition to complete flowthrough was measured as before.

IMAC Metal Loading Quantification

The amount of metal bound to each membrane was quantified using an Optima 7000 DV inductively coupled plasma optical emission spectrometer (ICP-OES). Samples of membrane were collected using a 6 mm biopsy punch. Each 6 mm diameter circle of membrane was then digested in 14% TraceMetal™ grade nitric acid for 15 minutes. The cellulose and nitric acid solution was then filtered through a 0.45 µm PVDF filter, and diluted to 2% nitric acid. Samples were then analyzed against a series of known standards and measured at 228.616 nm (Co(II)), 206.200 nm (Zn(II)), 231.604 nm (Ni(II)) and 224.700 nm (Cu(II)).

Scanning Electron Microscopy (SEM) Binding Analysis

The binding capabilities of the metal ligands was investigated using energy dispersive spectroscopy (EDS) on a Zeiss Merlin scanning electron microscope (SEM). Membranes were synthesized as described previously, but were washed with a solution of 25 mM L-cysteine before drying. A 144 mm^2 square of cysteine-washed membrane was affixed to a 12.7 mm diameter sample mount. All SEM samples were stored in desiccators after synthesis to maximize compatibility with the Zeiss SEM. Before analysis, all membranes were sputtered with gold for 80 seconds at a stage height of 57.5 mm. SEM/EDS analysis was performed at various magnifications using a 10 kV beam voltage for IDA samples and 20 kV for NTA-lysine samples.

Results and Discussion

IMAC Ligand Functionalization and Protein Binding Capacity

The theoretical protein binding capacity for both IDA and NTA was investigated using SEM/EDS to measure the ratio of L-cysteine, represented by the single detectable sulfur atom of the cysteine moiety, to the divalent metal on a Whatman Grade 3 FP membrane. The membrane was observed to bind M(II) evenly across the surface of the cellulose fibers, resulting in a relatively even distribution of bound sulfur atoms (Figure 2.2). While some areas of the membrane appeared to bind more sulfur than others, the aggregate values supported an overall even distribution (Table 2.2). These pockets of increased sulfur signal were hypothesized to be due to the variable porosity across the membrane surface created by the cellulose fibers. Elemental maps were unavailable for

NTA-lysine membranes as the low concentrations of bound atoms produced signal visibly indistinct from background.
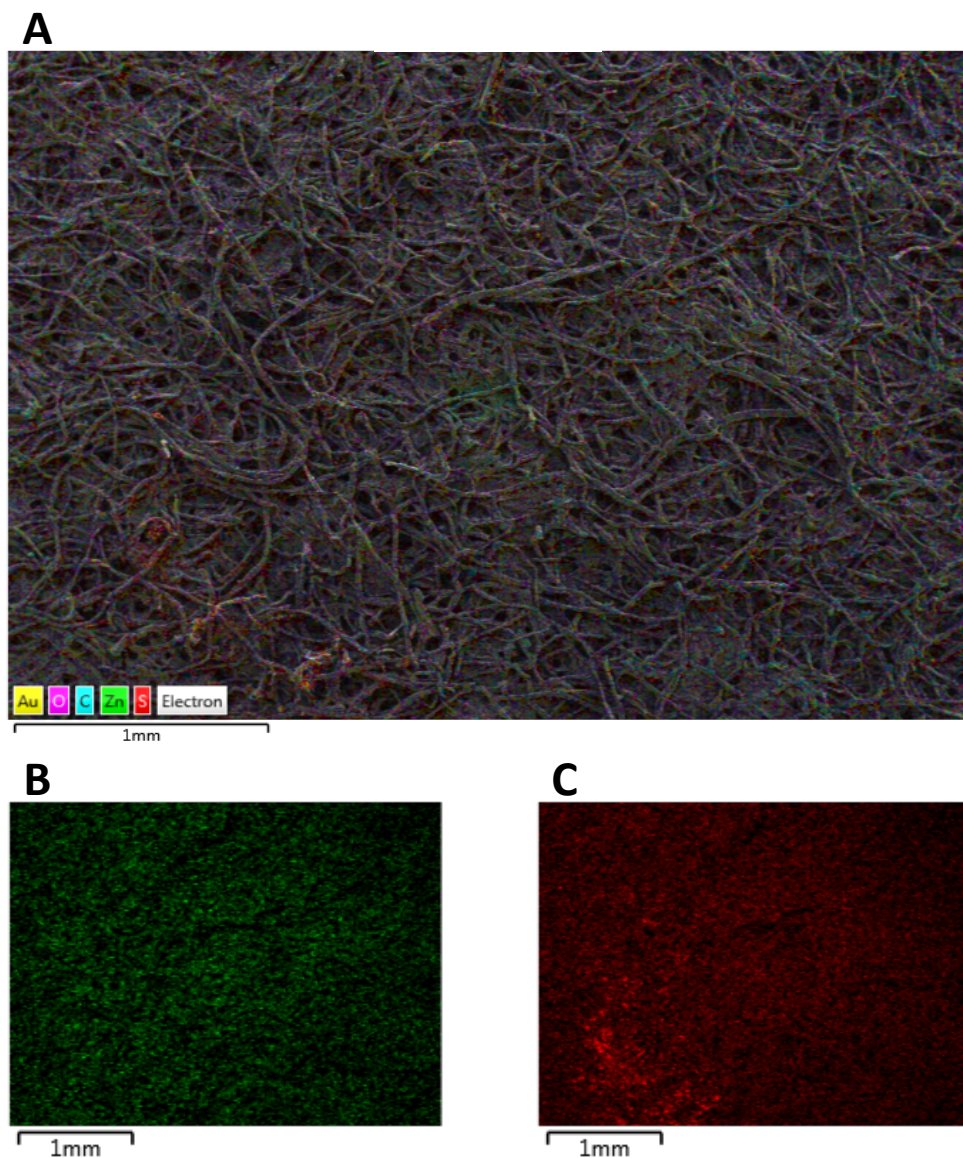
Figure 2.2. (A) Layered EDS-SEM elemental map of Grade 3FP cellulose membrane functionalized with Zn-IDA ligands and washed with L-cysteine. All membranes were sputtered with gold preceding analysis by SEM. Isolated maps showing only the distribution of (B) Zn(II) and (C) S atoms on the membrane.

In theory, tridentate ligands such as IDA use three atoms for metal chelation, leaving three available binding sites on the metal center for binding protein in solution. Tetradentate ligands such as NTA occupy four of the six binding sites in the coordination sphere, which leaves two available for protein binding. It was observed that, in agreement with the theoretical value, IDA-functionalized membranes were capable of binding L-cysteine to the membrane at a 3:1 ratio of sulfur to divalent metal (Table 2.2).

Table 2.2. Observed SEM-EDS weight percent and sigma values for the primary elements in IDA- and NTA-functionalized membranes washed with L-cysteine, where M (II) refers to the divalent metal.

	Weight Percent (%)	
Element	IDA	NTA
C	49.5 ± 0.1	52.95 ± 0.05
O	43.9 ± 0.1	46.30 ± 0.05
S	4.8 ± 0.1	0.45 ± 0.01
M(II)	1.6 ± 0.1	0.15 ± 0.01
S:M(II) ratio	3:1	2.72:1

However, it was also observed that the NTA-functionalized membranes bound at 2.72:1 ratio, slightly higher than the expected value of 2:1. This is likely due to steric inhibition of the coordination sites on the NTA-lysine molecule. The NTA-lysine derivative was selected in place of standard NTA to prevent binding of the on-membrane epoxide through one of the dentate arms, thus preserving the four distinct coordination sites. However, the addition of the lysine tail does not remove the other potential reaction sites within the NTA-lysine molecule. Therefore, it is possible that the ligand bound to the membrane in such a way that the subsequent binding of divalent metal was prevented by epoxide residues binding the NTA-core, rather than reacting through the nitrogen group

of the tail-end lysine as expected. Thus, the average ratio of sulfur atoms to M(II) could be slightly higher than expected. This steric hindrance and ligand misalignment is also likely responsible for the lower concentration of metal observed on NTA-lysine-functionalized membranes compared to IDA-functionalized membranes, as metal ion binding would be impacted by the misaligned binding of the NTA-lysine ligand.

Next, metal loading capacity, which here is defined as the molar quantity of M(II) bound to the cellulose membranes, was probed for each combination of IDA or NTA and the 4 most common divalent IMAC metals: cobalt(II), nickel(II), copper(II), and zinc(II) using ICP-OES. The ICP-OES experiments were initially performed using Whatman 17 Chr chromatography paper as the cellulose substrate, as it is easily available and amenable to use in flow-based devices based on the reported flow rate and air permeability (Table 2.1). As expected, all metals were found to bind successfully to the cellulose substrate; further, IDA-functionalized ligands bound significantly more metal per cubic centimeter of membrane than NTA-lysine-membranes, as observed on SEM-EDS. When the quantity of metal loaded on the membrane was plotted against the theoretical stability constant, K_s, for each metal-ligand pair, there was a clear trend of increasing loading capacity with increasing K_s (Figure 2.3). K_s is a reflection of the strength of the interaction occurring between the individual components of a complex, and thus it was expected that M(II)-ligand complexes with a higher theoretical K_s would be capable of binding more M(II) to the membrane.[82] The observed trend validates the expected affinity between each of the transition metals and the respective chelating ligand, as the highest reported K_s is directly correlated to the highest observed metal loading capacity for each ligand.
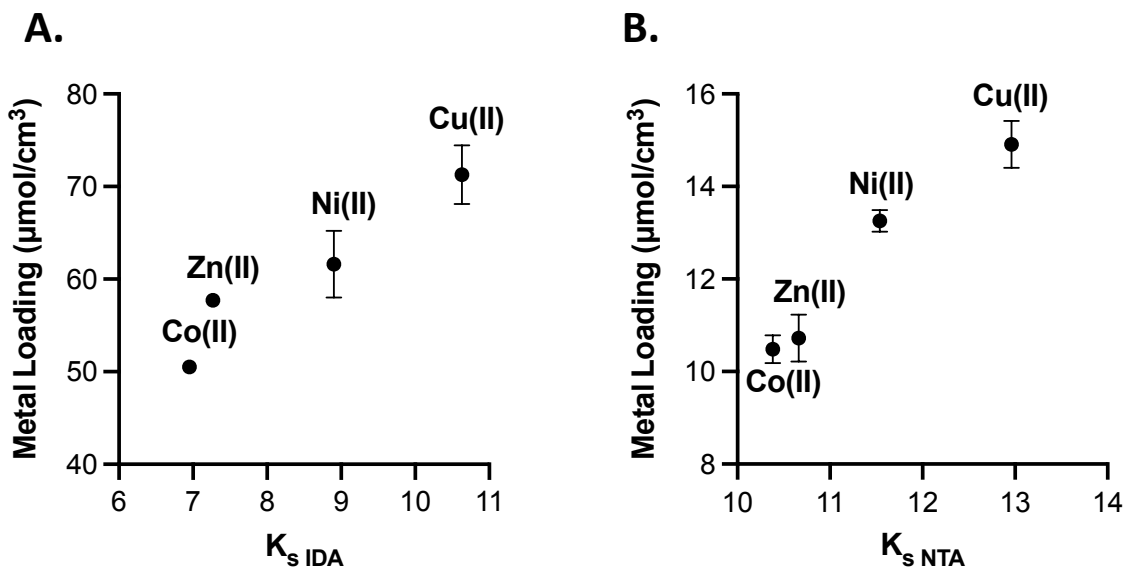
Figure 2.3. Metal loading on 17 Chr cellulose with each divalent metal ion using the (A) IDA ligand and (B) NTA ligand compared to the reported stability constant K_s for each divalent metal ion. Some error bars are not shown as the error lies within the point.

Further, the number of atoms of M(II) bound to a 144 mm^2 square of 17 Chr membrane were calculated and it was observed that there are between 8.36×10^{17} and 5.69×10^{18} metal ions bound depending on the synthesis method selected (Table 2.3).

Table 2.3. Average number of M(II) atoms bound to one 144 mm^2 square of 17 Chr cellulose (n=3).

	Number of M(II) atoms (x 10^{18})	
Element	*IDA*	*NTA*
Co(II)	4.03 ± 0.04	0.84 ± 0.04
Zn(II)	4.60 ± 0.29	0.86 ± 0.02
Ni(II)	4.92 ± 0.25	1.06 ± 0.04
Cu(II)	5.69 ± 0.06	1.19 ± 0.02

In comparison, a 250 µL sample of in-house D6 parasitized whole blood with a parasitemia of 10,000 parasites per µL is expected to contain 3.357 x 10^{12} molecules of the histidine-rich malaria biomarker HRP2. Additionally, a sample of the same volume with a parasitemia of 250,000 p/µL (the clinical threshold for severe malaria in nonimmune individuals) would contain 8.393 x 10^{13} molecules of HRP2.[83] Thus, a functionalized IMAC membrane contains several orders of magnitude more free M(II) atoms than HRP2 atoms present in a high-burden blood sample, further supporting its use in future malaria diagnostic applications.

Metal loading was also investigated for Cu(II) and Zn(II) alone using the 7 distinct cellulose membrane types detailed above (Figure 2.4). When compared by membrane thickness or area, there was a distinct increase in the molar quantity of both metals consistent with the increased surface area available in each membrane sample. Thus, 17 Chr was found to have the highest metal loading capacity compared to the mid-thickness membranes (3MM, 3 Chr, Grade 3 FP), or the thin membranes (1 Chr, 2 Chr, and 4 Chr).
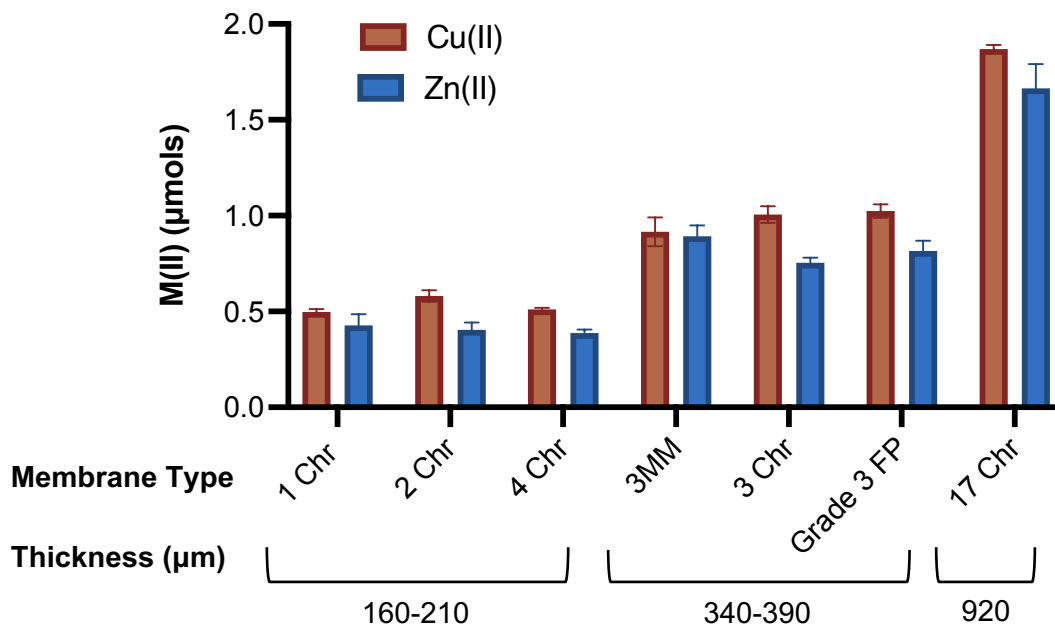
Figure 2.4. Zinc and copper ion loading for seven different cellulose membranes by increasing membrane thickness.

Vertical Flow Capability

Following assessments of ligand binding, each of the 7 potential membrane types was then examined for to their ability to process a sample via vertical flow (Figure 2.5) in preparation for use in a vertical protein capture and elution scheme discussed in Chapters 3 and 4.
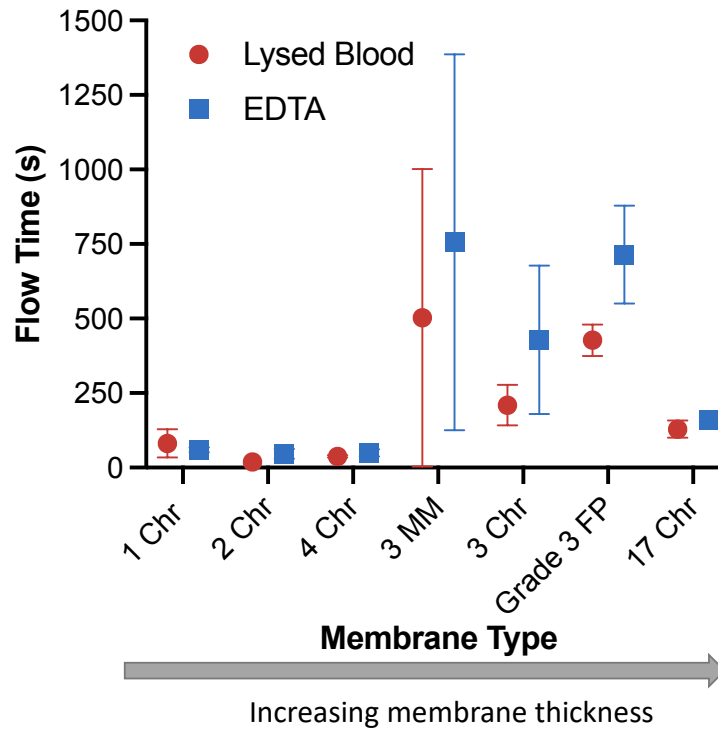
Figure 2.5. Time elapsed to complete vertical flow of a 500 µL sample of lysed blood and 500 µL 100 mM EDTA using different cellulose membranes of increasing thickness.

Thin membranes allowed liquid samples to flow through quickly with little variation, with vertical flow through the membrane occurring in a matter of seconds. Membranes of mid-range thickness had significantly longer flow times than the thinner membranes and showed significant variation, with maximum flow times exceeding 4 hours. Additionally, these middle-grade thickness membranes, which also had similar porosity values, appeared prone to clogging from blood residue and cell debris, causing significant increases in elution flow rate compared to thinner membranes. Interestingly, the thickest membrane, Whatman 17 Chr (920 µm) demonstrated remarkably fast vertical wicking speed for both blood and elution buffer and had little variation compared to the middle-

thickness membranes. This is consistent with its reported linear flow rate (190 mm/30 min) and Gurley permeability (9 sec/100 mL/in^2) (Table 2.1).

Cost Analysis

In order to appropriately utilize this technology as a point-of-care, low-resource protein enrichment tool, the cost of creating these IMAC membranes must be assessed. In Table 2.4, the cost per component is shown, for both a full 25 cm^2 membrane synthesis and an individual 14 mm^2 square used in the protein enrichment workflow.

While many of these reagents and materials are comparable in cost, it is critical to note that commercial NTA-lysine represents a staggering increase compared to the rest of the necessary components. While the in-house synthesized NTA-lysine derivative described in this chapter was able to be produced at a much lower cost (approximately $8.70 USD/gram excluding solvent costs), the synthesis was substantially limited by long lead times, production bottlenecks, and starting reagent constraints, making it impractical for large-scale experimentation. Thus, the exorbitant cost of commercial NTA-lysine, the difficulty in synthesizing in-house NTA-lysine, and the decreased metal loading capacity of the ligand compared to IDA were all significant considerations in downstream optimization of the IMAC membranes .

Table 2.4. Cost analysis for each component part of the IMAC membrane synthesis.

Materials	Amount Consumed per Synthesis	Cost per Synthesis ($ USD)	Amount Consumed per 1 Unit	Cost per 1 Unit ($ USD)
Cellulose Membranes				
1 Chr	25.0 cm^2	0.00681	1.44 cm^2	0.00039
2 Chr	25.0 cm^2	0.0325	1.44 cm^2	0.00187
3 Chr	25.0 cm^2	0.0549	1.44 cm^2	0.00316
4 Chr	25.0 cm^2	0.0334	1.44 cm^2	0.00192
3MM	25.0 cm^2	0.0361	1.44 cm^2	0.00208
Grade 3FP	25.0 cm^2	0.0465	1.44 cm^2	0.00268
17 Chr	25.0 cm^2	0.0965	1.44 cm^2	0.00556
Functionalization Reagents				
Epichlorohydrin	5.0 mL	0.2955	0.288 mL	0.017
NaOH	1.280 g	0.076	0.0737 g	0.00438
Chelating Ligands				
IDA	3.328 g	0.3521	0.1917 g	0.0203
NTA-lysine (commercial)	6.557 g	844.5	0.3777 g	48.65
M(II) Salts				
Zn(SO$_4$) heptahydrate	0.1797 g	0.0303	0.01035 g	0.00174
Cu(SO$_4$) pentahydrate	0.1561 g	0.0337	0.008989 g	0.00194
Ni(SO$_4$) hexahydrate	0.1643 g	0.0516	0.00946 g	0.00297
Co(SO$_4$) heptahydrate	0.1757 g	0.0659	0.01012 g	0.0038

Conclusion

In this chapter, a paper-based cellulose IMAC substrate was synthesized and characterized for future use in histidine-rich protein separations. Membrane-bound IMAC ligands were found to successfully bind to each of the four borderline transition metals evaluated: Co(II), Zn(II), Ni(II), and Cu(II). Additionally, the ability for the functionalized membrane to bind protein from solution was examined as a proof-of-concept using L-cysteine washes. This showed that the substrate-bound M(II) ligands were capable of binding protein from solution with minimal loss compared to the theoretical values. Further, the low cost associated with laboratory-scale production indicates that this paper-based separation technique may be imminently feasible to implement in LMICs, as it adds approximately $0.05 USD to the cost of production, and this cost could likely be driven down further with scale-up for mass production.

Acknowledgements

CHAPTER 3

APPLICATION OF IMAC MEMBRANES TO POINT-OF-CARE HISTIDINE-RICH

MALARIA BIOMARKER CAPTURE AND ENRICHMENT[3]

Introduction

Between 2010 and 2019, 2.7 billion RDTs for malaria were sold, and 80% (2.16 billion) of those were supplied directly to countries in sub-Saharan Africa.[8] Although there has been some plateauing observed in the RDT market in 2019 and 2020 with the onset of the global COVID-19 pandemic, RDTs are still considered the most commonly deployed malaria diagnostic method in public and community healthcare facilities.[84] This was further supported by the WHO in 2010, when malaria treatment guidelines were expanded to specifically include the recommendation that suspected cases be confirmed by either microscopy or RDT.[85] As discussed in Chapter 1, RDTs are inexpensive, quick, simple-to-use, and readily available to healthcare workers in primary or community care settings. Thus, broad rollouts of RDTs have removed several barriers related to malaria diagnosis in low-resource and rural areas. In 2017, it was estimated that approximately 75% of malaria diagnosis in sub-Saharan Africa was performed using RDTs as opposed to PCR, blood-smear microscopy, or other laboratory-based methods.[47] Additionally, following the onset of a broad-scale RDT rollout in sub-Saharan Africa, the percentage of children diagnosed via parasitological methods increased from 14% to 40%.[8]

---

[3] Portions of this chapter are reprinted here with permission from *Journal of Chromatography B*, submitted for publication. Unpublished work © Elsevier 2021.

The most common RDTs for malaria target the *Plasmodium falciparum*-specific biomarker HRP2, with over 90% of tests in circulation designed to detect this biomarker.[86] HRP2 is a 30 kDa water-soluble protein produced by *falciparum* parasites and released into the body by infected red blood cells.[87,88] The protein's sequence predominantly consists of histidine and alanine residues, which make up 34% and 37% of the protein, respectively.[87] To date, HRP2 has been detected in serum, plasma, cerebrospinal fluid, and urine, although many commercial HRP2-based tests for malaria detect the protein in small whole blood samples.[88]

Between these point-of-care rapid tests, there is significant variation in sensitivity, particularly at low parasite densities. As stated in Chapter 1, the WHO has recommended that commercially available RDTs be able to detect parasite burdens of at least 200 parasites per µL of whole blood.[45] However, many asymptomatic patients harbor parasite burdens far below the detectable range. Asymptomatic malaria infections are present in populations with widely varied levels of disease incidence (Figure 3.1) and several studies have observed asymptomatic infection rates near or above 50% regardless of risk.[89–94] This represents a significant threat to malaria control and elimination efforts, as asymptomatic patients remain capable of transmitting parasites despite their lower overall parasite burden.[29] Additionally, control and elimination efforts focused on asymptomatic malaria patients are further compounded by a lack of healthcare utilization among asymptomatic adults with subpatent infections.[95]
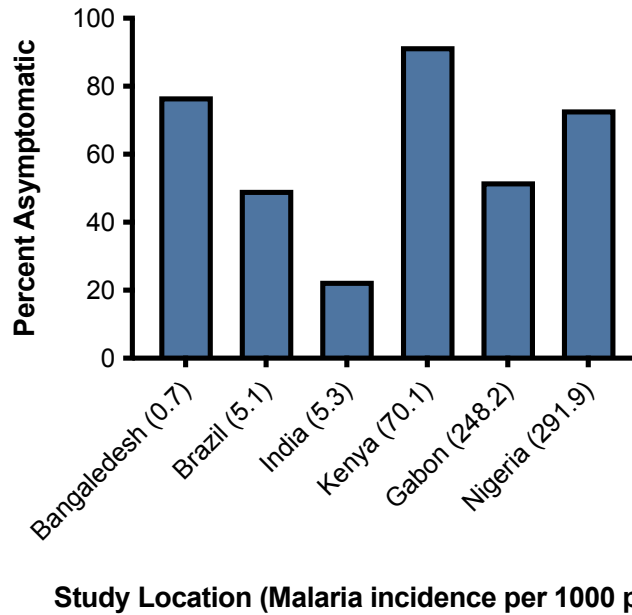
Figure 3.1. Percent of asymptomatic malaria infections determined for a specific region, ordered by increasing incidence of malaria in 2018. Data adapted from Refs. 88-93.

Recent modeling efforts have shown that the currently established diagnostic threshold of 200 parasites per µL is only sufficient for detecting 55% of the total infectious reservoir.[37] Increased sensitivity, for instance by 10-fold or 100-fold, would increase the percentage of the infectious reservoir being detected by 28% or 40% respectively. Thus, investigators have begun to seek additional sample preparation methods to enrich biomarkers of interest to within this range.

The simplest method to increase diagnostic sensitivity is to increase the volume of sample being analyzed, proportionally increasing the amount of biomarker present in the sample and the amount of biomarker that can be isolated at the test line of an RDT. However, previous work investigating large-volume sample addition on commercial RDTs found that using blood volumes of 15 µL of more resulted in clogged nitrocellulose test strips and little to no blood clearance.[96] The lack of blood clearance on these tests masked

the appearance of the test line and made tests effectively impossible to read. However, as mentioned briefly in Chapter 2, alternate enrichment methods using resin and magnetic beads require significant infrastructure to perform, and represent an added expense in manufacturing.[72,73,97] The initial resin bead-based method features a pipette tip embedded with a bed of packed resin beads. This method inherently relies on the ubiquity of handheld pipettes and modified pipette tips, which are uncommon outside of a laboratory and are unsuited to the rigors of field use. Further, the prototype was estimated to add an additional cost of $2.08 to each test, effectively double the cost of the most expensive RDT kits (estimated cost $0.60-$1 USD).[97,98] Later prototypes utilizing magnetic beads functionalized with IMAC ligands decreased this cost to $0.09 USD per test for the beads alone, and noted that the total cost of the assay was $0.25 per use if it was assumed that the test device survives 500 uses.[73] However, despite the ability of previous researchers to dramatically lower the price of enrichment methods, the method still required separate mixing using a battery-powered vortex device, and several sample transport steps, making it cumbersome and difficult to employ directly at the point of care. By developing a paper-based sample preparation method and integrating this method into traditional LFA formats, a novel RDT could be designed which drastically increases the sensitivity of these tests without sacrificing usability or affordability. In this chapter, the IMAC-functionalized cellulose membranes synthesized and characterized in Chapter 2 are applied to point-of-care malaria diagnostics designed to detect the innately histidine-rich malaria biomarker HRP2.

Experimental

Materials

Pre-backed nitrocellulose lateral flow membranes (FF80HP, FF120HP), and wicking pads (CF7), as well as Whatman cellulose membranes (described in detail in Chapter 2) were purchased from Cytiva Life Sciences (Marlborough, MA, USA). 40 nm unconjugated gold colloids were purchased from Ted Pella Inc (Redding, CA, USA). Anti-HRP2 antibodies, ABMAL 0405 IgM and ABMAL 0404 IgG, were purchased from Arista Biologicals Inc (Allentown, PA, USA). Control goat-anti-mouse antibodies were purchased from Fitzgerald Industries International (Acton, MA, USA). Pooled gender human whole blood in citrate phosphate dextrose (CPD) anticoagulant was purchased from BioIVT (Westbury, NY, USA). All other reagents utilized were of reagent grade and sourced from Fisher Scientific and Sigma Aldrich.

HRP2 Protein Quantification

To prepare the samples, two methods were utilized (Figure 3.2). In the initial sample preparation method, a 79 mm^2 circle of functionalized membrane was placed in the bottom of a 2 mL plastic syringe (Figure 3.2.A). Human whole blood was spiked with D6 parasite culture (stock parasitemia: 43,600 parasites/µL) and lysed 1:1 with lysis buffer (phosphate buffer, pH=8, 300 mM NaCl, 2% Triton 100). 500 µL of parasitized lysed blood with a final parasitemia of 25 p/µL was added to the membrane within the syringe and allowed to flow vertically for one minute before being flushed with the plunger. The resulting filtrate was collected in an Eppendorf tube. Next, a 500 µL aliquot of 100 mM EDTA was added to the membrane within the syringe and similarly allowed to flow by

39

gravity filtration through the membrane for one minute before being flushed through with the plunger. The eluent was collected in a separate Eppendorf tube. All experiments were performed in method triplicate.

In this study, both the capture filtrate and eluent were quantified by the *Pf*HRP2 ELISA developed by Davis *et al*.[99] First, 100 µL of 1µg/mL anti-HRP2 IgM antibody in 1x phosphate buffered saline (PBS) was pipetted into each well of an Immulon 2HB 96-well plate. The plate was sealed with Parafilm and incubated for 1 hour on an orbital shaker. After 1 hour, the plate was removed and washed 3 times with 1x phosphate buffered saline containing 0.1% Tween 20 (PBST). Following this, 300 µL of a 5% (w/v) bovine serum albumin (BSA) blocking solution was added to each well. The plate was sealed with Parafilm and allowed to incubate on the orbital shaker for 2 hours. After blocking, the plate was washed 3 times with PBST. Samples, standard curves, and controls were diluted 2.5-fold using PBST with 0.1% BSA (w/v) to fall within the dynamic range of the ELISA. These samples, standard curves, and controls were then added to the plate, which was sealed and allowed to incubate on the orbital shaker for 2 hours. Following sample incubation, the plate was washed 4 times with PBST, and 100 µL of a 0.5 µg/mL anti-HRP2 IgG detection antibody conjugated to HRP was added to each well. The detection antibody was suspended in PBST with 0.5% BSA. The plate was sealed with Parafilm and protected from light, and the detection antibody solution was incubated on the orbital shaker for 1 hour. The plate was then washed 5 times before developing with 100 µL of TMB One solution. The TMB One solution was incubated for 10 minutes on the orbital shaker, sealed and protected from light, before the reaction was quenched with

100 µL of 2 M H_2SO_4. The absorbance values for the quenched reaction were read at 450 nm using a BioTek Synergy H4 microplate reader (Winooski, VT, USA).

To more realistically mirror a potential field-based RDT setting, a second HRP2 capture workflow was developed (Figure 3.2.B). In this method, a 144 mm^2 square of IMAC-functionalized membrane was placed into a membrane holder and secured with binder clips. A 500 µL sample of parasitized lysed blood was pipetted onto the membrane and allowed to completely flow through the paper into the sample collection well. The sample was removed from the well before elution buffer (100 mM EDTA) was pipetted onto the paper and allowed to flow through into the sample well. All collected samples were analyzed using the *Pf*HRP2 ELISA described above.[99] Capture and elution values were evaluated for statistical significance using a one-way ANOVA test with Tukey's multiple comparisons test.

Metal interference was analyzed by titrating different concentrations of metal into parasitized and non-parasitized lysed blood samples in triplicate. Photographs were taken immediately after addition of the samples to the 96-well plate. All samples were evaluated by the HRP2 ELISA described above. The differences in the ratio of parasitized metal-containing samples to parasitized metal-free controls for each concentration of M(II) were examined using multiple unpaired t-tests.
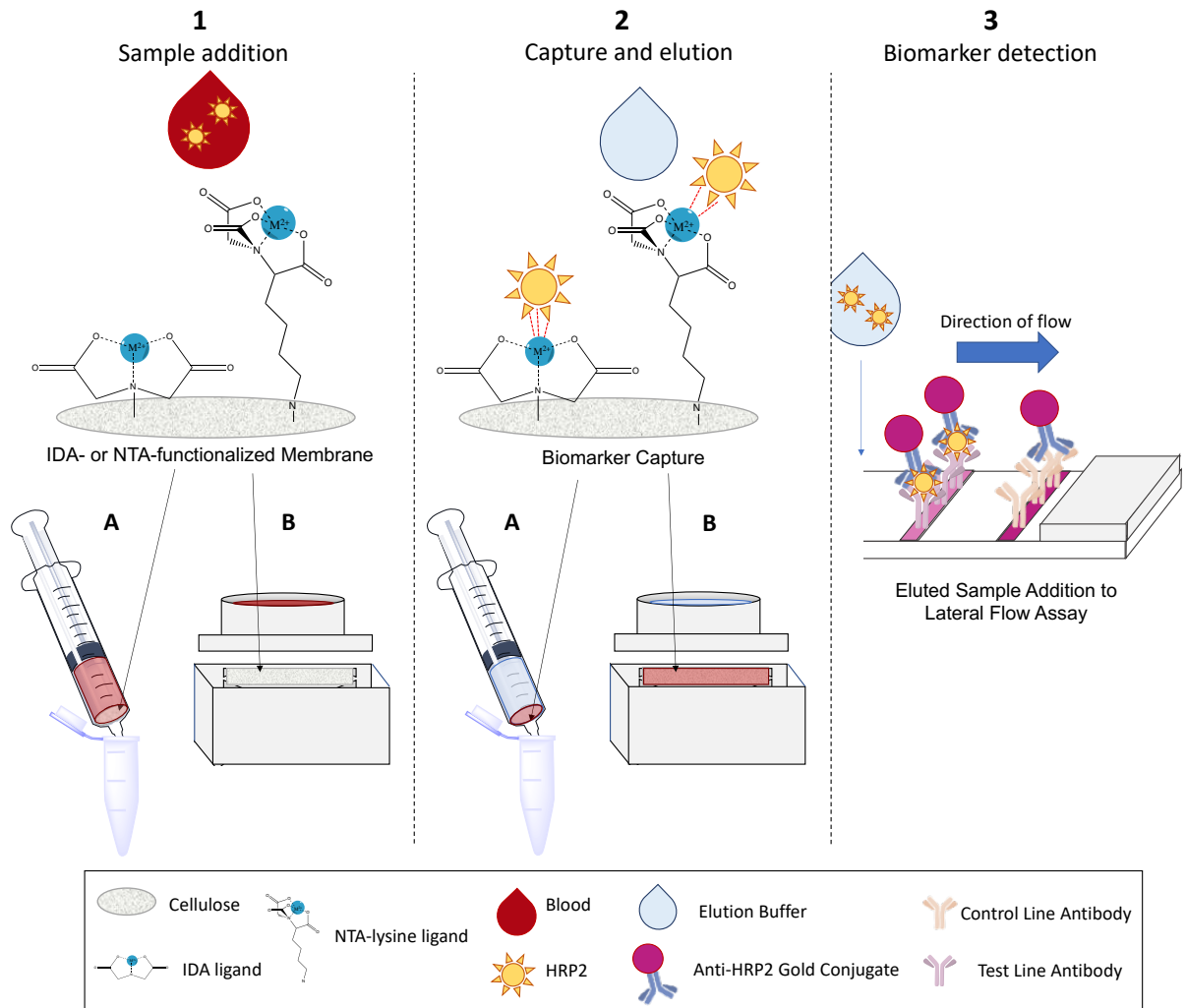
Figure 3.2. Overall workflow for IMAC membrane integration into a lateral flow assay workflow. (1) Cellulose membranes are functionalized with either IDA or NTA metal affinity ligands. For the syringe-based method (A), a 79 mm^2 circle of functionalized membrane is placed at the bottom of the syringe prior to sample addition. For the integrated membrane holder method (B), a 144 mm^2 square of IMAC-functionalized membrane is clamped into place between the lid of the holder, which contains a sample inlet, and the bottom, which contains an unobstructed flowthrough well. Sample is then added either to the syringe or to the sample inlet of the membrane holder and biomarker is aggregated on the membrane during vertical flow. (2) Metal affinity ligands capture HRP2 from a large-volume sample, as shown by the red color of the membrane. The filtrate is captured and removed for analysis and elution buffer is added to the same sample inlet as the initial blood sample. (3) The HRP2 eluted from the membrane can then be detected colorimetrically using an immunoassay such as a lateral flow assay (LFA, shown above) or ELISA.

Lateral Flow Assay Development

The HRP2 LFA was fabricated using a BioDot AD 1520 Array and Dispense Platform (Irvine, CA, USA). Anti-HRP2 IgM antibodies were immobilized at a concentration of 1 mg/mL in a horizontal stripe across a fast-wicking polystyrene-backed nitrocellulose membrane. Goat-anti-mouse IgG antibodies were then deposited in a parallel line downstream of the HRP2 test line. Tests were allowed to dry for 2 hours at 37 ℃ before being blocked with 5 mL of Pierce Protein Free blocking buffer. After blocking, test strips were dried for 3 hours at 37 ℃, and then cut into 5 mm strips using a BioDot CM 4000 high-precision lateral flow assay cutter. All tests were stored in a desiccated environment at room temperature before final assembly with wicking pad.

LFA conjugate was produced by incubating citrate-stabilized OD1 40 nm gold colloids with ABMAL 0404 anti-HRP2 IgG in 50 mM borate buffer for 1 hour on an orbital shaker. The gold colloids were then blocked with 10% BSA (w/v) in 50 mM borate buffer for 1 hour before centrifugation at 2500 g at 4℃ for 30 minutes. After centrifugation, the supernatant was removed, and the pellet was washed with a diluent buffer of 1% BSA and 10% Trehalose (w/v) in 50 mM borate buffer. The solution was then centrifuged again under the same conditions, the supernatant was removed, and the pellet was diluted to a final OD of 10.

Assessment of Integrated IMAC LFA

The efficacy of the IMAC sample enrichment step was analyzed by comparing the enhanced IMAC-integrated LFA to an unenhanced LFA. Enhanced LFAs were performed

using a titration series of parasite culture spiked into lysed whole blood and the sample preparation method detailed above. 10 µL of OD 10 anti-HRP2 gold nanoparticle conjugate was added to 125 µL of the mock elution sample, then an in-house LFA was dipped into the mixture and allowed to wick upwards for 15 minutes. The LFAs were then transferred to a running buffer of 50 mM borate buffer + 0.1% Tween 20 for 3 minutes to assist in membrane clearing.

Unenhanced LFAs were run as vertical dipstick tests, and consisted of a 10 µL sample of parasite-spiked lysed whole blood added to 115 µL of running buffer (1x borate buffer with 0.1% Tween 20). 10 µL of conjugate was added to the sample and an LFA was added to the mixture and allowed to wick for 15 minutes, followed by a 3-minute wash step.

Both IMAC-enhanced and unenhanced lateral flow test strips were analyzed on a Qiagen ESEQuant lateral flow reader (LFR) (QIAGEN Lake Constance GmbH, Germany). The average test line peak area and standard deviation were calculated at each parasite density in the titration series and the limit of detection was calculated using $3SD_{blank}$ divided by the slope of the regression of the linear region of the data.

Results and Discussion

On-Membrane HRP2 Capture and Recovery

First, each of the ligand-metal combinations were tested for HRP2 binding capacity in a membrane-based vertical flowthrough assay using the 17 Chr cellulose membrane

44

as a starting point. While all metal complexes yielded high HRP2 capture percentages (>80%), the recovery values varied widely (Figure 3.3).
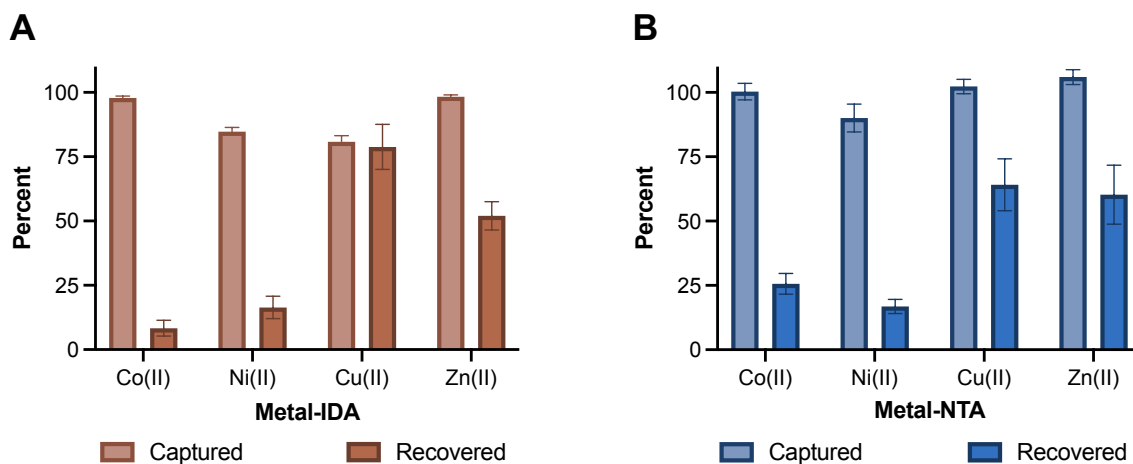
Figure 3.3. Percent HRP2 captured and recovered using each divalent metal ion bound to either the IDA ligand (A) and NTA ligand (B).

For IDA membranes, the capture between Co(II) and Zn(II) was not statistically different (p=0.9839, 95% CI), nor was capture between Ni(II) statistically different from Cu(II) (p=0.0540, 95% CI). However, the difference between Co(II) and Zn(II) compared to Ni(II) and Cu(II) was found to be significantly different (p <0.0001, 95% CI). Despite this, the lowest capture percentage among the 4 metals was found to be 80.8% ± 2.4% (Cu(II)), and the highest-performing metals (Zn(II) and Co(II)) were found to capture more than 99% of the protein in solution. Using NTA-lysine, Co(II), Cu(II) and Zn(II) are not statistically distinct (p=0.9166 for Co(II) vs. Cu(II), p=0.3216 for Co(II) vs. Zn(II), p=0.6402 for Cu(II) vs. Zn(II), 95% CI) while Ni(II) has a distinctly lower capture percentage (p=0.0399, 0.0166, and 0.0036 at 95% CI when compared to Co(II), Cu(II), and Zn(II),

respectively) (Figure 3.3B). For both IDA and NTA ligands, Cu(II) and Zn(II) were shown to have the highest protein recovery. Using Cu-IDA membranes, 78.8% ± 8.8% of the total protein was recovered, whereas 52.0% ± 5.5% of the total HRP2 was recovered using Zn-IDA preparation. For the NTA-lysine-functionalized membranes, recovery was improved for Cu(II) and Zn(II) (64.1% ± 10.1% and 60.2% ± 11.5% respectively), although these increases were not statistically significant. Although there is not a large difference in capture efficiency among the four metal ions, the high capture efficiency of Co(II) and Zn(II) IDA membranes reflects the k_{on} observed in literature.[72] Cu(II) was previously reported to have the least desirable kinetic parameters when examined in the context of resin-based solution separation and biolayer interferometry, but here shows the most effective binding capabilities. However, Cu(II) was down-selected in this process as Cu-functionalized membranes showed adverse effects when treated with lysed or whole blood (Figure 3.4A). Upon coming into contact with Cu(II)-treated membranes, blood samples underwent a visible shift in color from red to brown and precipitated solid in the sample. Additionally, it was found that the presence of Cu(II) in small concentrations interfered with the results of immunogenic assays, evidenced by the change in signal for metal-containing samples with varied Cu(II) concentrations at the same parasitemia (Figure 3.4B).
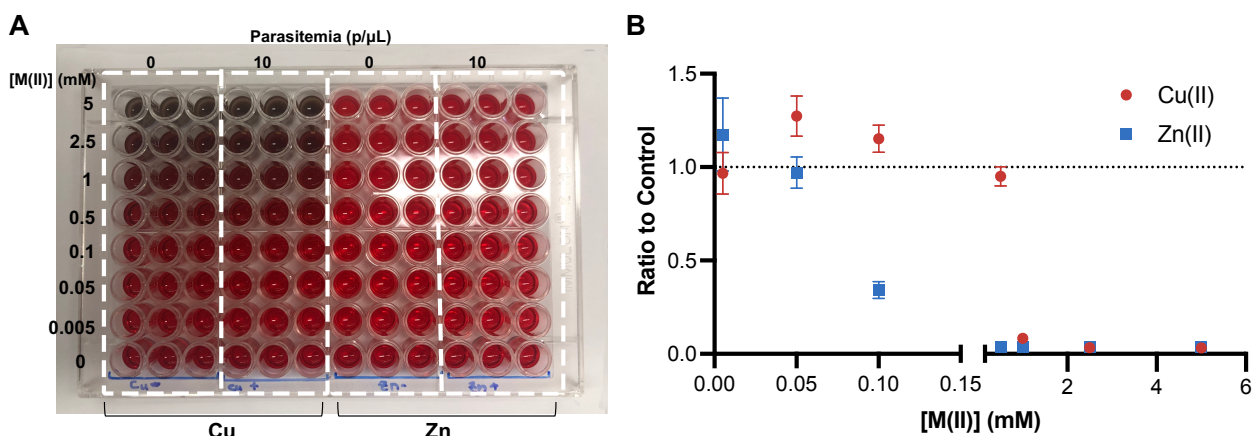
Figure 3.4. (A) Lysed whole blood samples titrated with Cu(II) and Zn(II), both without parasite culture (0 parasites/μL blood) and with parasite (10 parasites/μL blood). Parasite and Zn(II) do not have a visible effect on blood sample color, while the presence of Cu(II) drastically alters the color and texture of lysed blood. (B) Ratio of metal-containing positive samples against a metal-free control for parasitized blood containing increasing amounts of M(II).

When the HRP2 ELISA was tested in the presence of both Cu(II) and Zn(II), it was found that large amounts of M(II) in solution chelate HRP2 and prevent binding to the antibodies of the immunoassay (Figure 3.4B). There was little evidence that low concentrations of Cu(II) chelated HRP2 in such a way that prevented binding, as evidenced by the lack of decrease in signal. However, increasing concentrations of Zn(II) did appear to chelate HRP2 from the sample, shown by the decrease in the ratio of metal-containing sample to metal-free positive control. Additionally, small concentrations of Cu(II) appeared to interfere with the immunoassay sandwich, artificially inflating signal such that the ratio of metal-containing sample to metal-free control is significantly higher than 1 (p= 0.00025, 0.00101, and 0.00076 for 0.1 M, 0.5 M, and 1.0 M Cu(II) respectively) (Figure 3.4B). While a slight increase in signal was seen in Zn(II) samples, this difference

from the metal-free positive control was not statistically different from 1. This, in combination with the detrimental effects of copper on the biological samples, led to the down selection of copper as an appropriate membrane IMAC metal. Thus, although Zn(II)-functionalized membranes resulted in slightly less protein recovery, the high capture percentage and lack of bioreactivity of the Zn(II) membranes made these a natural choice for further development. IDA was utilized as the preferred IMAC ligand due to the ease of availability and low cost compared to NTA-lysine (Chapter 2), as well as lower observed variation for capture using Zn(II).

Following the selection of Zn(II) as the ideal candidate metal and IDA as the preferred IMAC ligand for on-membrane protein enrichment, nonspecific binding of HRP2 to the entire ligand-metal system was investigated (Figure 3.5).
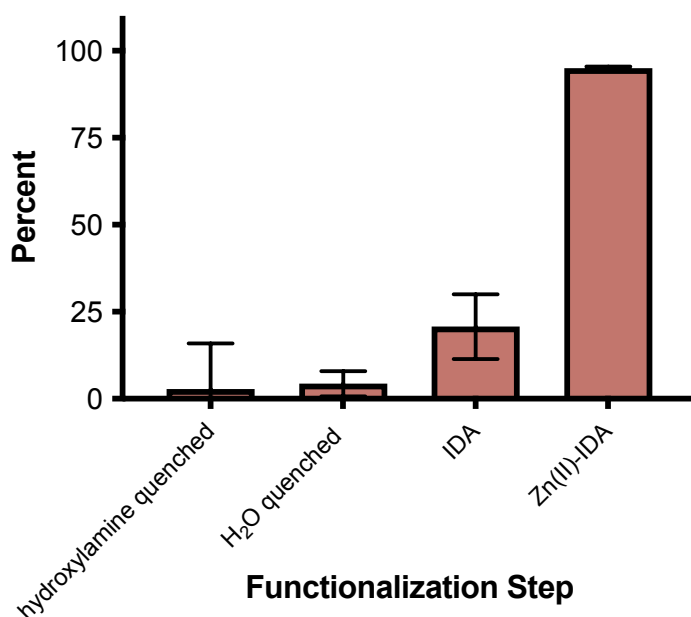
Figure 3.5. Percent HRP2 captured on membrane for each step of the M(II)-IDA functionalization procedure.

Binding was evaluated using membranes at each step of the functionalization procedure, and it was found that the entire Zn(II)-chelating ligand structure was necessary for significant capture of HRP2. While there was some nonspecific binding observed with ligand-only membranes, there was no binding evident for epoxidized membranes when quenched with water or hydroxylamine, indicating no free epoxides present on the membrane after the wash step of the functionalization. The minor nonspecific binding of HRP2 to the IDA-functionalized membrane was shown to be not statistically significant from the binding to either the hydroxylamine- or H_2O-quenched membranes using an ANOVA test with multiple comparisons (p=0.0828 and p=0.1155, respectively).

Following this affirmation that HRP2 binding was specific, each of the seven membrane types characterized previously was investigated for HRP2 binding capacity using Zn(II)-IDA functionalization (Figure 3.6).
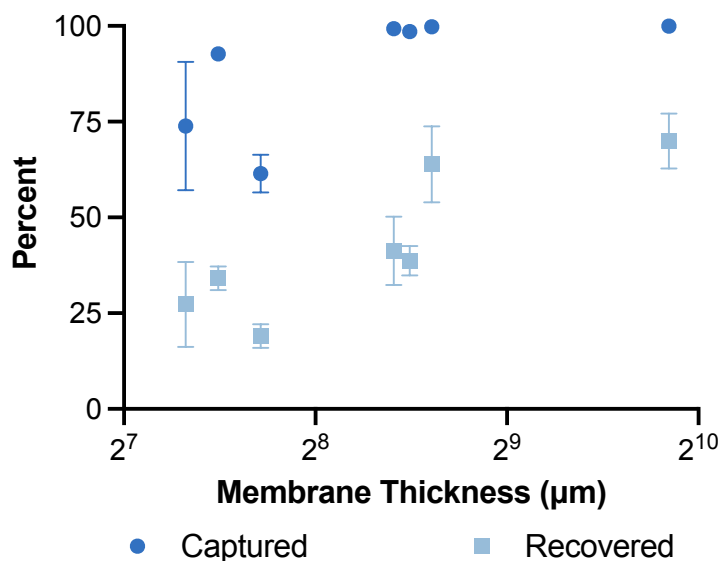
Figure 3.6. Percent HRP2 captured and recovered using Zn(II)-IDA functionalized membranes of increasing thickness.

While all membranes above 300 μm thick were observed to capture 100% of the protein from the sample, HRP2 recovery varied widely. 17 Chr, the thickest and fastest-flowing membrane, as discussed previously, outperformed the six other membranes tested, and thus remained the ideal candidate for use in LFA enhancement work. Specifically, 69.9% ± 7.2 of the total protein was recovered after elution using the 17 Chr cellulose membrane. The high proportions of both captured and recovered protein were expected due to the high molar concentration of M(II) observed on the thick 17 Chr membranes (discussed in further detail in Chapter 2). When compared to 17 Chr, Grade 3 FP had a similar recovery percentage of HRP2. However, it was not selected due to its significantly worse practical flow time (Chapter 2), which made it an inappropriate substrate for a rapid, field-usable diagnostic test.

All of the previously discussed capture and elution experiments were performed using the syringe method. The plunging and refilling of the syringe represents a several step process that would further limit the utility of this format at the point of care. During this process, the membrane dries while the syringe plunger is removed, and could be exposed to contaminants, or damaged or displaced by the force of the plunger removal. It is expected that in a traditional vertical flow workflow, relying only on the innate vertical flow of the membrane, the system would display the same capture and elution ability as the syringe-based system without the need for disruption of the membrane. As EDTA binds extremely tightly to Zn(II), (k_d approximately 10^{-16} M) changes to the flow method are expected to have minimal impact on the performance, particularly as the flow time only increases in the vertical flow method. Thus, in evaluating the enhancement with

regard to LFAs, the membrane holder was used to better mimic an integrated, hands-free, low-effort flow through system.

Lateral Flow Assay Enhancement

The unenhanced LFAs were performed using 10 µL of lysed blood, the highest possible volume as determined in the literature.[96] Using this value, the limit of detection (LOD) of the traditional LFA was found to be 109 parasites/µL (Figure 3.7) when using raw test line signal as the metric of interest. While this value represents a limit of detection significantly below the WHO accepted value for field-deployable tests of 200 parasites/µL, it is still not sufficient for detection of asymptomatic disease.

A

Parasitemia (p/µL)

6250 2500 1000 400 160 64 25.6 0

C

T

B

Parasitemia (p/µL)

2500 1000 400 160 64 25.6 10.2 0

C

T

C

LOD: 7 parasites/µL

LOD: 109 parasites/µL

● Unenhanced LFA   ■ IMAC Enhanced LFA
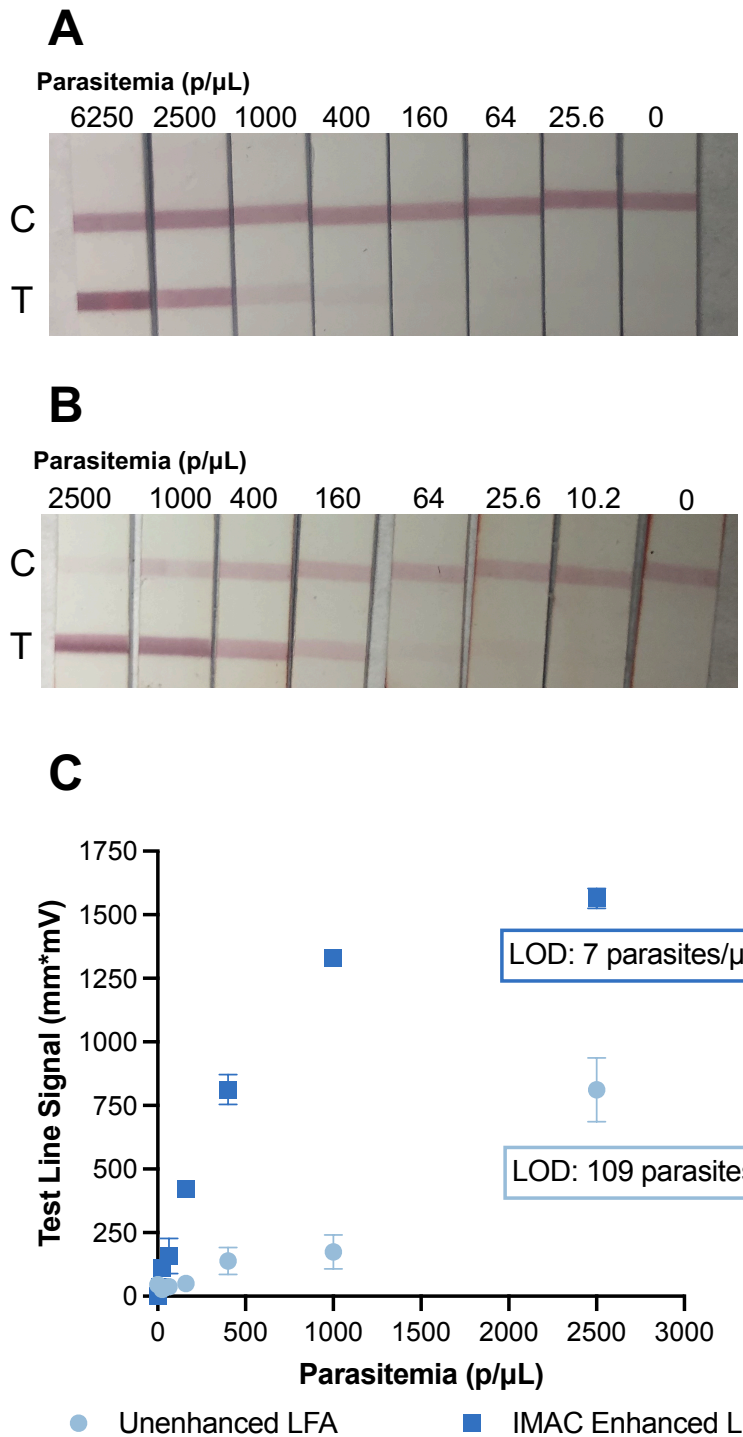
Figure 3.7. Limit of detection analyses were performed for the (A) unenhanced and (B) IMAC-enhanced LFA preparation using an 8-point spiked parasite titration series diluted by a factor of 2.5. (C) The IMAC-enhanced LFAs were observed to have an improvement factor of 15.6x compared to the traditional LFA method when utilizing test line signal as the metric of interest.

In comparison, the IMAC-enhanced LFAs were observed to have a LOD of 7 parasites per µL when using test line signal as the deciding metric. This results in a 15.6-fold enhancement compared to the unenhanced LFA. For enrichment of a 500 µL sample of lysed blood compared to a traditional 10 µL lysed blood sample, the enrichment factor is 50-fold. However, in this study, a 125 µL aliquot of the eluted HRP2 was used on the 5mm test strips. Additionally, the entire 500 µL sample volume was not recovered from the membrane. Due to the absorbent properties of the thick cellulose, there was on average, a remaining volume of 364 µL recovered from the membrane after flowthrough (n=12) rather than a full 500 µL aliquot. Thus, the 125 µL sample can be considered 34.3% of the total recoverable sample. With this in consideration, the true theoretical enhancement factor for this study is 17.2-fold compared to the unenhanced test, meaning that the IMAC-enhanced enrichment performed with 91.9% efficacy.

However, a loss of control line signal is observed in the enhanced diagnostics (Figure 3.7B), likely due to an over-enrichment of HRP2.[100,101] The enriched HRP2, even if not bound at the test line, could bind anti-HRP2 gold conjugate in such a manner that it impedes the binding of goat-anti mouse antibodies at the control line. This is easily remedied by the addition of more gold nanoparticle conjugate, or by using a different control line molecular recognition element. Nonetheless, the limits of detection observed for the enhanced LFA fall well within the proposed range of asymptomatic malaria parasitemias and could further be improved by using the full enriched sample volume.

There are some limitations to this study, including the persisting volume limitations of LFAs. Further work should be dedicated to enhancing LFA wicking capacity such that

an entire 364 µL elution volume could be utilized. In investigating the elution of all captured HRP2 into a usable 125 µL sample rather than the previously used 500 µL, it was found that the resultant protein recovery dropped significantly, even at increasing concentrations of EDTA (Figure 3.8). The increase in variation using a smaller volume sample is hypothesized to be due to the vastly different volumes recovered from the initial 125 µL sample. This could be due in part to the increased absorbance of the 17 Chr membrane, as it is the thickest and most absorbent of the membranes screened, and retains a significant amount of liquid samples and buffers. Thus, to maximize protein recovery, a large-volume elution buffer and downstream large-volume LFA are required for this system. Additionally, the wash step built into the LFA protocol, which assisted in clearing blood from the membrane before reading on the LFR, is unlikely to be practical in a field-based setting. However, a partitioned LFA cartridge could potentially make it possible as a further improvement to the technology available.
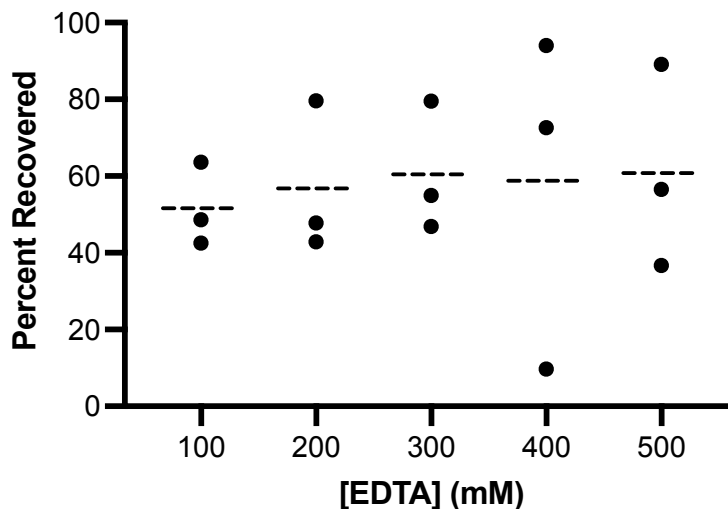
Figure 3.8. Percent HRP2 recovered using 125 µL of elution buffer at increasing concentrations of EDTA. The mean of each group is indicated by the dashed line (n=3 for each concentration of EDTA).

Cost Analysis

Using the reagents selected during optimization of the IMAC membranes, the total cost for a full synthesis at the laboratory scale could be under $1 USD, and the cost per single use would be as low $0.05 USD (Table 3.1). This represents a 5x decrease in cost compared to the previously discussed magnetic bead system[73] and an approximately 44x decrease in cost compared to other bead-based LFA enhancements.[96] It is possible that with commercial scale-up, this price could decrease further, making the added cost of IMAC membranes fractional cents.

Table 3.1. Cost analysis for each component part of the fully optimized IMAC membrane synthesis, total cost per synthesis, and cost per single use.

Materials	Amount Consumed per Synthesis	Cost per Synthesis ($ USD)	Amount Consumed per 1 Unit	Cost per 1 Unit ($ USD)
17 Chr	25.0 cm^2	0.0965	1.44 cm^2	0.00556
Epichlorohydrin	5.0 mL	0.2955	0.288 mL	0.017
NaOH	1.280 g	0.076	0.0737 g	0.00438
IDA	3.328 g	0.3521	0.1917 g	0.0203
Zn(SO$_4$) heptahydrate	0.1797 g	0.0303	0.01035 g	0.00174
Total		**$0.85**		**$0.05**

Conclusion

In this chapter, the IMAC-functionalized cellulose membrane presented in Chapter 2 was utilized as a simple-to-use, inexpensive supplement to traditional LFAs. Each

component of the IMAC membrane (e.g., cellulose substrate, chelating ligand, metal ion) was analyzed with respect to HRP2 capture and elution performance. While Zn(II)- and Cu(II)-functionalized membranes were observed to yield high percentages of recovered protein, the negative effects of copper on blood samples as well as the exorbitant cost of the NTA ligand led to Zn(II)-IDA being selected as the ideal ligand-metal combination for applied use. Using this combination of characteristics, the IMAC-enhanced LFA was found to have a 15.8-fold improvement in limit of detection compared to traditional tests at 1/5 the cost of previous interventions.

Acknowledgements

CHAPTER 4

USE OF IMAC MEMBRANES FOR NON-HISTINE-RICH BIOMARKER CAPTURE AND

ENRICHMENT[4]

Introduction

The vast majority of point-of-care rapid tests for malaria primarily detect HRP2, as

discussed in Chapter 3.[86] Despite their widespread use, rapid tests that rely solely on

HRP2 have several significant limitations to their utility. First, HRP2 is a *Plasmodium*

falciparum-specific biomarker, and is not produced by any other species of the

Plasmodium parasite.[87] Thus, tests specific only for HRP2 are incapable of detecting the

remaining 4 species of malaria that infect humans. While *Plasmodium falciparum* is the

most prevalent species of malaria parasite, *Plasmodium vivax* remains a threat in many

areas.[8] Outside of sub-Saharan Africa, *P. vivax* is the most geographically widespread

human-infecting malaria parasite.[102] Specifically, *P. vivax* makes up 76% of the malaria

infections in South and Central America, 46% of the infections in South-East Asia, and

27% of the infections in the Eastern Mediterranean region.[8] Furthermore, in nearly two-

thirds of the countries known to harbor several co-endemic malaria species, *P. vivax* is

the predominant malaria-causing pathogen.[103]

Further, HRP2 singleplexed tests (tests that only detect HRP2), are in danger of

becoming the first documented example of targeted "diagnostic resistance" as *P.*

falciparum parasites have begun to evolutionarily eliminate the *pfhrp2* and homologous

---

[4] Portions of this chapter are reprinted here with permission from *Journal of Chromatography B,* submitted for
publication. Unpublished work © Elsevier 2021.

pfhrp3 genes.[8,104,105] The *pfhrp2/pfhp3* gene deletion was first reported in the Peruvian Amazon river basin in 2010, and further studies have revealed the presence of this deletion in populations in 11 countries, including regions of Africa, India, Asia, and Central and South America.[8,105,106] For populations who lack both the *pfhrp2* and *pfhrp3* genes, or who express substantially altered versions of the genes, functional HRP2 is not expressed, and is thus not able to be detected using HRP2-specific RDTs.[104] The resulting false-negative diagnosis can then result in potentially lethal untreated infections.

Even for *P. falciparum* parasites that express HRP2 normally, HRP2 is far from the ideal biomarker for clinical case management. It has been shown that HRP2 can persist in infected individuals for several weeks after the clearance of the parasite, making it a poor marker of active infection.[107,108] In this instance, a residual positive test may result in the overtreatment of malaria-negative individuals.[109] As overtreatment is closely linked to the development of antimalarial resistance, a persistent problem in many endemic nations, this pitfall among diagnostics is significant.[110,111]

In order to address these shortcomings among HRP2 singleplexed diagnostic tests, multiplexed diagnostics have been developed that detect other biomarkers of *Plasmodium* parasites. Of these, *Plasmodium* lactate dehydrogenase (*P*LDH) is one of the most common. *P*LDH is a 35 kDa glycolytic enzyme, and it plays an essential part in anaerobic respiration during the asexual intraerythrocytic cycle of the *Plasmodium* parasite.[112] During their erythrocytic maturation, *Plasmodium* parasites lack a traditional Krebs cycle, and rely almost exclusively on the anaerobic fermentation of glucose as their primary source of energy.[113,114] *P*LDH is the terminal enzyme in this process, and catalyzes the interconversion of pyruvate and NADH to lactate and NAD⁺, making it

crucial for parasite survival.[115]   Importantly, *P*LDH is conserved between the different species of parasite, and is biochemically distinct from LDH produced by the human host.[113,115] Further, *P*LDH load in the human body closely correlates to the parasitemia during an active malaria infection; as effective treatment reduces the number of parasites in the blood, the enzyme concentration shows a corresponding decrease.[116] These factors combined make it a highly useful biomarker for pan-*Plasmodium* infections.

Unfortunately, *P*LDH has a lower circulating concentration which makes it more difficult to detect, particularly in patients with low parasitemias.[117] To mitigate this, previous work has investigated the use of artificially histidine-enriched antibodies against *P*LDH for in-solution IMAC enrichment of the protein before addition to and LFA for detection.[72] Use of this method resulted in a significant increase in *P*LDH test line signal on commercial LFAs. This method, however, relies on several complicated laboratory-based sample preparation steps that limit its direct use in the field. In this chapter, the previously developed IMAC-functionalized cellulose membrane has been combined with an enrichment method for *P*LDH for integration into a point-of-care diagnostic. This paper-based innovation has the potential to address the shortcomings of the previously developed laboratory-based enrichment method, and to increase the broad-scale utility of field-based malaria diagnostic tools.

Experimental

Materials

Whatman cellulose membranes (described in detail in Chapter 2) were purchased from Cytiva Life Sciences (Marlborough, MA, USA). 19g7 and 1201 anti-pan-malaria

*P*LDH antibodies were purchased from Vista Diagnostics International (Greenbank, WA, USA). 10-P09CS anti-pan-malaria *P*LDH antibodies were purchased from Fitzgerald Industries International (Acton, MA, USA). Recombinant *P. falciparum* LDH and *P. vivax* LDH were purchased from CTK Biotech (Poway, CA, USA). ICT Malaria Dual RDTs were purchased from ICT International (Cape Town, South Africa). Pooled gender human whole blood in citrate phosphate dextrose (CPD) anticoagulant was purchased from BioIVT (Westbury, NY, USA). C-Peg$_6$-H-H-H-H-H-H-Peg$_6$-Biotin (His$_6$-biotin) peptides were synthesized in-house. Dynabeads MyOne Streptavidin T1 magnetic beads were purchased from ThermoFisher Scientific. All other reagents utilized were of reagent grade and sourced from Fisher Scientific, Thermo Fisher, and Sigma Aldrich.

His$_6$ Anti-PLDH Antibody Conjugation

His$_6$-enriched anti-*P*LDH antibodies were used as a capture agent for *P*LDH. The His$_6$-enriched antibodies (HisAb) were conjugated using the protocol outlined by Bauer et al.[72] Briefly, anti-pan-*P*LDH antibodies (either 19g7 or 10-P09CS) were incubated with sulfosuccinimidyl 4-(N-maleimidomethyl)cyclohexane-1-carboxylate (sulfo-SMCC) for 30 minutes before removal of excess sulfo-SMCC using a 7k molecular weight cutoff Zeba desalting column. Following this, the His$_6$-biotin peptides were added and the solution was incubated again for 30 minutes. The HisAbs were then purified again using the same desalting column as in the previous step, diluted to a stock concentration of 2 mg/mL, and stored at -20°C.

BioLayer Interferometry (BLI) Quantification of Membrane-Bound HisAb

BLI quantification experiments were performed on a FortéBio Octet RED96 system (Sartorius AG, Goettingen, Germany). Aliquots of HisAb at 11.26 nM, 22.54 nM, and 112.6 nM were made in PBS. These concentrations correspond to theoretical 5x, 10x, and 50x molar excess of antibody in relation to the molar amount of *P*LDH expected in a 500 µL blood sample parasitized using in-house D6 parasite culture at a parasitemia of 500 p/µL. The HisAb solution was flowed through the Zn-IDA membrane described in Chs. 2 and 3 and both the pre-flowthrough solution and the recovered post-flow filtrate were collected for analysis. All collected samples were added to a black 96-well plate in triplicate with an 8-point serially diluted titration series, 5 µg/mL positive controls and 0 µg/mL negative controls, and analyzed using the Octet RED96 quantification software. HIS2 anti-His-tag octet biosensors were hydrated in an Octet buffer that consisted of: 50 mL 1x PBS, 0.1% BSA, and 0.02% Tween 20 for 600 seconds prior to sampling. The sampling time for the assay was set at 600 seconds.

Immunoassay Quantification of IMAC-Captured and Recovered PLDH

Samples for *P*LDH capture and recovery were created by first adding a 500 µL sample of HisAb directly to the IMAC membrane in the vertical flow membrane holder (Figure 4.1). This aliquot of HisAb was allowed to flow completely through the membrane, functionalizing Zn-IDA ligand with HisAb. The filtrate of this flowthrough was discarded. Following HisAb functionalization of the membrane, a 500 µL sample of D6 *Plasmodium falciparum* (stock parasitemia: 43,600 parasites/µL) spiked PBST or whole blood lysed 1:1 with lysis buffer (phosphate buffer, pH=8, 300 mM NaCl, 2% Triton 100) was added

to the membrane and allowed to flow to completion. The filtrate of this flowthrough was collected for analysis. Then, 500 µL of 100 mM EDTA was added to the membrane and allowed to flow completely through. The filtrate of this step was also recovered for analysis.
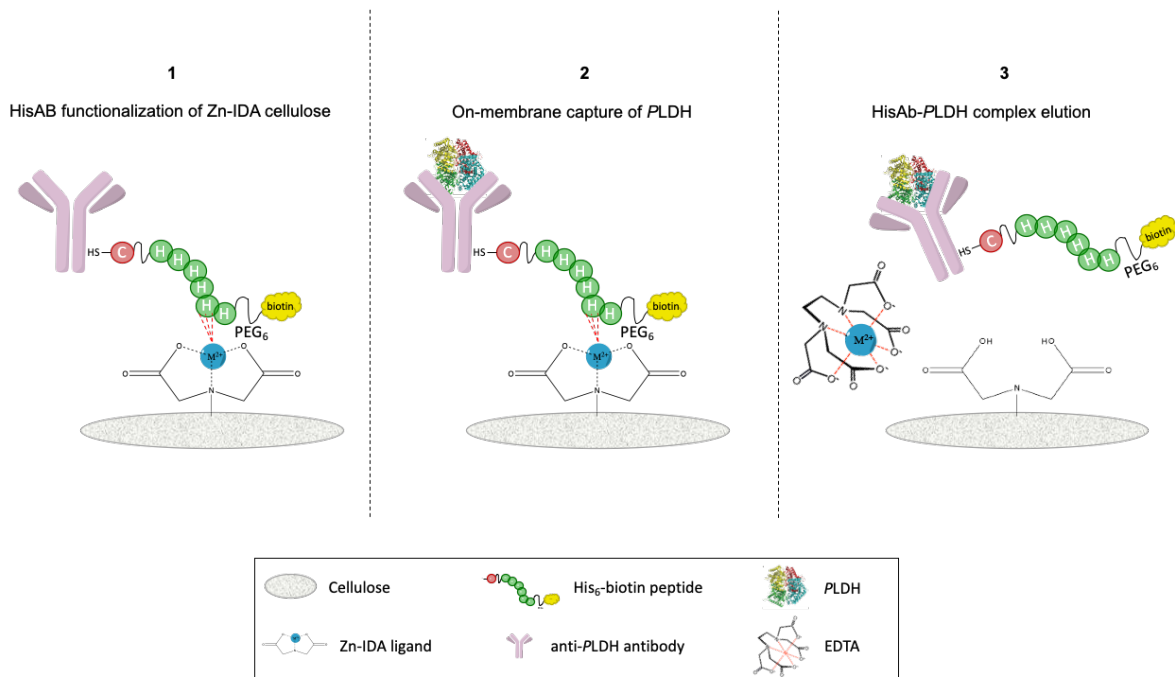
Figure 4.1. Workflow of on-membrane *P*LDH capture and elution. (1) The Zn-IDA membrane was treated with HisAb specific for PLDH. (2) A *P*LDH-containing sample of blood or buffer was added to the membrane. Free *P*LDH within the sample is immobilized on the membrane by the HisAb. (3) The *P*LDH-HisAb complex is eluted from the membrane using EDTA, which complexes the Zn(II), liberating the immobilized HisAb.

*P*LDH capture and recovery on the IMAC membrane were each analyzed using a separate *P*LDH-specific ELISA. To assess capture, free *P*LDH from the first flowthrough of the blood sample was quantified. To do this, first, 100 µL of a 0.5 µg/mL solution of 19g7 anti-*P*LDH capture antibody were added to an Immulon 2HB 96-well plate. The plate

was then sealed with Parafilm and incubated on an orbital shaker for 1 hour. After incubation, the plate was removed and each well was washed 4 times with 275 µL of PBST. Following this wash step, 275 µL of PBST with 5% (w/v) BSA was added to each well. The plate was again sealed and incubated for 2 hours. The plate was then washed 3 times with PBST. After blocking with BSA, 100 µL each of samples, controls, and the titration series were added to the plate. The titration series consisted of an 8-point two-fold serial dilution, from a concentration of 400 p/µL to 0 p/µL (400, 200, 100, 50, 25, 12.5, 6.25, and 0 parasites/µL). All samples, controls, and titration series concentrations were analyzed in triplicate. The plate was incubated for 1 hour. Following sample incubation, the plate was washed 4 times with PBST. 100 µL of a 1 µg/mL solution of 1201 anti-*P*LDH antibody conjugated to horseradish peroxidase (HRPx) was then added to each well of the washed plate and incubated, protected from light, for 1 hour. The plate was then washed 5 times before developing with 100 µL of TMB One solution. The TMB One solution was incubated for 10 minutes on the orbital shaker, sealed and protected from light, before the reaction was quenched with 100 µL of 2 M H_2SO_4. The absorbance values for the quenched reaction were read at 450 nm using a BioTek Synergy H4 microplate reader.

For quantification of protein recovery, a separate ELISA was used that allowed for detection of the eluted HisAb-*P*LDH complex in place of free *P*LDH. This assay was performed in the same manner as described above with minor changes. First, the capture antibody solution consisted of 2 µg/mL of 19g7 anti-*P*LDH antibody and 10-P09CS HisAb was used for detection. For samples not containing already 10-P09CS HisAb, e.g., titration series solutions and positive/negative controls, 100 µL of a 1 µg/mL of 10-P09CS

HisAb antibody solution was added to the sample wells and incubated, protected from light for one hour. Additionally, a strep-HRPx binding step was added following detection antibody addition and prior to TMB One addition. This step consisted of 100 µL of streptavidin:HRPx solution and was allowed to incubate, protected from light, for 1 hour.

Malstat Assay for Quantification of IMAC-Captured and Recovered PLDH

PLDH capture and elution were also analyzed using the Malstat assay[118], which adapted into an on-bead format by Markwalter et al.[115] For this assay, flowthrough samples were made by first flowing 500 µL of a 0.05 mg/mL solution of HisAb through the membrane. The filtrate of this functionalization step was discarded. Next, 500 µL of either tris-buffered saline with 0.05% Tween-20 (TBST) or lysed blood spiked with in-house D6 *Plasmodium falciparum* parasite culture (stock parasitemia: 43,600 parasites/µL) at varying concentrations described below, was flowed through the membrane. The filtrate of this flowthrough step was collected for analysis of PLDH capture. Following capture, 500 µL of 100 mM EDTA was flowed through the membrane to elute the captured HisAb-PLDH complex. This filtrate was collected for analysis of PLDH recovery.

Positive and negative controls and titration series dilutions were incubated with 19g7 HisAb at a final HisAb concentration of 0.05 mg/mL for 30 minutes, to match the concentration of HisAb expected in the flowthrough samples. The titration series consisted of an 8-point two-fold serial dilution, from a concentration of 3,000 p/µL to 0 p/µL (3,000, 1,500, 750, 375, 187.5, 93.75, 46.875 and 0 parasites/µL). All samples, controls, and titration series concentrations were analyzed in triplicate. After incubation, all samples, titration series concentrations, and controls were added to a non-coated

polystyrene 96-well plate with 25 µL of washed streptavidin magnetic beads. The plate was sealed and incubated on an orbital shaker for 30 minutes. After 30 minutes, the beads were isolated on a magnetic rack for 2 minutes and washed 3 times with TBST. After the third wash, the beads were resuspended in 25 µL of TBST. Next, 125 µL of Malstat solution (0.714 M sodium L-lactate, 0.218 M tris(hydroxymethy)aminomethane, and 0.664 mM 3-acetylpyridine adenine dinucleotide in deionized water) and 25 µL of a nitroblue tetrazolium/phenazine ethosulfate (NBT/PES) solution (7.83 mM NBT, 0.957 mM PES diluted in deionized water) were added to each well. The plate was sealed and incubated, protected from light, for 30 minutes. After incubation, the plate was placed on a magnetic rack for 2 minutes to isolate the magnetic beads. The supernatant was separated from the beads in each well and all samples were moved to clean wells. Finally, the absorbance was measured at 580 nm using a BioTek Synergy H4 microplate reader.

IMAC-Membrane Enhancement of Commercial Dual LFA

As a proof-of-concept study, the IMAC membranes were used to enhance commercial dual malaria diagnostics specific for both HRP2 and *P*LDH (ICT Malaria Dual RDT test kit). In this proof-of-concept experiment, the syringe format was utilized for sample preparation. First, 500 µL of a 0.0025 mg/mL HisAb solution was added to a 1 cm diameter circle of IMAC-functionalized membrane. The filtrate of this flowthrough was discarded. Next, 500 µL of parasitized PBS was flowed through the membrane-containing syringe, and the filtrate was similarly discarded. Finally, 500 µL of 100 mM EDTA was added to the syringe, and the solution was collected.

For the eluted fraction to be run on a commercial RDT, it was first concentrated to a traditionally usable volume, using an Amicon Ultra 0.5 mL 10 kDa cutoff centrifugal filter (Millipore Sigma). The eluted samples were added to spin filters and centrifuged for 30 minutes at 14,000 g. The filters were then removed from the centrifuge and inverted, before being centrifuged again for 2 minutes at 1,000 g. The resulting small-volume samples were added to the ICT Dual Malaria RDT following manufacturer protocols and analyzed on a Qiagen ESEQuant LFR. Unenhanced dual RDT LOD analysis was performed using 5 µL aliquots of each sample concentration on each test according to manufacturer instruction. All samples were analyzed in method triplicate.

Results and Discussion

BLI Quantification of HisAb Capture

BLI was utilized to quantify the amount of 10-P09CS HisAb bound to the membrane after samples of the artificially histidine-enriched antibodies were allowed to flow through the Zn-IDA functionalized cellulose. The antibody loading concentrations were chosen to provide a theoretical excess of binding sites for free *P*LDH in a blood sample. For the 10:1 (22.54 nM) and 5:1 (11.26 nM) samples, the resultant binding curve after flowthrough showed no detectable HisAb remaining in solution, whereas at a 50:1 (112.6 nM) ratio, 95.9% of the free HisAb in solution was found to have been bound to the membrane (Figure 4.2), indicating successful immobilization of the His_6 functionalized HisAbs on the Zn-IDA membrane. This result was expected, as the number of His-binding Zn(II) molecules bound to the Zn-IDA membrane outnumber the HisAb by approximately 5 orders of magnitude at the highest concentration evaluated (Chapter 2). Further, given

this excess of available membrane binding sites, the amount of HisAb bound to the membrane could easily be varied to account for more or less free PLDH in a given sample.
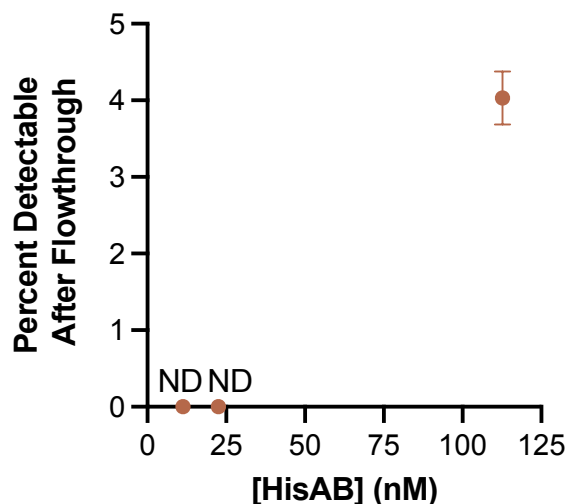
Figure 4.2. Percentage of HisAb in solution after flow through the Zn-IDA functionalized 17 Chr membrane (ND = not detectable).

Immunoassay Analysis of On-Membrane Capture

Following confirmation that the histidine-enriched 10-P09CS HisAb could be successfully bound to the Zn-IDA membranes, the PLDH capture efficiency of immobilized HisAb was investigated by subtraction assay. As concentrations of HisAb added to the membrane were increased, the amount of PLDH captured from solution also increased. A 10-fold increase in HisAb was observed to improve PLDH capture from 52.8% ± 7.6 to 64.8 ± 5.3, and a 100-fold increase in HisAb improved PLDH capture to 78.7% ± 11.2 (Figure 4.3). Increased concentrations of HisAb were not investigated during this particular trial due to reagent constraints. However, in future experiments, the

concentration of HisAb was able to be increased to a maximum of 200-fold due to increased availability.
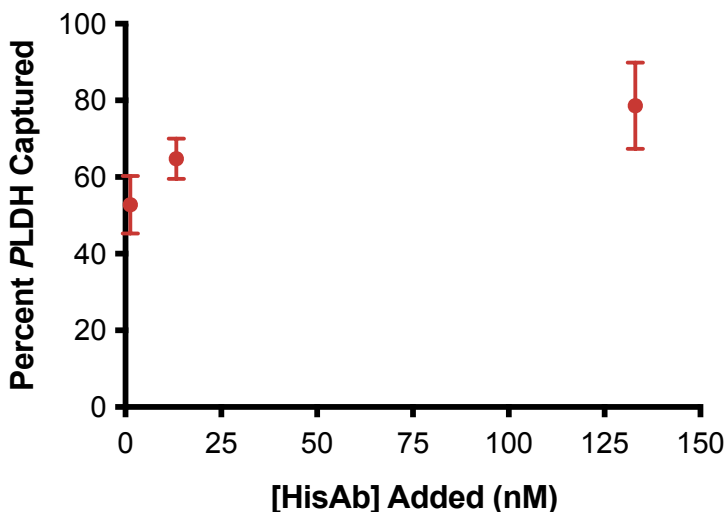
Figure 4.3. Percent of free *P*LDH captured from a parasitized blood sample using Zn-IDA membranes functionalized with increasing concentrations of 10-P09CS HisAb.

Taking into account the high level of HisAb capture on the membrane (Figure 4.2), it can be assumed that there is little to no free HisAb in the recovered capture filtrate. However, it was evident in the eluted fraction that there was significant interference on the ELISA when the 10-P09CS HisAb was present in solution, and the decrease in signal to noise ratio is even more pronounced when the antibody is present in combination with EDTA (Figure 4.4).
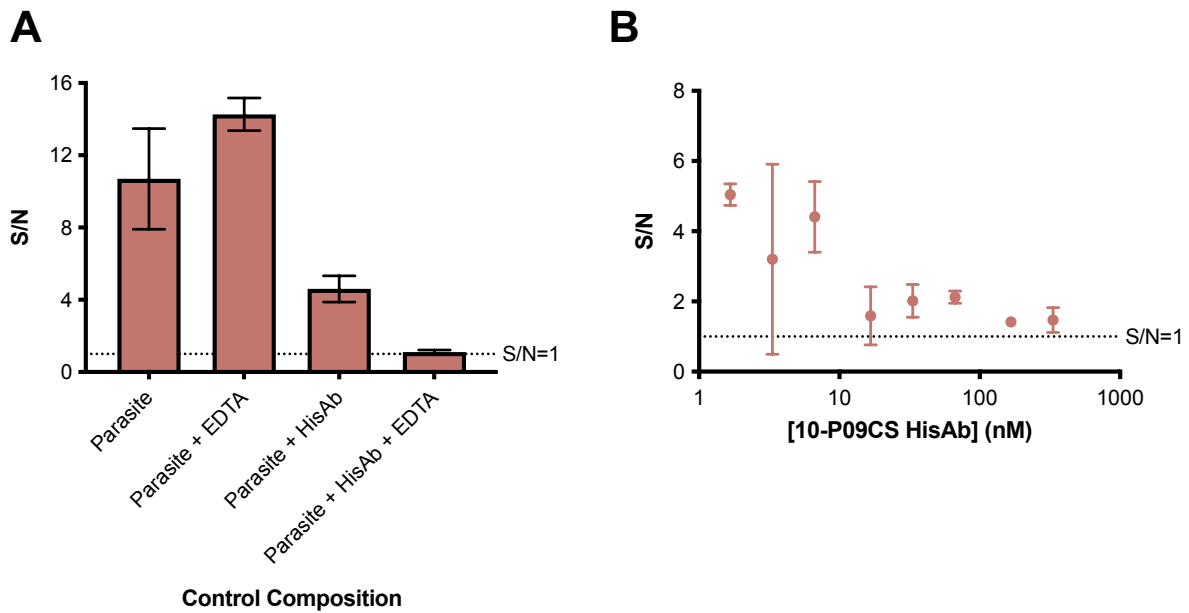
Figure 4.4. Signal-to-noise ratio for (A) samples of different compositions reflecting the different samples being processed, and (B) samples containing parasitized buffer with increasing concentrations of 10-P09CS HisAb.

This interference was unable to be mitigated with assay optimization (e.g., changing blocking buffer reagents, concentrations, detection methods, increasing wash steps), and was evident at most of the concentrations required for sufficient on-membrane capture of *P*LDH. It is believed that there are two possibilities for this interference. First, it is possible that the interference was caused by the overwhelming excess of HisAb in the sample, which was unable to be cleared from the sample wells. In the 10-P09CS ELISA analysis, the HisAb acts as both the on-membrane capture agent, and the in-well detection agent, due to the biotin moiety contained in the His_6 tag. This biotin moiety binds to streptavidin:HRP in the ELISA to generate the downstream colorimetric signal. However, it is also possible that the presence of EDTA caused artificial turnover of the enzymatic substrate. The presence of EDTA in immunoassay samples, as is present in the HisAb-

containing eluent samples, has been documented to alter the results of immunoassays, particularly those reliant on enzymatic turnover for generation of signal.[119–121] Thus, moving forward, the Malstat assay was used to quantify *P*LDH recovery.

Malstat Assay Quantification of Recovered HisAb-PLDH Complex

Previous work in the Wright laboratory indicated that the binding of certain antibody clones (Vista 12g1) prevented the redox reaction on which the Malstat assay relied, while other antibodies (Vista 19g7 and 17e4, Fitzgerald 10-P09DS) allowed the reaction to proceed as normal. Thus, to confirm their utility in this project, both the 10-P09CS HisAb (HisAb1) and a newly functionalized 19g7 HisAb (HisAb2) were tested simultaneously. As shown in Figure 4.5A, the presence of the 10-P09CS hHisAb1 decreased the signal observed on the Malstat assay significantly compared to 19g7. As 19g7 has also been shown to have particularly high affinity for many species of *P*LDH compared to other commercially available antibodies, the 19g7 HisAb2 was selected for analysis moving forward.[122,123]

Following this, the Malstat assay was investigated for interference based on the presence of EDTA in solution (Figure 4.5B). Although there was some variation between the samples containing no EDTA and those that did contain EDTA, there was not a significant difference between the EDTA-containing samples and the samples that contained the HisAb2 alone. This was a promising indication that the presence of both HisAb2 and EDTA in the eluted *P*LDH flowthrough sample would not affect downstream quantification.
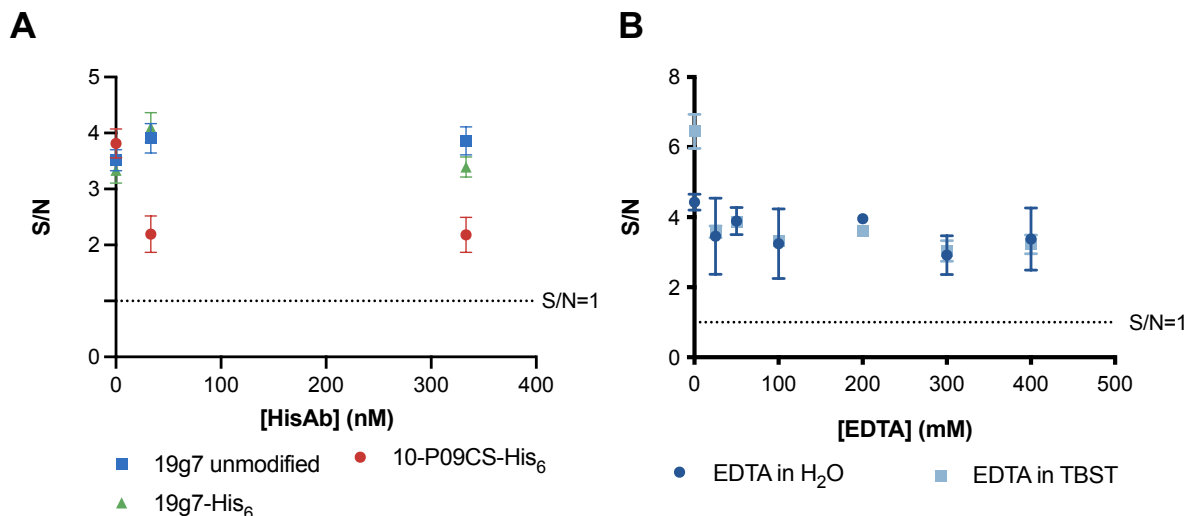
Figure 4.5. Signal-to-noise ratio for (A) the Malstat assay containing increasing concentrations of the 10-P09CS HisAb1, 19g7 HisAb2, and unmodified 19g7 antibodies (shown in previous work not to interfere with Malstat signal) and (B) the Malstat assay with increasing concentrations of EDTA in solution in both deionized water and the Malstat buffer (TBST).

As a result of the ability to quantify samples with both HisAb and EDTA, the Malstat assay was used to quantify the percentage of PLDH that was eluted from the Zn-IDA membrane, using the highest available concentration of HisAb2. In TBST, the percentage of recovered PLDH was found to be 85.4% ± 10, and in lysed blood, the percentage of recovered PLDH was found to be 57.4% ± 26 (p=0.1571) (Figure 4.6). Although there is a slight decrease observed in protein recovery between blood and buffer, this difference is not statistically significant. The increased variation in the blood samples was expected as blood is a vastly more complex matrix than TBST and likely contains interferents not present in a laboratory-derived buffer sample.[124] Despite this, a high proportion of PLDH was recovered from the samples, further indicating the benefits of the IMAC membrane system for enriching complex biomarkers from biologic matrices.
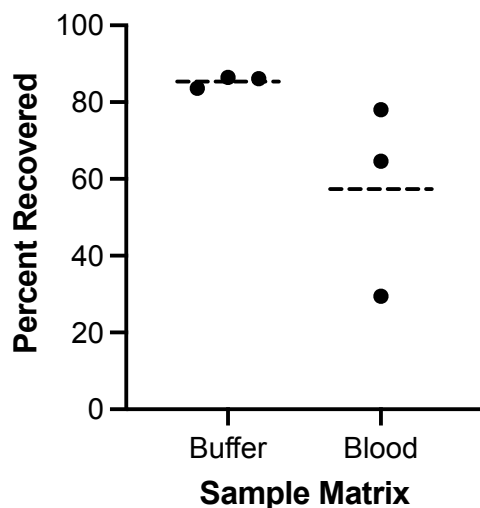
Figure 4.6. The percentage of free *P*LDH recovered from a sample of parasitized Malstat buffer, and from a sample of parasitized lysed blood. The mean of each group is indicated by the dashed line (n=3 for each condition).

IMAC-Membrane Enhancement of a Commercial Dual Malaria RDT

Following the successful confirmation of *P*LDH capture and elution using the previously optimized Zn-IDA membrane, *P*LDH enhancement on a commercial dual malaria biomarker RDT was investigated. With visual inspection, the unenhanced IDT Dual tests were negative until a faint positive HRP2 line appeared at a concentration of 50 p/µL (Figure 4.7A). However, no *P*LDH test line appeared at any concentration of the unenhanced test, including the WHO-standard concentration of 200 p/µL. For the enhanced tests, a faint HRP2 signal was apparent to the naked eye at 12.5 p/µL and the *P*LDH test line became visible at 200 p/µL (Figure 4.7B). This result was confirmed using the LFR: there was a significant increase in signal at the HRP2 test line, as evidenced by the differences in slope of the line of best fit (m) (Figure 4.7C). While the increase in *P*LDH signal was minimal, the increase in slope between the linear portion of the unenhanced

results and the linear portion of the enhanced test line results was significant (p=0.0006) (Figure 4.7D).
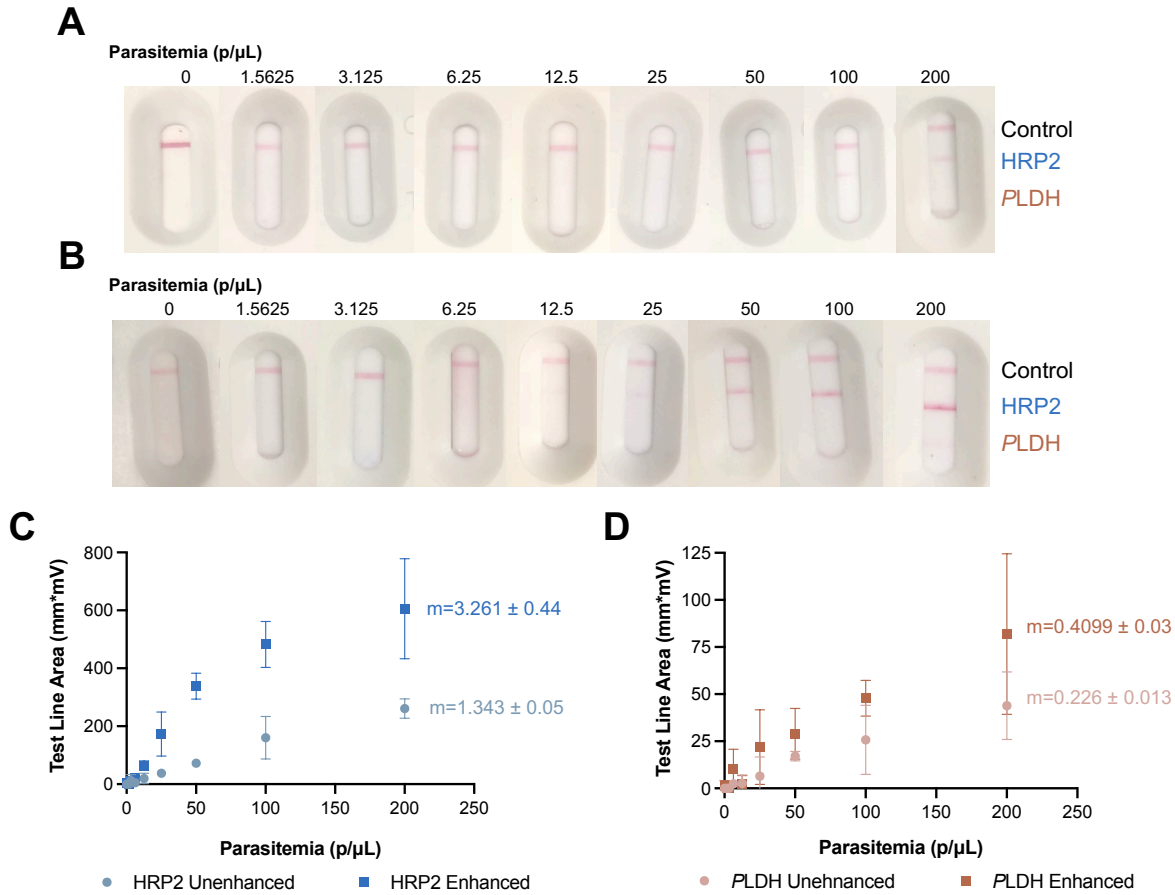
Figure 4.7. Titration series of (A) unenhanced samples and (B) IMAC membrane functionalized-syringe/centrifugation concentrated samples on the ICT Dual Malaria RDT. The comparisons of enhancement at both the (C) HRP2 and (D) *P*LDH test lines (quantified by LFR), with slope of the linear regression for each series (m).

The increases observed in this study were not as high as expected based on the observed results in Ch. 3, likely due to several factors. First, the reliance on both the syringe method of sample collection and centrifugation to achieve a sample volume capable of being tested on a commercial LFA likely led to loss of biomarker. This may

also have led to the increase in variation between the enhanced and unenhanced tests. While the increase in variation was not as pronounced for the HRP2 titration, there was a large increase in variation for PLDH, as shown in Figure 4.7D. Second, in the case of PLDH, it has been previously documented that the presence of the HisAb-PLDH complex likely interferes with signal generation on commercial RDTs, as the orthogonally-binding anti-PLDH antibodies at the test line and on the gold nanoparticle conjugate are blocked from forming the traditional signal generating 'sandwich'.[72]

Limitations and Directions for Future Studies

Preliminary work was performed to investigate the possibility of developing a larger-volume in-house LFA, as was done in Chapter 3. However, the presence of the HisAb creating a 'three-antibody problem' complicated the process (Figure 4.8). The three-antibody problem refers to the idea that orthogonal binding pairs are disrupted by the presence of a third capture antibody, such as the HisAb, through steric hinderance or the occupation of conserved binding epitopes.
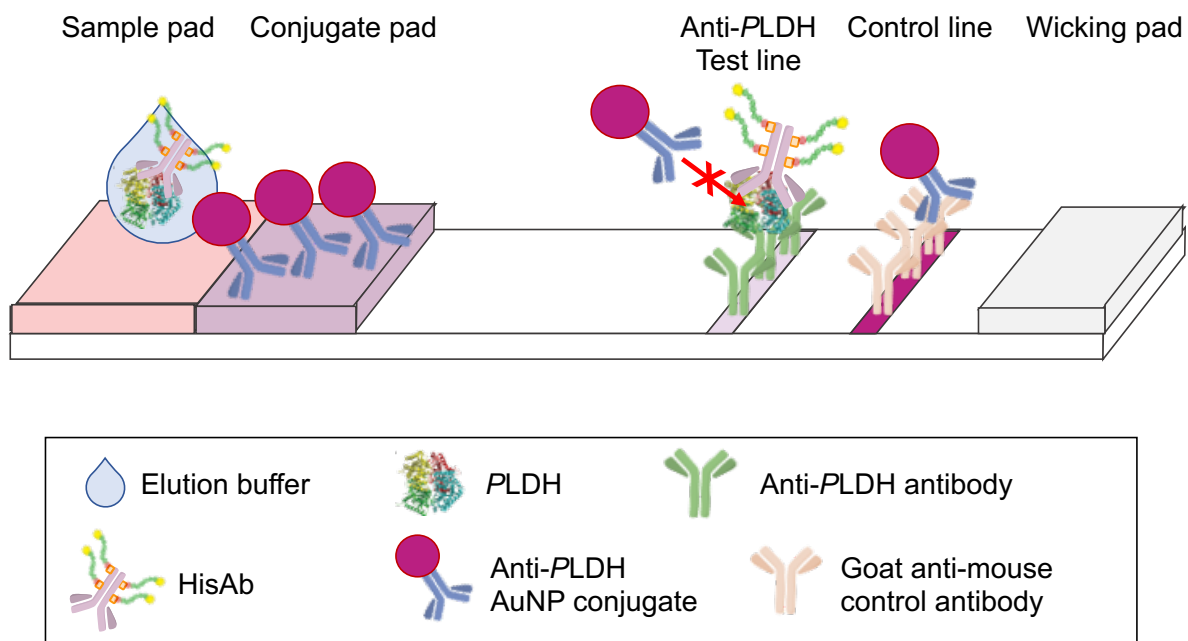
Figure 4.8. Illustration of the 'three-antibody problem' on a typical *P*LDH-specific LFA.

As was shown previously on commercial tests, signal was blocked on all antibody-based test lines for *P*LDH as well as several different iterations of streptavidin test lines. It is likely that an all-antibody-based test like a traditional LFA will not be viable with this method, and future work should concentrate on the development of promising technologies such as aptamer-based capture[125,126] or synthetic *de novo* binding reagents[127]. Additionally, an on-paper Malstat assay, which has been investigated for use at the point of care, may be a further solution to the pressing issue of downstream complex detection.[126] Further, the cost of the antibodies used in this enrichment method is substantial. For each membrane HisAb treatment, the antibody costs $2.50 USD, at laboratory standard pricing. At higher-volume manufacturing costs, this can be driven down to $1.50 per test, which is still likely an insurmountable upcharge for healthcare

workers and patients living in malaria-endemic LMICs. To further pursue this method of test enhancement for non-histidine-rich biomarkers such as *P*LDH, lower-cost alternatives must be investigated, or large-scale manufacturing decisions must be made to further decrease the cost incurred. However, despite these limitations, this method still offers an increase in signal for both HRP2 and PLDH, and has been shown to be an effective means of capture and recovery for non-histidine-rich biomarkers through the use of artificially histidine-enriched monoclonal antibodies.

Conclusion

Overall, cellulose-based IMAC membrane enhancement of non-histidine-rich proteins was shown to be successful, but at a lower proportion compared to the initial success of innate HRP2 enrichment. Artificially histidine-enriched monoclonal antibodies against *P*LDH were used to capture over 80% of the free enzyme in a lysed blood sample on the surface of the cellulose membrane, and a conserved elution strategy was employed to recover high percentages in both buffer and in the complex lysed blood matrix. While this method has shown promise for use in a malaria diagnostic setting, this method could be used for nearly any disease diagnostic for which a molecular recognition element exists. However, future work must focus on resolving the 'three-antibody problem' as well as the steep cost of implementing this specific method before it can be considered ready for broad distribution.

Acknowledgements

CHAPTER 5

DEVELOPMENT AND IMPLEMENTATION OF MOBILE PHONE-BASED

SURVEILLANCE TOOLS FOR MALARIA DIAGNOSIS AND DATA AGGREGATION IN

RURAL ZAMBIA[5]

Introduction

Approximately half of the world's population is at risk of malaria infection, and

current literature proposes that these estimates may be significantly underestimating the

true burden of disease.[58–60] The WHO relies on national and regional programs within

each country of interest to collect and report epidemiologic data and have published

guidelines for operation of these systems.[128] From these guidelines, 'good-quality' malaria

surveillance data is understood to be a data set that contains diagnostic results for every

potential malaria patient, which were obtained by validated microscopy or rapid diagnostic

testing. Additionally, collection of good-quality data ensures that all diagnostic results are

classified correctly, are reported in a complete and consistent manner, and that there is

a mechanism in place to verify or audit the collected data[128]. These recommendations

outline the gold standard for malaria surveillance and data collection.

---

[5] Portions of this chapter have been previously published as:
Moore, C., Scherr, T., Matoba, J. *et al.* mHAT app for automated malaria rapid test result analysis and aggregation: a pilot study. *Malar J.,* **20**, 237 (2021). Reproduced and adapted with permission under the Creative Commons 4.0 open-access license (http://creativecommons.org/licenses/by/4.0/)
and
Scherr, T., Moore, C., *et al.* Evaluating Network Readiness for mHealth Interventions Using the Beacon Mobile Phone App: Application Development and Validation Study. *JMIR mHealth uHealth.,* **8(7)**, e18413, (2020). Reproduced and adapted with permission under the Creative Commons 4.0 open-access license (http://creativecommons.org/licenses/by/4.0/).

Within these guidelines, however, the distinct objectives of disease control and elimination campaigns necessitate disparate approaches for surveillance. Countries whose disease burdens are low are less likely to carry out the universal coverage and testing that defines some malaria control campaigns.[129] In general, as disease prevalence in these countries decreases due to the sweeping interventions and widescale testing that accompany control campaigns, these campaigns become more expensive and unwieldy for detection of single cases or very small pockets of disease. Conversely, elimination programs tend to be characterized by decentralized testing and a focus on individual loci of transmission.[129,130] One popular strategy for this type of program is active case detection (ACD).[131,132] ACD focuses on the detection of individual malaria cases at the community and household level within high-risk populations.[130,133] In Zambia and other LMICs approaching elimination, ACD has manifested in the form of a "test and treat" strategy: febrile patients or at-risk asymptomatic patients are tested for infection and treated accordingly.[130,134,135] However, although effective, a universal test and treat strategy has the potential to be expensive and time-consuming based on the prevalence of disease and the intended length of the program.[136,137] As public health stakeholders push for worldwide elimination, many LMICs are interested in simple, effective, and inexpensive methods for improving the collection and aggregation of surveillance data collected by these programs.

With the current tools, even the most well-equipped health outpost in a high-burden, low-resource setting may struggle to meet the WHO goals for surveillance data. This is particularly true when attempting to implement an infrastructure-heavy intervention such as test and treat. The majority of the available healthcare in LMICs consists primarily

of treatment from community health workers (Level 0).[4,21] To this point, Africa has the lowest average health worker density in the world, with 90 percent of countries reporting below 10 medical doctors per 10,000 people.[138] Thus, while factors like travel and cost can be prohibitive, difficulty in accessing potentially malaria-positive patients with diagnostic tools is also compounded by the lack of available healthcare workers.[139,140]

In the last decade, mobile health (mHealth) has become a popular tool to address the challenges associated with traditional healthcare systems. mHealth is the utilization of mobile communication technology to connect users directly with healthcare services and providers. The effect has been especially powerful in areas underserved by traditional brick-and-mortar medical facilities, like LMICs.[50,141]. This is well-illustrated by a 2013 HIV monitoring program in Mozambique.[142] The Mozambique Ministry of Health implemented web-based data collection for decentralized HIV monitoring in which point-of-care CD4 count devices equipped with wireless capabilities were distributed to health facilities across the country. Using this network, healthcare workers were able to relay surveillance data directly to the Ministry of Health, including number of tests performed each day, any errors encountered, and quality control checks. As the program scaled up, clinic errors were reduced from 13% to 5% and have remained stable, increasing confidence in the reliability and quality of the decentralized testing facilities across the country.

An increasing number of mHealth interventions have followed as a natural consequence of the high penetration of mobile phones into LMICs and subsequent developments in mobile network capacity, which have accelerated over the last two decades (Figure 5.1).[51]
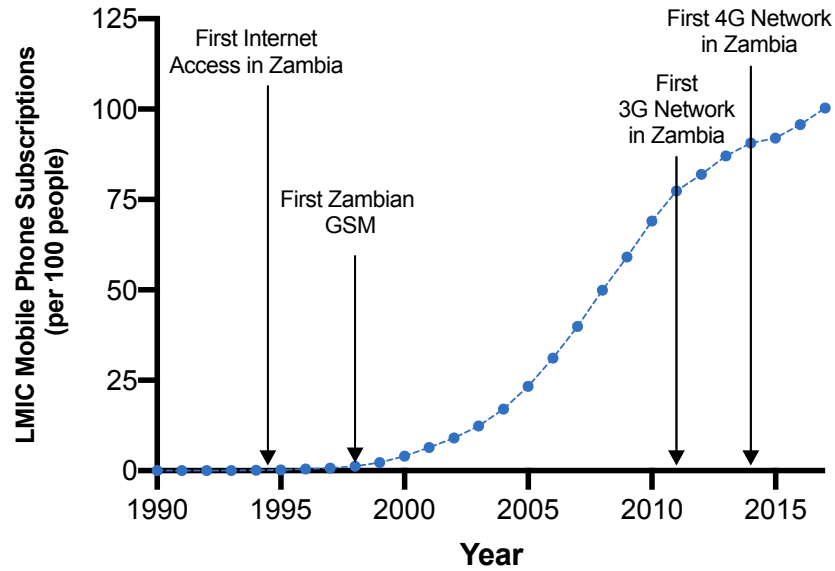
Figure 5.1. The number of mobile phone subscriptions per 100 people in World Bank LMICs from 1990 to 2017. Arrows represent important developments in the telecommunications landscape of Zambia, including: internet access, the introduction of a Global System for Mobile Communication (GSM), and enhanced mobile network additions (e.g. 3G and 4G service).

Studies have already been undertaken to investigate the role of mobile phones in malaria case management.[143–145] Many of these interventions utilize short message service (SMS) messaging to convey reminders regarding drug adherence or report collected data on RDT detection rates. However, there has been little application of mobile phones in analysis and automated data recording and reporting. The challenges involved with developing confidential, accurate, and integrated systems for healthcare information may discourage developers from attempting to go beyond surface-level mHealth interventions, and some currently available applications are hampered by poor sensitivity compared to visual interpretation of tests.[146,147]

Despite the high cell phone penetration into populations that was unimaginable two decades ago, the implementation of new mHealth interventions in some developing

nations has been met with apprehension from key stakeholders and decision makers.[148–151] A major source of this skepticism is the lack of growth from current projects in the field. Concerns over poor connectivity and limitations on accessibility have hampered the success of previous mHealth interventions and these barriers limit pilot projects from developing into sustainable, large-scale programs. In Uganda alone, between 2008 and 2009, 23 mHealth projects did not progress beyond pilot testing.[152,153] The failure of these programs to develop beyond preliminary investigations into widespread, integrated mHealth systems further promotes hesitation, and mobile networks remain an underutilized healthcare resource in LMICs.

Many of these pilot studies fail to move forward because they could not overcome the limitations of working with mobile devices in resource-limited settings. So, while there is network infrastructure in place, even with clear room for improvement, these pilots never succeeded in harnessing that network to produce improved health outcomes. There remains a marked need not only for improved healthcare interventions, but also for tools that could be employed to give uninformed mHealth interventions a more complete understanding of the mobile landscape, particularly in the more remote areas of LMICs where this information is scarce.

Mobile technology is uniquely poised to improve malaria surveillance campaigns. In this chapter, both Beacon, an app designed to evaluate a setting's capacity for basic mobile health interventions, and the mobile health and treat system (mHAT) are presented as solutions to the challenges that elimination campaigns currently face. Beacon is a native mobile platform designed to evaluate a global health setting's infrastructure for readiness to implement mobile health interventions. While there are

several existing methods to measure cellular signal, these technologies are often limited because of a lack of generalizability, inability to differentiate errors, failure to permanently record any data collected, and repeated manual intervention required to initiate data collection. To rigorously document and assess a region's mHealth readiness, it is critical for the ideal tool to be broadly accessible and reliable, and to have automated data recording capabilities. As such, the software was designed to collect spatiotemporal data on cellular network capabilities and mimic certain necessities such as data transmission to and from research databases or electronic medical records.

mHAT is a mobile phone-based web application that utilizes image processing software to automatically detect test lines on commercially available RDTs and provides semi-quantitative results. These results are standardized within the platform and stored in a secure research database (REDCap) for automated downstream analytical surveillance efforts. The mHAT system takes advantage of available healthcare infrastructure through the use of RDTs and community healthcare workers, while also leveraging the ubiquity of mobile phones and their native reporting capabilities for surveillance with improved accuracy and speed. For this pilot study, the data collected using the Beacon and mHAT applications are analyzed to (1) create a granular image of the mobile network surrounding the Macha Research Trust in Macha, Zambia, and (2) compare mHealth interventions to current data collection and surveillance practices in a highly functioning LMIC healthcare setting in Southern Province, Zambia that has had renowned success with active case detection (Figure 5.2).
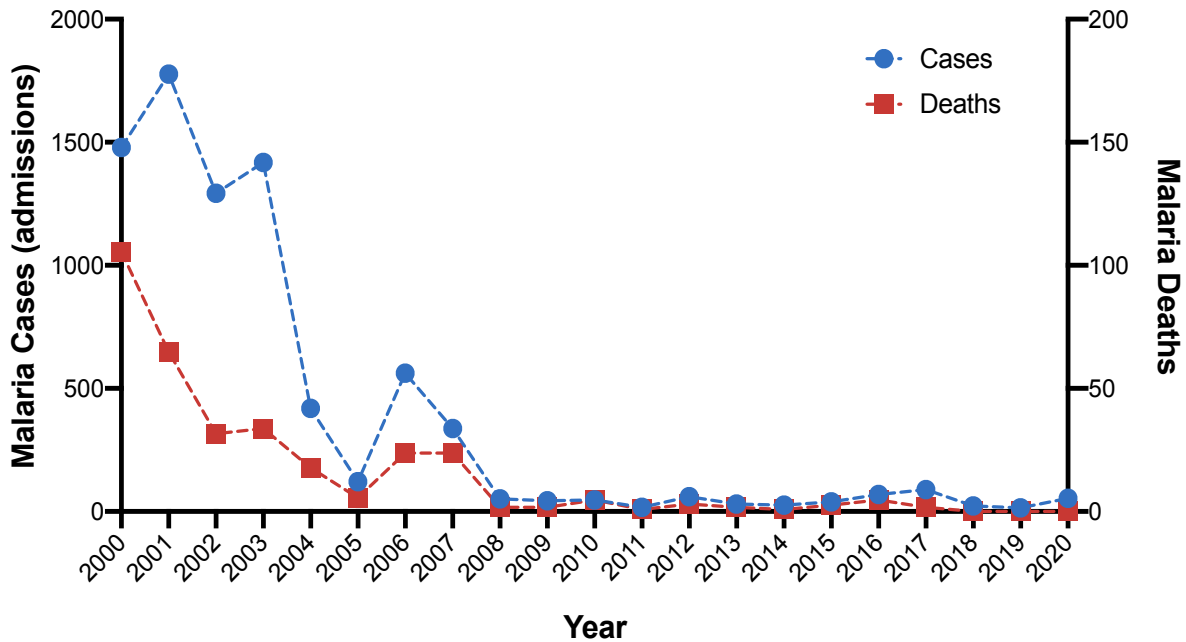
Figure 5.2. Malaria admissions and deaths at the Macha Hospital Children's Ward after the initiation of a test and treat campaign in 2002-2003.

Experimental

Beacon Application

A native mobile application was developed in the Swift programming language, using the XCode Integrated Development Environment, and deployed through the Apple App Store's Beta Testing program, TestFlight. The application has only a main screen for data collection, and a results screen for data transmission. The main view of the app has a simple interface with four components (Figure 5.3A): 1) a "on"/"off" switch that allows the user to start and stop data collection, 2) a slider that allows the user to select a frequency of data collection, 3) a table with the most recent data, and 4) a button to send the user to the Results table where they can transmit their results to REDCap (an electronic research database).[154]

Users can toggle on data collection using the on/off switch, at which point a timer is started with the duration specified by the user-input frequency. When the timer expires, the software asynchronously performs the following events using third party libraries (Alamofire v4.7 and PlainPing v0.4): 1) a timestamp is recorded, 2) GPS coordinates are recorded, 3) a ping is sent to a server at Vanderbilt University, 4) a file is downloaded from the same server to the phone, 5) a file is uploaded from the phone to the server. From these events, the following statistics could be measured or calculated: ping duration, download latency, total download duration, download speed, upload latency, total upload duration, upload speed. For work in remote regions of unknown connectivity, geolocation and timestamp were still recorded in the event that an upload, download, or ping failed. All of the data was entered into a data structure that could be visualized on the results screen. On the results screen, a table displayed an entry for each set of values that was collected (Figure 5.3B). The table row entry showed the timestamp of the data, and a check/x symbol depending on if there were any errors in that row's data entry. At the bottom of the screen, a button ("Check RC Connection") allowed the user to check whether their mobile device was able to connect to REDCap for data transmission. If this connection failed, the user was notified and the user's data remained in storage for a later upload. If a connection could be made, another button ("Send Data to RC") was enabled, which, when clicked, transferred the entire data structure from the app to REDCap. Upon successful data upload to REDCap, the number of data entries uploaded is shown and the data table is cleared.
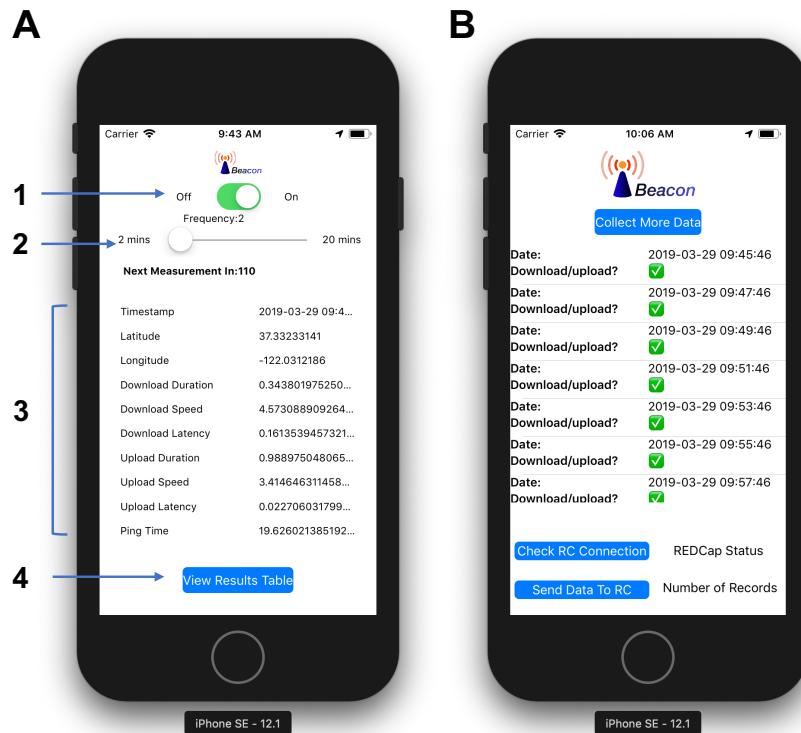
Figure 5.3. The two main screens of the Beacon application: (A) the data collection screen, and (B) the results table and data transmission screen. The main screen features (1) an on-off toggle switch, (2), a collection frequency slider, (3) a table of the most recently collected data, and (4) a button linked to the full results screen.

The software was tested for compatibility on multiple iOS devices, including an iPhone 8 and an iPhone X. The data collection in Macha was performed on multiple iPhone SE (2017) phones, all running iOS 12.1.3. While Apple products are less common globally than they are in the United States, this model has comparable hardware to commonly used mobile devices, including: processor, memory, camera. This makes it a reasonable device for this testing, with the understanding that the software could readily be ported to Android devices, which are more common in LMICs. Data collection was performed on the three primary cellular networks operating in and around Macha, Zambia: Airtel, MTN, Zamtel. While evaluation of a particular carrier's performance is an expected

usage of Beacon in practice, in this work each network was randomly assigned an alphabetical code to explicitly avoid identifying network performance.

Mobile Network Performance Testing

At the onset of data collection, the timer was initiated in the app. Once the timer was toggled on, the mobile device was placed into Guided Access mode. This allows the user to turn off interactions with the screen or device buttons, thus permitting the app to collect data uninterrupted by inadvertent screen taps. The phone or phones running the Beacon app were stored in a backpack connected to a portable charger and data was collected during the course of routine field work in and around the Macha Research Trust between the months of February and August in 2019. Users were provided instructions and documentation on how to use the app, but were not given any other instructions related to data collection frequencies, locations to visit or to avoid, or how often to upload their results to REDCap. Data was downloaded from REDCap for offline statistical analysis.

mHAT Application

The mHAT application is a mobile-friendly, web application hosted on a development server at Vanderbilt University. For the duration of the study, it was accessible in any web browser by its public IP address (now disabled).

mHAT was designed as a web application, hosted by a webserver and running in the browser of a mobile device, rather than a native application that is downloaded and runs locally on the device. This decision was guided by our expected use case, and was

influenced by the broad device compatibility, and the ease and speed with which software updates can be deployed for web applications. The architecture described above can work on any web-connected device (i.e., phones, tables, laptops, desktops) and interchangeably across operating systems. The mHAT app does require network connectivity, but new developments that enable progressive web apps will allow future versions of the software to have similar functionality offline as well.

Computer vision for analysis of rapid diagnostic tests is a substantial endeavor. These algorithms must be tolerant of lighting and background variations, and different camera resolutions. To use the app, users first input any information they would like to associate with this test (e.g., case ID, test ID, any other notes). From within the app, the user presses a button to take a photograph of the RDT they would like to analyze. Prior to taking the photograph, the web app asks to access the user's GPS coordinates to assist with spatial infectious disease surveillance. Preliminary image processing is performed and determines if the photograph must be retaken, or if it is suitable for full analysis. If the preliminary photograph is suitable, a preview image is presented to the user with annotations of key test features. The user has the choice to accept this image and proceed with analysis, or they can elect to take another photograph and restart the process. If the user proceeds with analysis, the full results are presented to the user, including: a qualitative "Positive"/"Negative" as well as the numerical values for test line signal, control signal, and signal ratio. The result is transferred to a custom REDCap (a widely-used, customizable research electronic database)[154–156] project for storage, along with the user that uploaded the test information, the GPS coordinates, and a timestamp. This information facilitates spatio-temporal surveillance, as well as allowing national

healthcare systems to observe the locations of individual community healthcare workers and their teams.

For any new test, computer vision and image processing features must be experimentally optimized. This is a result of the different shapes of cassettes, the colors of the test and control line signals, markings and brandings on the test cassettes, different spatial differences during manufacturing of each test. However, this process is relatively straightforward, and with minimal effort, can enable the use of the software to analyze a variety of tests. This optimization was performed for several malaria tests (including multiplexed tests with multiple test lines), multiple HIV test kits, schistosomiasis test kits, pregnancy and ovulation test kits. Since the algorithm utilizes feature recognition, it has the potential to automatically detect the type of test from the photograph, without additional user input. This would have obvious utility for organizations that heavily rely on point-of-care testing.

Laboratory RDT Image-Processing, Training, and Validation

Initial image-processing optimization was performed using SD Bioline Malaria Ag P.f. tests (Standard Diagnostics, South Korea). D6 *Plasmodium falciparum* parasite was cultured in-house. Human whole blood (pooled, CPD) was purchased from BioIVT. Samples were prepared by spiking whole blood with D6 parasite culture at 5,000 p/μL and diluting serially. A whole blood control with no parasite culture was used as a negative control. These mock specimens were applied to the RDTs, which were run according to manufacturer's instructions. Briefly, a 5 μL sample was added to the specimen well of the test. 4 drops of proprietary running buffer were then added to the diluent well, and the test

was allowed to develop for 15 minutes at room temperature. After 15 minutes, photos were taken in the web-based mHAT application on both an iPhone 8+ (Apple, USA) and Samsung Galaxy J3 (Samsung, South Korea). All tests were analyzed in triplicate. All mHAT results were automatically recorded and stored in a pre-configured REDCap project. Immediately after mobile phone imaging, each test was removed from its plastic casing and the nitrocellulose lateral flow test strips were analyzed on a Qiagen ESEQuant lateral flow reader (QIAGEN Lake Constance GmbH, Stokach, Germany).

RDT Collection and Imaging in Southern Zambia

RDT collection was performed in collaboration with the outpatient clinic (OPC) triage team and the field research team at Macha Research Trust (MRT) (Macha, Zambia), the latter as part of an existing IRB-approved malaria epidemiology study. All patients were first screened by underarm temperature. In the OPC, SD Bioline Malaria Ag *P.f.* tests were performed for all patients presenting with a temperature at or above 37°C. In the field, SD Bioline Malaria Ag *P.f* RDTs were performed for all patients presenting with a fever at or above 38°C. Positive tests were collected by the field team for further laboratory analysis.

Upon completion of an RDT, the administering MRT clinical worker recorded the result in a physical ledger along with patient name age, village, history of travel, weight, blood pressure, pulse, and temperature. This data was not available to the MHAT app team. Once the MRT clinicians had recorded the necessary data for their records, the RDT was then imaged using the mHAT application and the result was recorded and stored in the REDCap database. The number of image re-takes prior to analysis and the

90

binary mHAT result were additionally recorded. The image orientation and photo acceptance features were improved iteratively over the course of this pilot study.

Analysis of Current Data Collection and Aggregation Systems

As one of the leading medical research sites in Southern Zambia, and an active participant in the Zambian malaria elimination effort, MRT has a well-developed system for collection and verification of malaria RDT results. Data collection is performed using a network of clinic-based healthcare workers who summarize recorded data from clinic record legers at the end of each week. Every Monday, one healthcare provider from each clinic aggregates the data from the past 7 days and enters it into an SMS message. This SMS is then sent to a member of the MRT data aggregation team who collates the data from the satellite sites into a single spreadsheet, which is then manually entered into a REDCap project.

Verification of this SMS data is performed quarterly. To verify the data, the verification team travels to each of the satellite clinics and compares reported data to the physical clinic ledger. All changes to the data are recorded on a physical copy of the SMS aggregate spreadsheet, and changes are recorded digitally upon return to the laboratory. The verified and corrected data is then uploaded to REDCap.

Observational analysis of this system was performed by collecting and evaluating the corrected spreadsheets from January 2017-February 2019. The number of corrections was determined by comparing the number of correct (unaltered) data points to the number of corrected (altered) data points for each clinic over time. Date and time data were collected from SMS records between November 2018-February 2019.

Statistical Analysis

Experiments to determine the limit of detection of were performed in triplicate, with the average and standard deviation being calculated at each parasite density. The limit of detection was calculated using $3SD_{blank}$ divided by the slope of the regression of the linear region of the data. Receiver operating characteristic (ROC) curves were generated for both iOS and Android mobile phones using test line signal and test line to control line signal ratio as the dependent variable. Youden's J statistic and the Euclidian distance from the top left corner of the ROC curve were calculated for all systems.

Results and Discussion

Mobile Network Strength in Macha, Zambia

The Beacon app was used to compare the three primary mobile phone carriers operating in or near Macha, Zambia. Figure 5.4 shows the results of this comparison, delineated by the transmission success rate of each individual modality: downloads, uploads, and pings. While Carriers A and B performed with high success (97% and 89% of downloads, and 95% and 84% of uploads completed respectively), Carrier C was observed to complete only 5% of file downloads and 0% of file uploads, despite a high rate of successful pings. These results agree with anecdotal evidence reported by Macha residents. The remaining data shown in this chapter will focus on Carrier Network A, and, as two of the most tangible metrics of cellular network performance, upload and download speed.
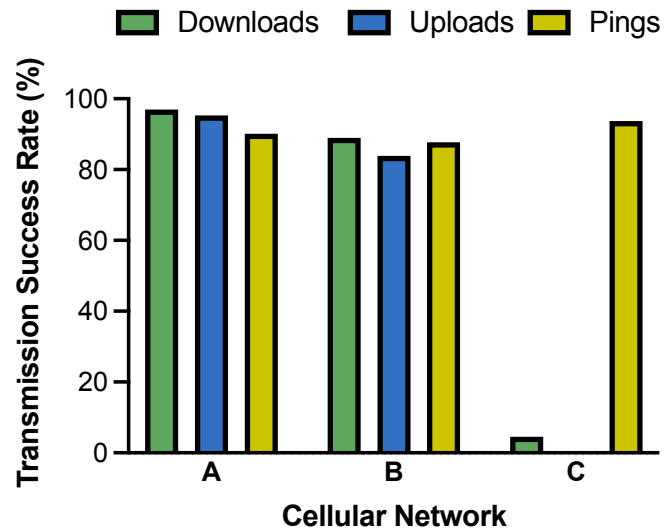
Figure 5.4. Success and error rates of different modalities of data transfer (download, upload, ping) across three different Zambian cellular provider networks.

Data collection was not fixed at a single defined frequency throughout the entire study, resulting in a nonuniform distribution of record counts based on day and time of collection, with the most data collected mid-day and on weekends. As the system was designed, the number of download attempts matched the number of upload attempts. Errors were mostly observed to increase proportionally as total data count increased, thus sampling bias was not observed in these results. However, there was slight disagreement between the number of download errors and the number of upload errors recorded, indicating that success of one mode of transmission did not guarantee success of another.

A distribution of the upload and download durations recorded for successful data transmissions on Carrier A are shown in Figure 5.5. On average, downloads occurred faster and with a narrower range than uploads. To this point, 50% of downloads were

completed in under 8.5 seconds and 75% were completed in under 13 seconds, whereas 50% and 75% of uploads were completed in 21 and 30.5 seconds, respectively; the fastest and slowest downloads occurred in 3.7 seconds and 21.2 seconds, respectively, while the fastest and slowest uploads occurred in 8.4 and 53.8 seconds, respectively. The average download latency is larger than upload latency (1.8 seconds and 0.8, respectively).
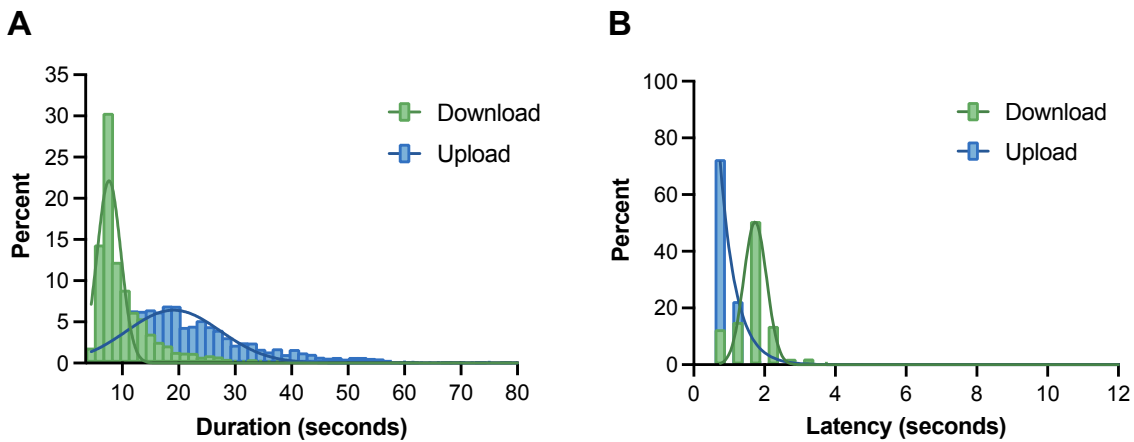
Figure 5.5. Distribution of upload and download (A) duration and (B) latency for mobile Carrier A during the course of the Beacon pilot study.

All data collected using the Beacon app was tagged with both a GPS location and timestamp. As shown in Figure 5.6A, signal strength can be overlaid on a map as a point map with respect to the coordinates from which it was collected. The primary study site for this pilot study was in Macha (a rural village in the Southern Province of Zambia), and the overwhelming majority of the data was collected in and around Macha. However, users were not geographically constrained and data was collected at other sites, including a larger town (Choma, 50 km away) and a larger city (Livingstone, 190 km away). The

durations of successful downloads and uploads are shown as a function of Haversine distance from the Macha Research Trust in Figure 5.6B and 5.6C. While measuring distance away from Macha does not have explicit directionality, and thus by itself can not explicitly confirm location (for instance, a user could have traveled 50 km in the opposite direction and this plot would show the data points next to Choma), confirmation of GPS coordinates shows that the overwhelming majority of data points near 50 km and 190 km away from the Macha Research Trust were collected in Choma and Livingstone, respectively. Near Macha Research Trust, the full range of download and upload durations were observed, while in Choma and Livingstone, the cellular signal was more consistent in general, but still with the occasional outlier. In the regions between these cities, higher numbers of errors were reported, which is likely directly related to the distance from cell towers along the routes traveled, and thus more indirectly related to the lack of densely populated areas between cities.
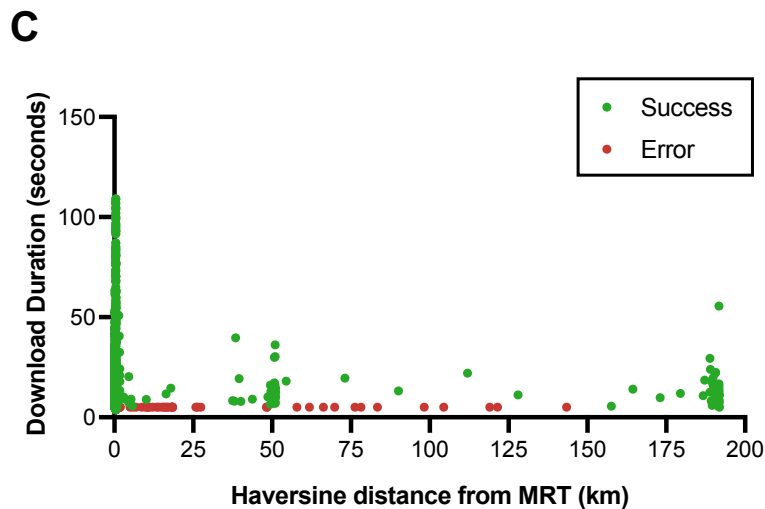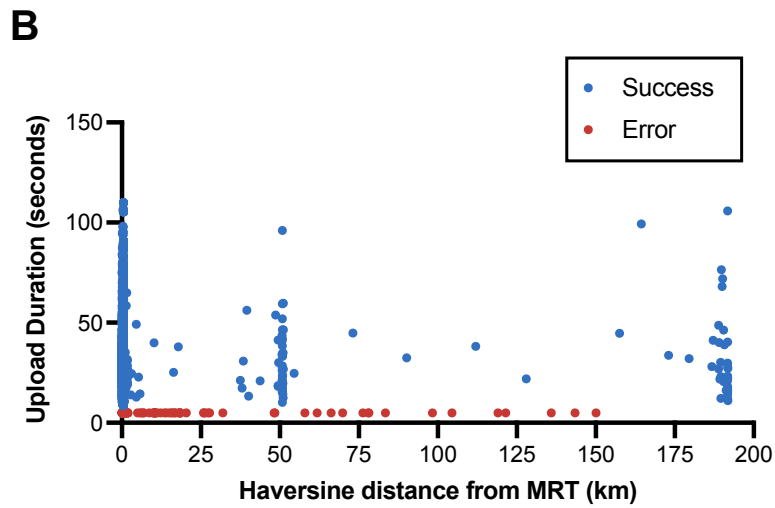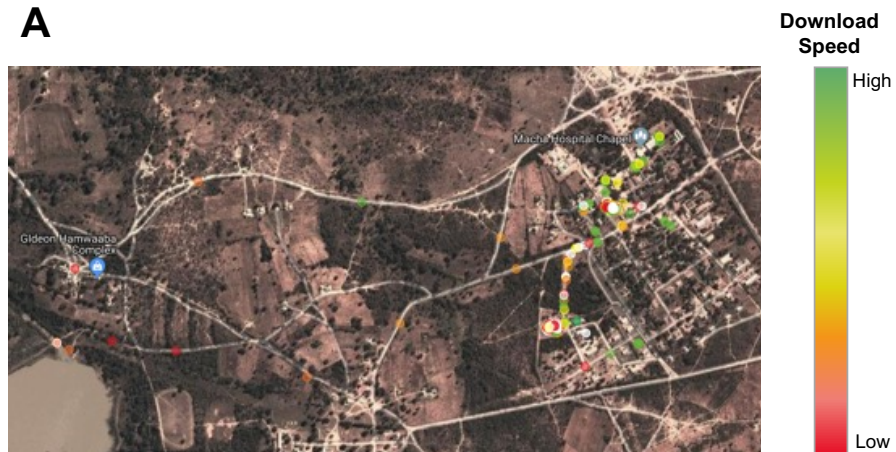
Figure 5.6. (A) Download speed mapped by GPS coordinates around MRT, where download speed is denoted on a scale from green (high) to red (low). (B) Download and (C) upload durations, as well as errors in each mode, as a function of Haversine distance from the Macha Research Trust.

When data was grouped by hour of day (Figure 5.7), download durations appear short early in the morning (from 2am - 5am), followed by an increase from 5am - 8am). They remain roughly constant from 8am-4pm, with a slight decrease at 2pm. Download durations experience a significant increase in the evening hours beginning at 5pm and lasting through 11pm, until they begin to decrease again (12am - 2am). A similar, but slightly less pronounced and noisier trend is observed for upload speed. When the data is grouped by day of the week, download durations are, on average, fastest on Monday (10.8 seconds) and slowest on Tuesday (15.5 seconds); upload durations are, on average, fastest on Sunday (21.8 seconds) and slowest on Friday (31.6 seconds).
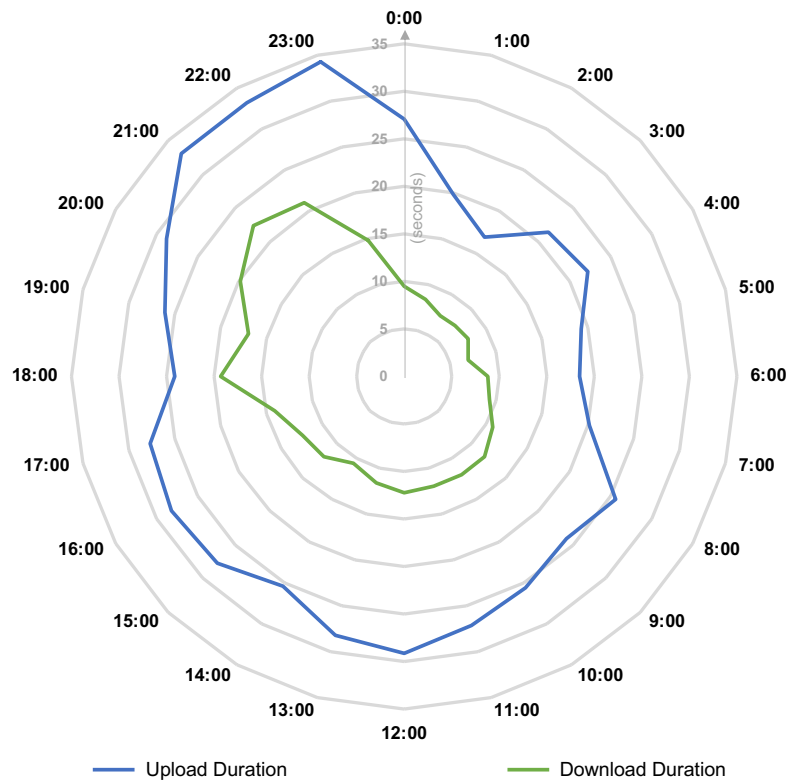
Figure 5.7. Average download and upload durations for each hour of the day.

From this data, it was possible to identify the best-performing cellular network for use in potential mHealth interventions, and in this case, validate the anecdotal experiences of Macha residents. Although significant differences were observed between the available networks, variations in network performance are to be expected in any environment. Network performance is a function of many elements, including but not limited to: number and locations of available cell towers, obstructions between towers (e.g. buildings), cell tower hardware, mobile unit hardware, and current network load at a given time.[157] Many of these factors can be determined before or during testing, and, combined with Beacon verification, can further influence decisions reached by mHealth researchers.

In addition to a comparative evaluation of multiple networks, Beacon was used to quantitatively measure upload and download metrics around the pilot site. From anecdotal experience, download speed in Macha was observed to be faster than upload speed, and this was confirmed during data collection. In most scenarios, this is to be expected, due to the asymmetric design and operation of cellular networks.[158] However, despite increased speed compared to uploads, download latency was observed to be slower than upload latency. This result is counterintuitive in light of the trends observed in total download/upload duration, but may be related to the asymmetry of network configurations. However, overall latency in both directions was fast, and did not exceed the acceptable latency for single-item transfer, which is a positive finding given the physical distance between the mobile phone (Macha, Zambia) and the home server (Vanderbilt University, Nashville, TN).[159]

Even the simple raw data from Beacon can be transformed into more information-dense results, for instance by grouping temporally (by time-of-day and day-of-week). No discernible trend for upload or download speed was observed based on day of the week, however, the hourly data did appear to correlate with times of high human activity in the catchment area. Between approximately midnight and 6:00 am, upload and download durations are at their lowest level, and begin to increase between 6:00 am and 8:00 am. This presumably relates to many people waking and beginning to use their mobile devices. During working hours, this moderate activity remains. This continues until approximately 5:00 pm, when phone-users leave work and more freely engage with their mobile devices. For mHealth interventions, this data is useful, as it provides both an optimal window for any large-volume data transfer or other network activities, and a proxy for when users are on their mobile devices. As a result of this information, an mHealth implementation team may decide to schedule large data backups in the early hours of the morning, when the burden on the local network is low and would thus be more capable of high-capacity use, but that lightweight SMS interventions may be more successful at times of higher network activity.

The spatial resolution of Beacon is also a strength for mHealth researchers planning interventions. Plots of signal strength mapped over topographical or satellite images can help visualize the digital landscape and can be useful to denote strength based on distance from landmarks such as cell towers, hospitals, or airports. This, in turn, can help inform researchers interested in implementing both localized and broadly-spaced interventions. Further collaboration between mHealth researchers, local

99

municipalities, and internet service providers could use this data to inform strategic infrastructure improvements.

As mentioned previously, users were not provided any instruction regarding the frequency of data collection. One of the strengths of the Beacon app is the ability to easily power the app on and off, as well as the ability to adjust the frequency of data collection over a broad range. While high-frequency data collection provides more granular temporal and spatial data, it does come at a higher overall cost. With a small file size and at the minimum collection rate (collection every 20 minutes), Beacon costs less than 30 Kwacha per week, equivalent to approximately $2 USD ; these operating costs would be expected to increase proportionally with higher frequency or larger download/upload file size, but high spatiotemporal data can still be collected for <$100 USD/month. This potential increase in cost experienced by varying these parameters may more closely approximate a site's actual intervention, and therefore may prove to be worthwhile to mHealth investigators when using Beacon-based surveillance. Although sampling bias was not observed during this initial pilot test, the potential for variable sampling frequency to introduce bias into a preliminary study must be noted. For instance, if rolling outages were to occur during a certain time of day in a study location and collection frequency was increased during this time, further analysis of sampling practices may be required to account for the higher volume of signal errors. This requires diligent monitoring and analysis, or, the more straightforward solution, the implementation of a strict data collection frequency that reflects the needs of the planned mHealth intervention. However, for the purposes of this mHealth pilot study, the mobile network surrounding MRT was found to be adequate.

mHAT RDT reader performance validation

The limit of detection for the mHAT application was determined to be comparable to commercial lateral flow readers (Figure 5.8A). For all devices used, signal intensity monotonically increases as the parasite density in the sample increases; at higher concentrations, the rate of increase slows, and the test line signal intensity begins to plateau. Both test line signal and the ratio of test line and control line signal were considered as threshold metrics. Using the test line signal, the limits of detection were found to be 15.0 ± 3 parasites/μL, 14.9 ± 4 parasites/μL, and 6.12 ± 2 parasites/μL using the iPhone 8+, Samsung Galaxy J3, and ESEQuant LFR respectively (Figure 5.8B). The two mobile devices used in this study have substantially different camera hardware (iPhone 8+, 12 MP camera with dual lens; Samsung Galaxy J3, 8 MP camera), and previous work has shown that similar algorithms are also effective when using earlier model devices that have lower resolution cameras.[160] When considering signal ratio (test line signal over control line signal) as the readout measure, the mHAT application limits of detection increased slightly but not significantly (Figure 5.8C). The limits of detection were found to be 23.2 ± 8 parasites/μL and 20.9 ± 6 parasites/μL while the EQEQuant LFR was found to have a limit of detection of 6.15 ± 2 parasites/μL.
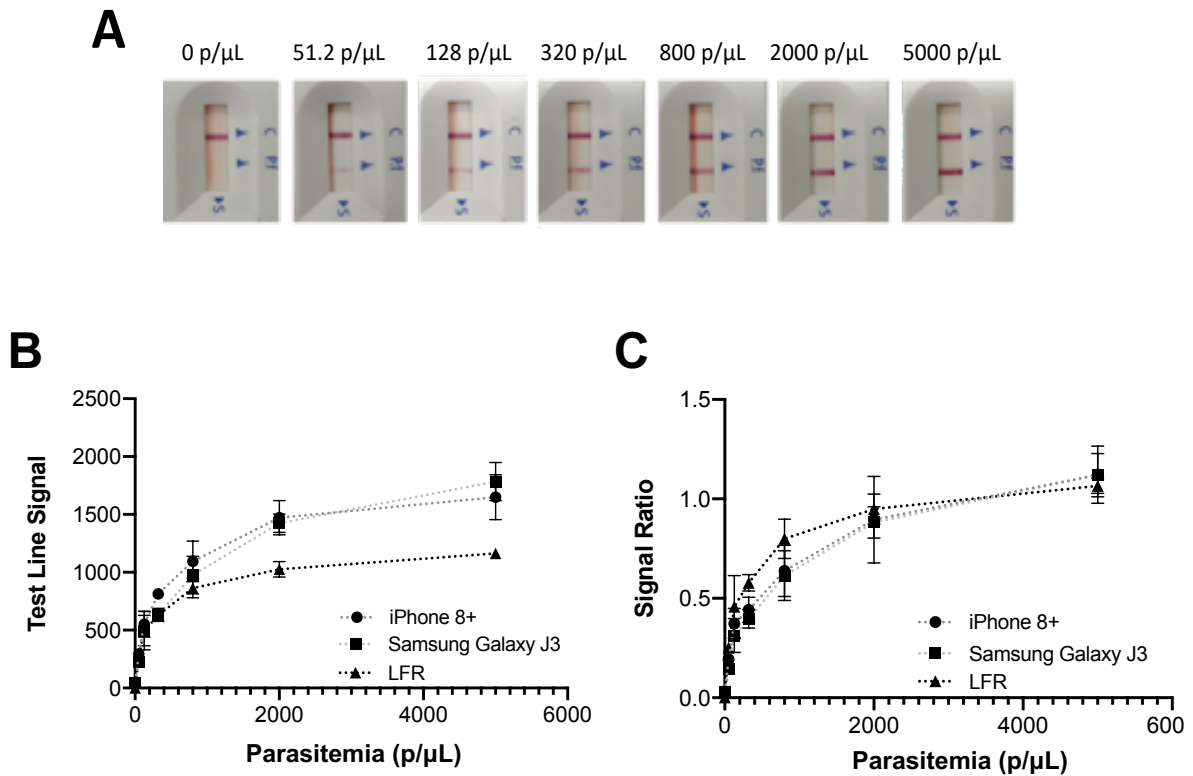
Figure 5.8. iPhone images of the RDT titration series used to determine the mHAT limit of detection (A). Analytical sensitivity for the mHAT application on iOS and Android

mHAT optimization for field performance

A controlled laboratory environment is an idealized setting for a mobile application that uses computer vision to analyze global health rapid diagnostic tests. To mitigate potential errors in photography resulting from an uncontrolled field setting, the app incorporated: 1) an automated checkpoint where the algorithm attempts to automatically determine if a photograph is satisfactory for processing and 2) a manual checkpoint where a user can determine if the photograph should be retaken. In addition, it was anticipated that adjustments to the image-processing algorithms may improve field performance.

102
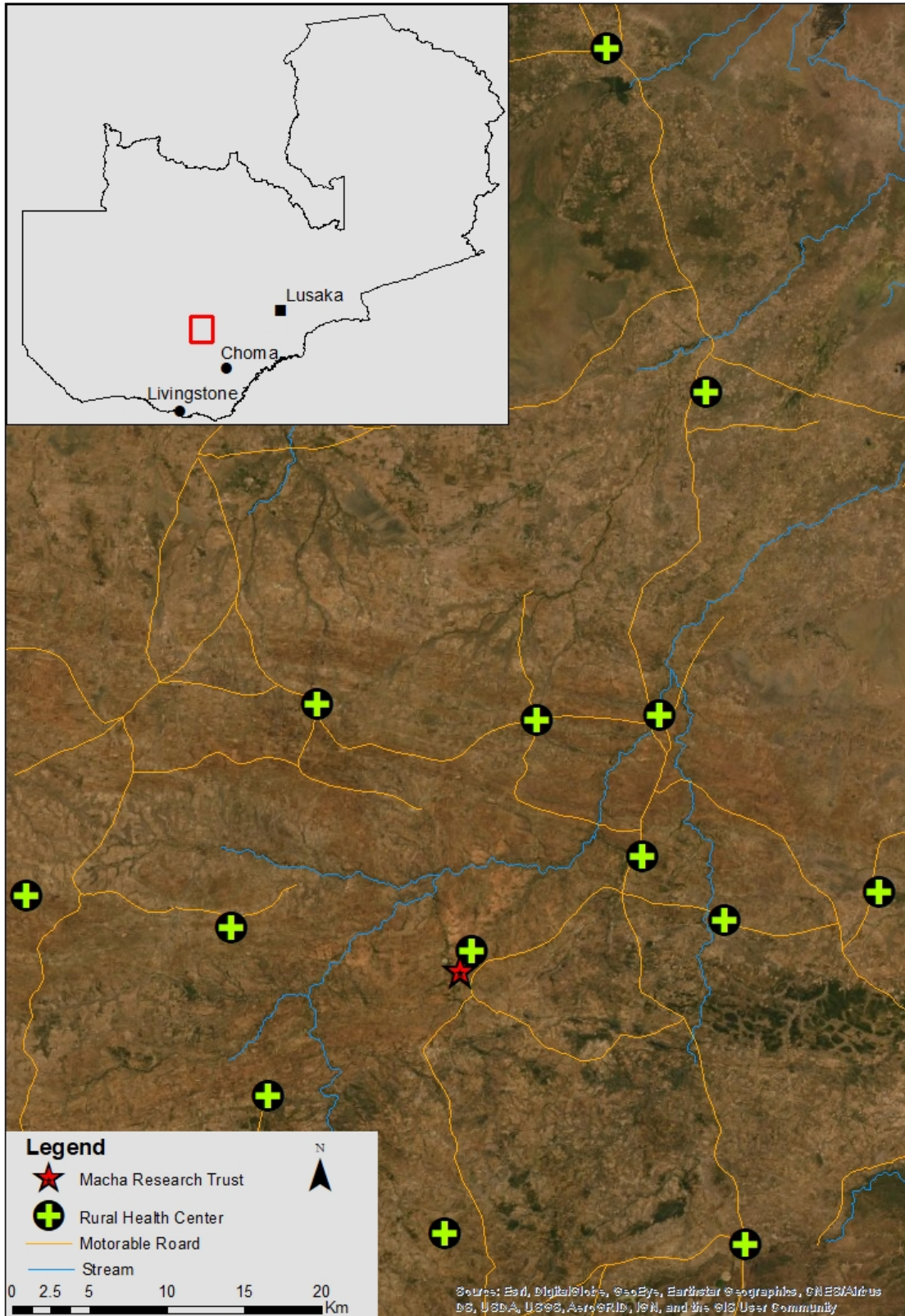
Figure 5.9. Map showing Macha Research Trust (MRT, red star) and each of the 14 rural clinics within the MRT catchment area (green crosses).

Quantification of data reporting and aggregation in active case detection

MRT is an ideal implementation of the WHO guidelines, and they have used ACD to effectively reduce their malaria burden (Figure 5.2). MRT relies on several teams of researchers, physicians, and community healthcare workers to collect surveillance data and provide treatment for the population in and surrounding Macha, using a hub-and-spoke model of satellite clinics. Aggregate surveillance data is validated quarterly by an independent team of MRT researchers, and collected weekly from each of the 14 MRT outposts in the area (Figure 5.9). MRT is not immune to the variety of challenges that arise with data collection in low-resource settings, and this work sought to quantify the impact of these obstacles.

For the 14 spoke clinics, surveillance data is aggregated by mobile messaging. Physical records of malaria RDT data are summarized by community healthcare workers (CHWs) at each clinic and reported by short message service (SMS) every Monday. To assess the temporal efficacy of this system, SMS records were collected spanning the period between November 2018 and February 2019. Of the 96 weeks of data analyzed, only 55.2 percent of the data packages were received on the Monday which it was expected (Figure 5.10A). When data was received late, it was typically received within 1-2 days of when it was expected, but over 25 percent of the time, the report was received over a week late. This could be due to any number of factors, including the number of patients being seen at each clinic, seasonal environmental factors, or weak mobile phone signal.

During this pilot study, the accuracy of reported data was also assessed. Data at MRT is verified by a team of researchers who travel to each clinic quarterly. The verification team examines the physical records kept by the CHWs at each clinic, and counts every entry describing either positive and negative RDT result, noting the date and totaling for each week. This data is then compared to what was reported by SMS. If the tallies are divergent, the verification team resolves the disparity through a record re-count. The final corrected tally is noted in red ink on a physical copy of the collated SMS data. When analyzing physical data from January 2017 to February 2019, it was found that most weekly data packets were reported correctly and required no revision by the verification team; however, 36 percent of the weekly data points did require correction (Figure 5.10B). Of the weeks in which data was corrected, most required at least two data points to be corrected, and almost half required three or more points to be corrected. The most common error observed in this data was incorrect entry, where the counts were correct but correct numbers for two categories (positive RDT, negative RDT) had been exchanged. Approximately 6 percent of the data was not verified at the time of the analysis due to external causes including environmental factors that limit the ability of the verification team to reach clinics, physical damage to clinic records, or lost records.
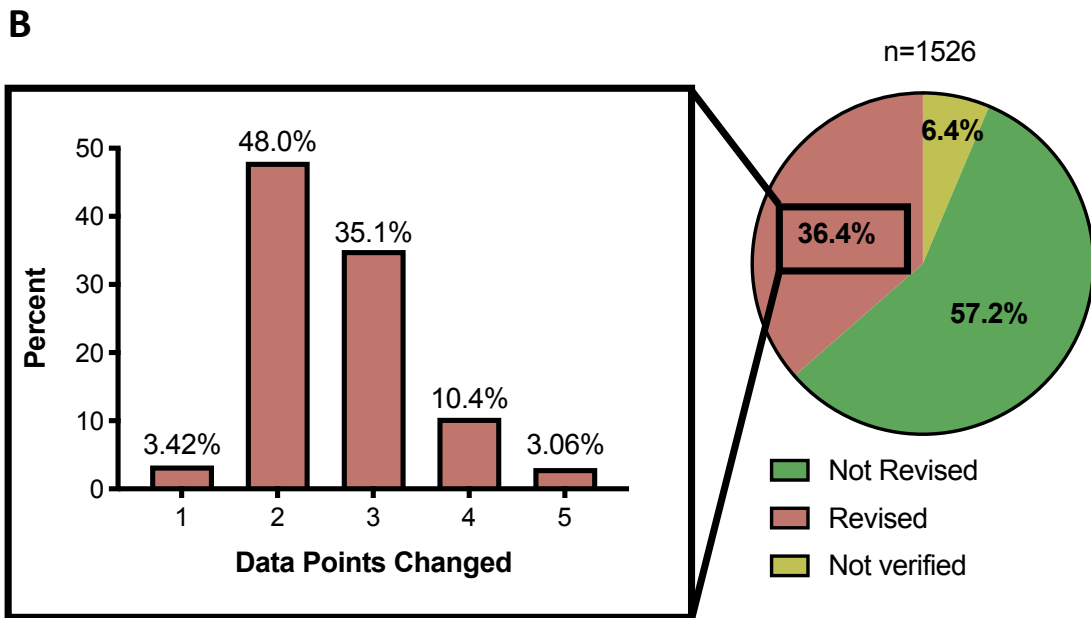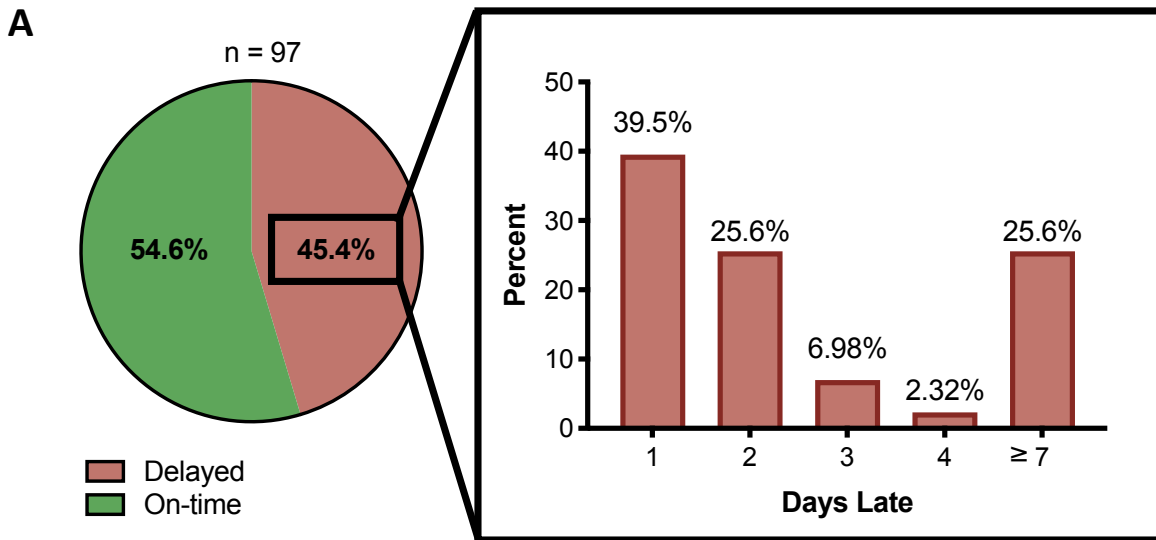
Figure 5.10. (A) Percentage of reported surveillance data that was received after the expected date of arrival. The box to the right shows the histogram of late reports binned by the number of days past the due date at which the data was received. (B) Percentage of recorded surveillance data that was revised upon review by the MRT remote verification team. The box to the left shows the histogram of revised data points binned by the number of data points altered per report.

This pilot study was performed in Macha, Zambia in order to understand how the app could complement existing surveillance campaigns. The Macha Research Trust has had success in decreasing the malaria burden in the region through active and reactive case detection and has implemented the standards set out by the WHO with regard to data collection, reporting, and verification.[134] To ensure reporting data accuracy, MRT has established an independent data validation team, which works to authenticate collected surveillance data on a quarterly basis. It was anecdotally known that data collection before validation was occasionally subject to time delays and misinformation possibly caused by input from multiple disparate healthcare workers or physical damage or loss of records, but this delay had not been previously quantified. While the validation technique used by MRT has proven to be successful, many low-resource settings will not have access to resources of this type and may not be able to validate data with the required level of rigor, leaving their reporting open to delays and inaccuracies.

mHAT application field performance

The most common method for RDT analysis in the field is visual inspection. Although in many locations, CHWs may not be explicitly trained in RDT analysis, the healthcare workers in and around MRT have a high level of familiarity with the tests. Thus, for this study, the mHAT application was compared to visual interpretation of RDTs by these experienced CHWs as a gold standard. All RDTs were identified as positive or negative by a CHW at the point of care, and validated by the researcher using the mHAT application. Iterative improvement of the image analysis software was required over the

span of the trial to account for differences between photo quality in a controlled laboratory setting and the field (Figure 5.11).
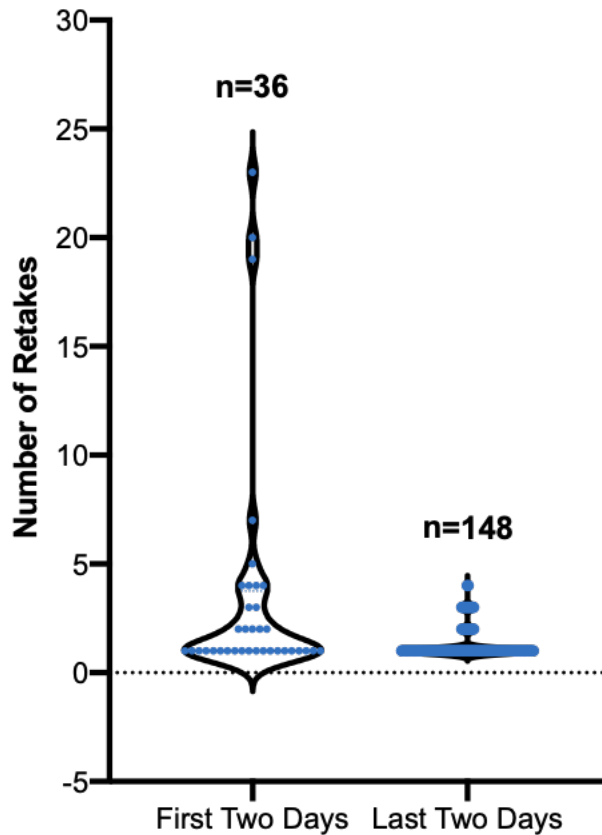
Figure 5.11. Number of photo retakes needed to achieve an mHAT accepted image on any device during the first two days of the field study, and the last two days of the field study. The mean number of retakes needed in the first two days was 3.5 (5.46), compared to 1.3 (0.670) on the final two days of the field trial.

In this analysis, both the signal at the test line and the ratio of test line and control line signal were evaluated as potential readout values and ideal thresholds for each signal metric were determined (Figure 5.12). Both values were assessed on iOS and Android devices.
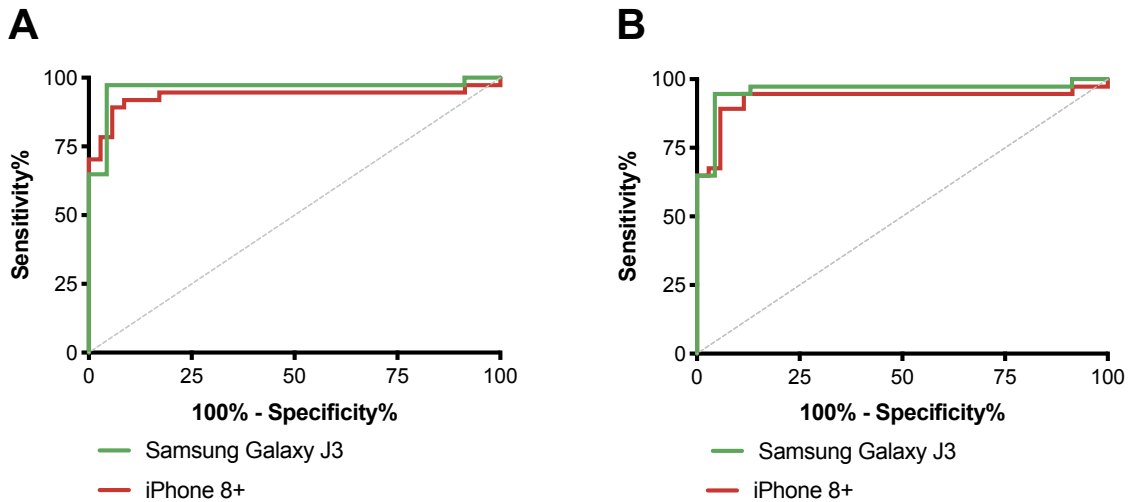
Figure 5.12. Receiver operator characteristic (ROC) curves for the mHAT application using test line signal (A) and test line to control line ratio (B), when compared to visual interpretation of RDTs by an experienced healthcare worker.

When analyzing iOS devices, Youden's J statistic and top left analysis were in agreement with respect to the threshold for signal ratio, which was determined to be 0.283. However, when analyzing test line signal alone, Youden's J statistic and top left analysis were in disagreement: the ideal threshold based on Youden's J statistic was 169.1, whereas the ideal threshold by top left analysis was 106.2. Ultimately, 106.2 was selected as the operating threshold for analysis based on test line signal alone, as it maximized the sensitivity of the application, allowing mHAT users to confidently detect all patients who have a positive RDT result. When analyzing Android devices, Youden's J statistic and top left analysis were in agreement for both test line signal and test to control line signal ratio and the optimal threshold values were found to be 82.35 and 0.222 respectively.

Test line to control line signal ratio was ultimately utilized as the determinant for mHAT test results. While significant batch-to-batch variation between RDTs was not

observed, the decision to use signal ratio as a metric rather than test line signal alone, offers protection from this issue and is supported by the literature.[161] Sensitivity for signal ratio analysis on iOS devices was found to be 94.6 percent (CI: 80, 100) and specificity was 88.6 percent (CI: 70, 100). Using an Android device, sensitivity was 94.6 percent (CI: 80, 100) and specificity was 95.6 percent (CI: 80, 100). When both device types were analyzed, the combined sensitivity was then observed to be 94.6 percent (CI: 80, 100) and specificity was 88.6 percent (CI: 70, 100). Using test line signal alone, sensitivity on iOS devices was found to be 91.9 percent (CI 80, 100) and specificity was found to be 91.4 percent (CI 80, 100). Using an Android device, sensitivity with test line signal was found to be 97.3 percent (CI 90, 100), and specificity 95.6% (CI 80, 100). The combined sensitivity for iOS and Android devices was found to be 91.9% (CI 80, 100) and specificity was 91.4% (CI 80, 100).

Positive predictive value (PPV) and negative predictive value (NPV) for the mHAT application on Android phones were observed to be 0.923 and 0.952 respectively. For iOS hardware, the mHAT application was found to have a PPV of 0.854, and an NPV of 0.935. However, while PPV and NPV are capable of determining the proportion of patients who receive a positive result and who truly have the disease, or the proportion of patients who receive a negative result and are truly disease-free, the positive and negative likelihood ratios are likely a more appropriate metric for determining the utility of the mHAT application. Likelihood ratios express a change in the odds of receiving a diagnosis for patients who test positive or negative using the method of interest. For iOS devices, the positive likelihood ratio was observed to be 5.5, and the negative likelihood ratio was observed to be 0.065. For Android devices, the positive and negative likelihood ratios

were found to be 7.5 and 0.031, respectively. These results indicate a moderate shift in post-test probability for positive patients, and a large shift in post-test probability for negative patients, regardless of device used.

The mHAT app also allowed users to note test defects during analysis. Common test defects included: blood failing to clear from the nitrocellulose membrane (blood clearance), missing control line, physical damage to the test or casing (test defect), or interfering environmental defects. During laboratory analysis, blood clearance was the only observed defect, common to many RDTs which utilize blood as a sample matrix[96] (Figure 5.13). However, during field testing, tests were found to have several defects, including lack of blood clearance, missing test lines, and several test defects such as writing or breakage along the exterior of the plastic casing. The ability to note and record all of these defects in a single database, alongside a picture of the test in question, illustrates a level of transparency in malaria surveillance data that has previously been lacking.
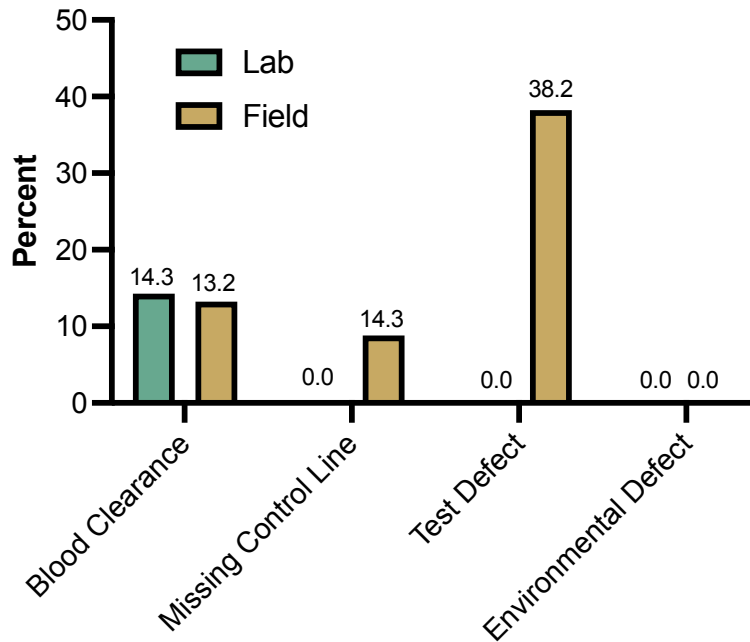
Figure 5.13. Percent of tests that were observed to have each of the 4 mHAT errors: blood failing to clear from the nitrocellulose membrane (blood clearance), missing control line, physical damage to the test or casing (test defect), or interfering environmental defects.

The application is ideal for low-resource uses because it requires minimal training, provides results in seconds[162], and automatically collates data into a single accessible database—without the errors that can arise in manual data recording. In addition to the flexibility mHAT offers, the app has several strengths, including minimal up-front investments in trained personnel or infrastructure, and relatively low operating costs. The app requires no further instrumentation (e.g., readers, dongles, phone attachments) than a camera-enabled smartphone, which, as outlined earlier, can be easily found in many LIMC settings (Figure 5.1). Data use for this app is low, and can cost below $1 US per week.[162] However, the main limitation of the current version of the mHAT software is that it does require a consistent internet connection, which may not be available in all settings where RDT analysis is performed. In order to address this shortcoming, both mobile and

web-based applications capable of offline operations and asynchronous data transfer are being developed for use in instances where dependable internet access cannot be maintained.

Conclusion

mHealth interventions, even without continuous connectivity, have genuine potential to improve global health outcomes. Although many countries have high mobile phone penetration, not all locations are capable of supporting mHealth. The lack of infrastructure and high costs may be prohibitive, but proper planning and tailoring of these interventions based on the infrastructure available greatly increases the likelihood of success. The small cost of piloting a short signal mapping study, such as was included in the above work, would be negligible compared to blind implementation of an intervention that is destined to fail. The Beacon mobile app represents a valuable mobile health tool that can assist in determining a site's readiness for mHealth interventions. By combining temporal and spatial tags with measurements of cellular signal strength, researchers are able to better understand the digital landscape around their potential intervention site. In this chapter, the Beacon app was used to probe the area around MRT to determine the capacity of the surrounding mobile network to support the mHAT mobile intervention.

Although the focus in this effort centered on the accuracy of the results generated by the mHAT application, and the comparison to traditional surveillance reporting systems, there are many additional features that make mHAT a complete surveillance tool. These features include: healthcare worker training guides, case maps, timelines, calendars, a user hierarchy which allows for delineation of privileges, administrator

access and an administrator dashboard for user monitoring, and secure authentication, transmission, and storage of data. Combined, these features represent a rapid, fully functional, user-friendly mobile healthcare experience. The targeted use-case for this application was for low-resource disease surveillance. However, with little additional effort, it could have immediate relevance to the current COVID-19 pandemic which has resulted in dozens of rapid diagnostic tests receiving Emergency Authorization Use status from the US Food & Drug Administration. This further underscores the importance of support for global health initiatives and their ability to drive innovation that can have unexpected positive impacts, even in domestic settings.

REFERENCES

1. World Health Organization. World health statistics 2020: Monitoring health for the SDGs, sustainable development goals. WHO, Geneva, Switzerland; 2020.
2. Stevens, P. Diseases of poverty and the 10/90 Gap. International Policy Network, London, United Kingdom; 2004.
3. World Health Organization. WHO Medicines Strategy: Countries at the Core (2004-2007). WHO, Geneva, Switzerland; 2004.
4. World Health Organization. Tracking Universal Health Coverage: 2017 Global Monitoring Report. WHO, Geneva, Switzerland; 2017.
5. Kruk, M. E. *et al.* Mortality due to low-quality health systems in the universal health coverage era: a systematic analysis of amenable deaths in 137 countries. *Lancet.* **392**, 2203–2212 (2018).
6. Roser, M. & Ritchie, H. Malaria. *Our World in Data.* (2019).
7. Egbendewe-Mondzozo, A., Musumba, M., McCarl, B. A. & Wu, X. Climate Change and Vector-borne Diseases: An Economic Impact Analysis of Malaria in Africa. *Int J Environ Res Public Health,* **8**, 913–930 (2011).
8. World Health Organization. World Malaria Report 2020: Years of Global Progress and Challenges. WHO, Geneva, Switzerland; 2020.
9. World Health Organization. World malaria report: 2016. WHO, Geneva, Switzerland; 2016.
10. Worrall, E., Basu, S. & Hanson, K. Is malaria a disease of poverty? A review of the literature. *Trop Med Int Health,* **10**, 1047–1059 (2005).
11. Datoo, M. S. *et al.* Efficacy of a low-dose candidate malaria vaccine, R21 in adjuvant Matrix-M, with seasonal administration to children in Burkina Faso: a randomised controlled trial. *Lancet*, S0140673621009430, (2021).
12. Eisele, T. P., Larsen, D. & Steketee, R. W. Protective efficacy of interventions for preventing malaria mortality in children in Plasmodium falciparum endemic areas. *Int J Epidemiol,* **39**, i88–i101 (2010).
13. Wilson, A. L. and IPTc Taskforce. A Systematic Review and Meta-Analysis of the Efficacy and Safety of Intermittent Preventive Treatment of Malaria in Children (IPTc). *PLOS ONE* **6**, e16976 (2011).
14. World Health Organization. Treating malaria. WHO, Geneva, Switzerland; 2021. https://www.who.int/activities/treating-malaria.
15. Institute of Medicine. *Saving Lives, Buying Time: Economics of Malaria Drugs in an Age of Resistance*. National Academies Press, Washington, DC; 2004.
16. Shibeshi, M. A., Kifle, Z. D. & Atnafie, S. A. Antimalarial Drug Resistance; Novel Targets for Antimalarial Drug Discovery. *Infect Drug Resist,* **13**, 4047–4060 (2020).
17. Rogerson, S. J. *et al.* Identifying and combating the impacts of COVID-19 on malaria. *BMC Medicine* **18**, 239 (2020).
18. Boseley, S. Demand for coronavirus tests raises concerns over HIV and malaria. *the Guardian* (2020). http://www.theguardian.com/world/2020/may/01/demand-for-coronavirus-tests-raises-concerns-over-hiv-and-malaria
19. Raman, J. Why malaria treatment shouldn't take a back seat to COVID-19. *The Conversation* (2020). http://theconversation.com/why-malaria-treatment-shouldnt-take-a-back-seat-to-covid-19-138444.

20. Khan, M. S. & Hashmani, F. N. Political and technical barriers to improving quality of health care. *Lancet,* **392**, 2146–2147 (2018).
21. World Health Organization. World Health Organization Model List of Essential In Vitro Diagnostics. WHO, Geneva, Switzerland; 2018.
22. Jacobs, B., Ir, P., Bigdeli, M., Annear, P. L. & Van Damme, W. Addressing access barriers to health services: an analytical framework for selecting appropriate interventions in low-income Asian countries. *Health Policy and Planning* **27**, 288–300 (2012).
23. Peeling, R. W. Testing for sexually transmitted infections: a brave new world? *Sex Transm Infect,* **82**, 425–430 (2006).
24. Land, K. J., Boeras, D. I., Chen, X.-S., Ramsay, A. R. & Peeling, R. W. REASSURED diagnostics to inform disease control strategies, strengthen health systems and improve patient outcomes. *Nat Microbiol* **4**, 46–54 (2019).
25. Markwalter, C. F., Kantor, A. G., Moore, C. P., Richardson, K. A. & Wright, D. W. Inorganic Complexes and Metal-Based Nanomaterials for Infectious Disease Diagnostics. *Chem Rev,* **119**, 1456–1518 (2019).
26. Hawkes, M. & Kain, K. C. Advances in malaria diagnosis. *Expert Rev Anti-Infect Ther,* **5**, 485–495 (2007).
27. Ragavan, K. V., Kumar, S., Swaraj, S. & Neethirajan, S. Advances in biosensors and optical assays for diagnosis and detection of malaria. *Biosens Bioelectron,* **105**, 188–210 (2018).
28. World Health Organization. *World malaria report 2017.* WHO, Geneva, Switzerland; 2017.
29. Laishram, D. D. *et al.* The complexities of malaria disease manifestations with a focus on asymptomatic malaria. *Malar J,* **11**, 29 (2012).
30. Green, M.R., Sambrook, J. Polymerase Chain Reaction (PCR).*Cold Spring Harb Protoc*, **6**, (2019).
31. Johnston, S. P. *et al.* PCR as a Confirmatory Technique for Laboratory Diagnosis of Malaria. *J Clin Microbiol* **44**, 1087–1089 (2006).
32. Hänscheid, T. & Grobusch, M. P. How useful is PCR in the diagnosis of malaria? *Trends Parasitol,* **18**, 395–398 (2002).
33. Omo-Aghoja, L. O., Abe, E., Feyi-Waboso, P. & Okonofua, F. E. The challenges of diagnosis and treatment of malaria in pregnancy in low resource settings. *Acta Obstet Gynecol Scand,* **87**, 693–696 (2008).
34. Canier, L. *et al.* An innovative tool for moving malaria PCR detection of parasite reservoir into the field. *Malar J,* **12**, 405 (2013).
35. Okell, L. C., Ghani, A. C., Lyons, E. & Drakeley, C. J. Submicroscopic Infection in *Plasmodium falciparum* –Endemic Populations: A Systematic Review and Meta-Analysis. *J Infect Dis,* **200**, 1509–1517 (2009).
36. Murray, C. K., Gasser, R. A., Magill, A. J. & Miller, R. S. Update on rapid diagnostic testing for malaria. *Clin Microbiol Rev,* **21**, (2008).
37. Slater, H. C. *et al.* Assessing the impact of next-generation rapid diagnostic tests on Plasmodium falciparum malaria elimination strategies. *Nature,* **528**, S94–S101 (2015).

38. Bell, D., Fleurent, A. E., Hegg, M. C., Boomgard, J. D. & McConnico, C. C. Development of new malaria diagnostics: matching performance and need. *Malar J,* **15**, 406, s12936-016-1454–8 (2016).

39. Ochola, L., Vounatsou, P., Smith, T., Mabaso, M. & Newton, C. The reliability of diagnostic techniques in the diagnosis and management of malaria in the absence of a gold standard. *Lancet Infect Dis,* **6**, 582–588 (2006).

40. McMorrow, M. L., Aidoo, M. & Kachur, S. P. Malaria rapid diagnostic tests in elimination settings—can they find the last parasite? *Clin Microbiol Infect,* **17**, 1624–1631 (2011).

41. Mukkala, A. N. *et al.* An Update on Malaria Rapid Diagnostic Tests. *Curr Infect Dis Rep,* **20**, (2018).

42. Makler, M. T. & Piper, R. C. Rapid malaria tests: where do we go after 20 years? *Am J Trop Med Hyg,* **81**, (2009).

43. Wilson, M. L. Malaria Rapid Diagnostic Tests. *Clin Infect Dis,* **54**, 1637–1641 (2012).

44. Geertruida A. Posthuma-Trumpie & Aart van Amerongen*. Lateral Flow Assays. in *Antibodies Applications and New Developments* 175–183 (Bentham Science Publishers, 2012).

45. World Health Organization. Malaria rapid diagnostic test performance: Results of WHO product testing of malaria RDTs: round 1-7 (2008-2016). WHO, Geneva, Switzerland, 2017.

46. Amoah, A. S. *et al.* Sensitive diagnostic tools and targeted drug administration strategies are needed to eliminate schistosomiasis. *Lancet Infect Dis,* **20**, e165–e172 (2020).

47. World Health Organization. World Malaria Report 2018. WHO, Geneva, Switzerland, 2018.

48. Kayyali, R. *et al.* Awareness and Use of mHealth Apps: A Study from England. *Pharmacy,* **5**, 33 (2017).

49. Shapiro-Mathews, E. & Barton, A. J. Using the Patient Engagement Framework to Develop an Institutional Mobile Health Strategy: *Clin Nurse Spec,* **27**, 221–223 (2013).

50. Steinhubl, S. R., Muse, E. D. & Topol, E. J. Can Mobile Health Technologies Transform Health Care? *JAMA* **310**, 2395 (2013).

51. International Telecommunication Union. Mobile cellular subscriptions (per 100 people). *World Telecommunication/ICT Development Report and database.* https://data.worldbank.org/indicator/IT.CEL.SETS.P2.

52. Portulans Institute. The Networked Readiness Index 2020: Accelerating Digital Transformation in a post-COVID Global Economy. Washington, DC, USA; 2020.

53. Elliott, R. Mobile Phone Penetration Throughout Sub-Saharan Africa. *GeoPoll* (2019). https://www.geopoll.com/blog/mobile-phone-penetration-africa/

54. Global System for Mobile Communications Association. The State of Mobile Internet Connectivity 2020. London, United Kingdom; 2020.

55. Bloomfield, G. S. *et al.* Mobile health for non-communicable diseases in Sub-Saharan Africa: a systematic review of the literature and strategic framework for research. *Glob Health,* **10**, 49 (2014).

56. Long, L.A., Pariyo, G. & Kallander, K. Digital Technologies for Health Workforce Development in Low- and Middle-Income Countries: A Scoping Review. *Glob Health Sci Pract,* **6**, S41–S48 (2018).

57. Agarwal, S., Perry, H. B., Long, L.-A. & Labrique, A. B. Evidence on feasibility and effective use of mHealth strategies by frontline health workers in developing countries: systematic review. *Trop Med Int Health,* **20**, 1003–1014 (2015).

58. World Health Organization. World malaria report 2019. WHO, Geneva, Switzerland; 2019.

59. Alonso, P. & Noor, A. M. The global fight against malaria is at crossroads. *Lance,t* **390**, 2532–2534 (2017).

60. The Lancet. Malaria: control vs elimination vs eradication. *Lancet,* **378**, 1117 (2011).

61. Everson, R. J. & Parker, H. E. Zinc binding and synthesis of eight-hydroxy-quinoline-agarose. *Bioinorg Chem,* **4**, 15–20 (1974).

62. Porath, J. & Olin, B. Immobilized metal affinity adsorption and immobilized metal affinity chromatography of biomaterials. Serum protein affinities for gel-immobilized iron and nickel ions. *Biochemistry,* **22**, 1621–1630 (1983).

63. Porath, J. Immobilized metal ion affinity chromatography. *Protein Expr Purif,* **3**, 263–281 (1992).

64. Chen, B. *et al.* Evaluation and optimization of the metal-binding properties of a complex ligand for immobilized metal affinity chromatography: Liquid Chromatography. *J Sep Sci,* **39**, 518–524 (2016).

65. Gaberc-Porekar, V. & Menart, V. Perspectives of immobilized-metal affinity chromatography. *J Biochem Biophys Methods,* **49**, 335–360 (2001).

66. Todorova, D., and Vijayalakshmi, M.A. Chapter 10: Immobilized Metal-Ion Affinity Chromatography. in *Handbook of Affinity Chromatography*. 257-286 (Taylor & Francis, 2006).

67. Block, H. *et al.* Chapter 27: Immobilized-Metal Affinity Chromatography (IMAC). in *Methods in Enzymolog.y* vol. 463, 439–473 (Elsevier, 2009).

68. Liesienė, J., Račaitytė, K., Morkevičienė, M., Valančius, P. & Bumelis, B. Immobilized metal affinity chromatography of human growth hormone Effect of ligand density. *J Chromatogr A,* **764**, 27–33 (1997).

69. Bornhorst, J. A. & Falke, J. J. Chapter 16: Purification of proteins using polyhistidine affinity tags. in *Methods in Enzymology,* vol. 326, 245–254 (Elsevier, 2000).

70. Hu, H.-L., Wang, M.-Y., Chung, C.-H. & Suen, S.-Y. Purification of VP3 protein of infectious bursal disease virus using nickel ion-immobilized regenerated cellulose-based membranes. *J Chromatogr B,* **840**, 76–84 (2006).

71. Opitz, L., Hohlweg, J., Reichl, U. & Wolff, M. W. Purification of cell culture-derived influenza virus A/Puerto Rico/8/34 by membrane-based immobilized metal affinity chromatography. *J Viroll Methods,* **161**, 312–316 (2009).

72. Bauer, W. S. *et al.* Metal Affinity-Enabled Capture and Release Antibody Reagents Generate a Multiplex Biomarker Enrichment System that Improves Detection Limits of Rapid Diagnostic Tests. *Anal Chem,* **89**, 10216–10223 (2017).

73. Bauer, W. S. *et al.* Magnetically-enabled biomarker extraction and delivery system: towards integrated ASSURED diagnostic tools. *Analyst,* **142**, 1569–1580 (2017).

74. Pearson, Ralph G. Hard and soft acids and bases, HSAB, part II: Underlying theories. *J Chem Educ,* **45**, 643–648 (1968).
75. Ayers, P. W. An elementary derivation of the hard/soft-acid/base principle. *J Chem Phys,* **122**, 141102 (2005).
76. Ayers, P. W. The physical basis of the hard/soft acid/base principle. *Faraday Discuss,* **135**, 161–190 (2007).
77. Poti, K.E., Sullivan, D.J., Dondorp, A.M., and Woodrow, C.J. HRP2: Transforming Malaria Diagnosis, but with Caveats. *Trends Parisitol*, **36** (2), 112-116 (2020).
78. M. DeSousa, J. *et al.* Inductively coupled plasma optical emission spectroscopy as a tool for evaluating lateral flow assays. *Anal Methods,* **13,** 2137-2146 (2021).
79. Panton, L. J. *et al.* Purification and partial characterization of an unusual protein of Plasmodium falciparum: histidine-rich protein II. *Mol Biochem Parasitol,* **35**, 149–160 (1989).
80. Baker, J. *et al.* Genetic diversity of Plasmodium falciparum histidine-rich protein 2 (PfHRP2) and its effect on the performance of PfHRP2-based rapid diagnostic tests. *J Infect Dis,* **192**, (2005).
81. Ke, Y.-M. *et al.* Preparation of the immobilized metal affinity membrane with high amount of metal ions and protein adsorption efficiencies. *Process Biochem,* **45**, 500–506 (2010).
82. Singh, J., Srivastav, A. N., Singh, N. & Singh, A. Chapter 3: Stability Constants of Metal Complexes in Solution. in *Stability and Applications of Coordination Compounds* (IntechOpen, 2019).
83. Trampuz, A., Jereb, M., Muzlovic, I. & Prabhu, R. M. Clinical review: Severe malaria. *Crit Care*, **7**, 315 (2003).
84. Makanjuola, R. O. & Taylor-Robinson, A. W. Improving Accuracy of Malaria Diagnosis in Underserved Rural and Remote Endemic Areas of Sub-Saharan Africa: A Call to Develop Multiplexing Rapid Diagnostic Tests. *Scientifica*, **2020**, 1–7 (2020).
85. Beshir, K. B. *et al.* Emergence of Undetectable Malaria Parasites: A Threat under the Radar amid the COVID-19 Pandemic? *Am J Trop Med Hyg,* **103**, 558–560 (2020).
86. Mbanefo, A. & Kumar, N. Evaluation of Malaria Diagnostic Methods as a Key for Successful Control and Elimination Programs. *Trop Med Infect Dis,* **5**, (2020).
87. Parra, M. E., Evans, C. B. & Taylor, D. W. Identification of Plasmodium falciparum histidine-rich protein 2 in the plasma of humans with malaria. *J Clin Microbiol,* **29**, 1629–1634 (1991).
88. Desakorn, V. *et al.* Stage-dependent production and release of histidine-rich protein 2 by Plasmodium falciparum. *Trans R Soc Trop Med Hyg,* **99**, 517–524 (2005).
89. Starzengruber, P. *et al.* High prevalence of asymptomatic malaria in south-eastern Bangladesh. *Malar J,* **13**, 16 (2014).
90. Idris, Z. M. *et al.* High and Heterogeneous Prevalence of Asymptomatic and Sub-microscopic Malaria Infections on Islands in Lake Victoria, Kenya. *Sci Rep,* **6**, (2016).

91. Chourasia, M. K. *et al.* Burden of asymptomatic malaria among a tribal population in a forested village of central India: a hidden challenge for malaria control in India. *Public Health,* **147**, 92–97 (2017).

92. Köster, K. B. *et al.* High Prevalence of Asymptomatic Plasmodium falciparum Infection in Gabonese Adults. *Am J Trop Med Hyg,* **77**, 939–942 (2007).

93. Krieger, H. *et al.* High prevalence of asymptomatic Plasmodium vivax and Plasmodium falciparum infections in native Amazonian populations. *Am J Trop Med Hyg,* **66**, 641–648 (2002).

94. The World Bank. Incidence of malaria (per 1,000 population at risk). World Bank Group, Washington, DC; 2018. https://data.worldbank.org/indicator/SH.MLR.INCD.P3?end=2018&start=2018&view=map.

95. Lindblade, K. A., Steinhardt, L., Samuels, A., Kachur, S. P. & Slutsker, L. The silent threat: asymptomatic parasitemia and malaria transmission. *Expert Rev Anti Infect Ther,* **11**, 623–639 (2013).

96. Ricks, K. M., Adams, N. M., Scherr, T. F., Haselton, F. R. & Wright, D. W. Direct transfer of HRPII-magnetic bead complexes to malaria rapid diagnostic tests significantly improves test sensitivity. *Malar J,* **15**, 399, (2016).

97. Bauer, W. S. *et al.* Rapid concentration and elution of malarial antigen histidine-rich protein II using solid phase Zn(II) resin in a simple flow-through pipette tip format. *Biomicrofluidics,* **11**, 034115 (2017).

98. World Health Organization. Cost-effectiveness of malaria diagnostic methods in sub-Saharan Africa in an era of combination therapy. WHO, Geneva, Switzerland; 2008. https://www.who.int/bulletin/volumes/86/2/07-042259/en/.

99. Davis, K. M., Swartz, J. D., Haselton, F. R. & Wright, D. W. Low-Resource Method for Extracting the Malarial Biomarker Histidine-Rich Protein II To Enhance Diagnostic Test Performance. *Anal Chem,* **84**, 6136–6142 (2012).

100. Gillet, P., Mori, M., Van Esbroeck, M., Ende, J. V. den & Jacobs, J. Assessment of the prozone effect in malaria rapid diagnostic tests. *Malar J,* **8**, 271 (2009).

101. Luchavez, J. *et al.* Laboratory demonstration of a prozone-like effect in HRP2-detecting malaria rapid diagnostic tests: implications for clinical management. *Malar J,* **10**, 286 (2011).

102. Hossain, M. S. *et al.* The risk of Plasmodium vivax parasitaemia after P. falciparum malaria: An individual patient data meta-analysis from the WorldWide Antimalarial Resistance Network. *PLOS Medicine,* **17**, e1003393 (2020).

103. Price, R. N., Commons, R. J., Battle, K. E., Thriemer, K. & Mendis, K. Plasmodium vivax in the Era of the Shrinking P. falciparum Map. *Trends Parasitol,* **36**, 560–570 (2020).

104. Mayor, A. & Bassat, Q. "Resistance" to diagnostics: A serious biological challenge for malaria control and elimination. *EBioMedicine*, **50**, 9–10 (2019).

105. Agaba, B. B. *et al.* Systematic review of the status of pfhrp2 and pfhrp3 gene deletion, approaches and methods used for its estimation and reporting in Plasmodium falciparum populations in Africa: review of published studies 2010–2019. *Malar J,* **18**, 355 (2019).

106. Rachid Viana, G. M. *et al.* Histidine-rich protein 2 (pfhrp2) and pfhrp3 gene deletions in Plasmodium falciparum isolates from select sites in Brazil and Bolivia. *PLoS ONE,* **12**, e0171150 (2017).

107. Gibson, L. E. *et al.* Plasmodium falciparum HRP2 ELISA for analysis of dried blood spot samples in rural Zambia. *Malar J,* **16**, 350 (2017).

108. Plucinski, M. M. *et al.* Posttreatment HRP2 Clearance in Patients with Uncomplicated Plasmodium falciparum Malaria. *J Infect Dis,* **217**, 685–692 (2018).

109. Dalrymple, U., Arambepola, R., Gething, P. W. & Cameron, E. How long do rapid diagnostic tests remain positive after anti-malarial treatment? *Malar J,* **17**, 228 (2018).

110. D'Alessandro, U. & Buttiëns, H. History and importance of antimalarial drug resistance. *Trop Med Int Health,* **6**, 845–848 (2001).

111. Gosling, R.D., Okell, L.,Mosha, J., and Chandramohan, D. The role of antimalarial treatment in the elimination of malaria. *Clin Micobiol Infect,* **17** (11), 1617-1623 (2011).

112. Shin, H.-I. *et al.* Polymorphism of the parasite lactate dehydrogenase gene from Plasmodium vivax Korean isolates. *Malar J,* **12**, 166 (2013).

113. Brown, W. M. *et al.* Comparative structural analysis and kinetic properties of lactate dehydrogenases from the four species of human malarial parasites. *Biochemistry,* **43**, (2004).

114. Chaikuad, A. *et al.* Structure of lactate dehydrogenase from Plasmodium vivax: complexes with NADH and APADH. *Biochemistry,* **44**, (2005).

115. Markwalter, C. F., Davis, K. M. & Wright, D. W. Immunomagnetic capture and colorimetric detection of malarial biomarker Plasmodium falciparum lactate dehydrogenase. *Anal Biochem,* **493**, 30–34 (2016).

116. Iqbal, J., Siddique, A., Jameel, M. & Hira, P. R. Persistent Histidine-Rich Protein 2, Parasite Lactate Dehydrogenase, and Panmalarial Antigen Reactivity after Clearance of Plasmodium falciparum Monoinfection. *J Clin Microbiol,* **42**, 4237–4241 (2004).

117. K Martin, S., Rajasekariah, G.-H., Awinda, G., Waitumbi, J. & Kifude, C. Unified parasite lactate dehydrogenase and histidine-rich protein ELISA for quantification of *Plasmodium falciparum. Am J Trop Med Hyg,* **80** (4), 516-522, (2009).

118. Makler, M. T. & Hinrichs, D. J. Measurement of the lactate dehydrogenase activity of Plasmodium falciparum as an assessment of parasitemia. *Am J Trop Med Hyg* **48**, (1993).

119. Davies, C. Chapter 1.3: Immunoassay Performance Measures, in *The Immunoassay Handbook: Theory and Applications of Ligand Binding, ELISA and Related Techniques,* 4th ed., 17-18, (Newnes, 2013).

120. Selby, C. Interference in Immunoassay. *Ann Clin Biochem,* **36**, 704–721 (1999).

121. Bhattacharyya, D. K., Adak, S., Bandyopadhyay, U. & Banerjee, R. K. Mechanism of inhibition of horseradish peroxidase-catalysed iodide oxidation by EDTA. *Biochem,* **298**, 281–288 (1994).

122. Piper, R. C., Buchanan, I., Choi, Y. H. & Makler, M. T. Opportunities for improving pLDH-based malaria diagnostic tests. *Malar J,* **10**, 213 (2011).

123. Markwalter, C. F., Ricks, K. M., Bitting, A. L., Mudenda, L. & Wright, D. W. Simultaneous capture and sequential detection of two malarial biomarkers on magnetic microparticles. *Talanta,* **161**, 443–449 (2016).
124. Ashri, N. Y. & Abdel-Rehim, M. Sample treatment based on extraction techniques in biological matrices. *Bioanalysis,* **3**, 2003–2018 (2011).
125. Kantor, A. G., Markwalter, C. F., Nourani, A. & Wright, D. W. An antibody-free dual-biomarker rapid enrichment workflow (AnDREW) improves the sensitivity of malaria rapid diagnostic tests. *Anal Biochem,* **612**, 114020 (2021).
126. Dirkzwager, R. M., Liang, S. & Tanner, J. A. Development of Aptamer-Based Point-of-Care Diagnostic Devices for Malaria Using Three-Dimensional Printing Rapid Prototyping. *ACS Sens,* **1**, 420–426 (2016).
127. Bishop, J. D., Hsieh, H. V., Gasperino, D. J. & Weigl, B. H. Sensitivity enhancement in lateral flow assays: a systems perspective. *Lab Chip,* **19**, 2486–2499 (2019).
128. World Health Organization. Malaria surveillance, monitoring & evalution: a reference manual. WHO, Geneva, Switzerland; 2018.
129. Bridges, D. J., Winters, A. M. & Hamer, D. H. Malaria elimination: surveillance and response. *Pathog Glob Health,* **106**, 224–231 (2012).
130. World Health Organization. Disease surveillance for malaria control: an operational manual. WHO, Geneva, Switzerland; 2012.
131. Wickremasinghe, R., Fernando, S. D., Thillekaratne, J., Wijeyaratne, P. M. & Wickremasinghe, A. R. Importance of active case detection in a malaria elimination programme. *Malar J,* **13**, (2014).
132. Smith Gueye, C. *et al.* Active case detection for malaria elimination: a survey among Asia Pacific countries. *Malar J*, **12**, 358 (2013).
133. Sturrock, H. J. W. *et al.* Reactive Case Detection for Malaria Elimination: Real-Life Experience from an Ongoing Program in Swaziland. *PLoS One,* **8**, (2013).
134. Deutsch-Feldman, M. *et al.* Efficiency of a Malaria Reactive Test-and-Treat Program in Southern Zambia: A Prospective, Observational Study. *Am J Trop Med Hyg,* **98**, 1382–1388 (2018).
135. Silumbe, K. *et al.* A qualitative study of perceptions of a mass test and treat campaign in Southern Zambia and potential barriers to effectiveness. *Malar J,* **14**, (2015).
136. Graz, B., Willcox, M., Szeless, T. & Rougemont, A. 'Test and treat' or presumptive treatment for malaria in high transmission situations? A reflection on the latest WHO guidelines. *Malar J,* **10**, 136 (2011).
137. Zikusooka, C. M., McIntyre, D. & Barnes, K. I. Should countries implementing an artemisinin-based combination malaria treatment policy also introduce rapid diagnostic tests? *Malar J,* **7**, (2008).
138. World Health Organization. World Health Statistics 2019: monitoring health for the SDGS, sustainable development goals. WHO, Geneva, Switzerland; 2019.
139. Bohren, M. A. *et al.* Facilitators and barriers to facility-based delivery in low- and middle-income countries: a qualitative evidence synthesis. *Reprod Health,* **11**, (2014).

140. Varela, C. *et al.* Transportation Barriers to Acess Health Care for Surgical Conditions in Malawi: a cross sectional nationwide household survey. *BMC Public Health,* **19**, (2019).

141. Istepanian, R. S. H. & AlAnzi, T. Mobile health (m-health). in *Biomedical Information Technology* 717–733 (Elsevier, 2020).

142. Jani, IIesh V., Quevedo, J. I. & Tobaiwa, O. Use of mobile phone technology to improve the quality of point-of-care testing in a low-resource setting. *AIDS,* **30**, 159–161 (2016).

143. Porter, G. Mobilities in Rural Africa: New Connections, New Challenges. *Ann Am Assoc Geogr,* **106** (2), 1–8 (2016).

144. Zurovac, D., Talisuna, A. O. & Snow, R. W. Mobile Phone Text Messaging: Tool for Malaria Control in Africa. *PLoS Medicine,* **9**, e1001176 (2012).

145. Prue, C. S. *et al.* Mobile phones improve case detection and management of malaria in rural Bangladesh. *Malar J,* **12**, 48 (2013).

146. Wallis, L., Blessing, P., Dalwai, M. & Shin, S. D. Integrating mHealth at point of care in low- and middle-income settings: the system perspective. *Glob Health Action*, **10**, (2017).

147. Visser, T. A comparative evaluation of mobile medical APPS (MMAS) for reading and interpreting malaria rapid diagnostic tests. *Malar J*, **20,** 39 (2021).

148. Lewis, T., Synowiec, C., Lagomarsino, G. & Schweitzer, J. E-health in low- and middle-income countries: findings from the Center for Health Market Innovations. *Bulletin of the World Health Organization,* **90**, 332–340 (2012).

149. Istepanian, R. S. H. & Woodward, B. *m-Health: Fundamentals and Applications*. (John Wiley & Sons, 2016).

150. Feng, D. D. *Biomedical Information Technology*. (Academic Press, 2019).

151. Labrique, A., Vasudevan, L., Mehl, G., Rosskam, E. & Hyder, A. A. Digital Health and Health Systems of the Future. *Glob Health Sci Pract,* **6**, S1–S4 (2018).

152. Lemaire, J. Scaling Up Mobile Health: Elements Necessary for the Successful Scale Up of mHealth in Developing Countries. Actevis Consulting Group, New York, NY; 2011.

153. Siedner, M. J. *et al.* Optimizing Network Connectivity for Mobile Health Technologies in sub-Saharan Africa. *PLoS ONE,* **7**, e45643 (2012).

154. Harris, P. A. *et al*. Research electronic data capture (REDCap)—A metadata-driven methodology and workflow process for providing translational research informatics support. *J Biomed Inform*, **42**, 377-381 (2009).

155. Harris, P. A. Research Electronic Data Capture (REDCap) - planning, collecting and managing data for clinical and translational research. *BMC Bioinformatics,* **13**, A15 (2012).

156. Harris, P. A. *et al*. The REDCap consortium: Building an international community of software platform partners | Elsevier Enhanced Reader. *J Biomed Inform*, **95**, 103208 (2019).

157. Chen, Y. *et al.* Understanding the complexity of 3G UMTS network performance. in *2013 IFIP Networking Conference.* 1–9 (2013).

158. Agarwal, S. K., Laifenfeld, M., Trachtenberg, A. & Alanyali, M. Using bandwidth sharing to fairly overcome channel asymmetry. In: Information Theory and

Applications Workshop. 2006 Presented at: Information Theory and Applications Workshop; February 2006; San Diego, CA.

159. Charzinski, J. Web Performance in Practice – Why We are Waiting. *AEU-Int J Electron Comm,* **55**, 37–45 (2001).

160. Scherr, T. F., Gupta, S., Wright, D. W. & Haselton, F. R. Mobile phone imaging and cloud-based analysis for standardized malaria detection and reporting. *Sci Rep,* **6**, (2016).

161. Colley, D. G. *et al.* Evaluation, Validation, and Recognition of the Point-of-Care Circulating Cathodic Antigen, Urine-Based Assay for Mapping Schistosoma mansoni Infections. *Am J Trop Med Hyg,* **103**, 42–49 (2020).

162. Scherr, T. F., Moore, C. P., Thuma, P. & Wright, D. W. Evaluating Network Readiness for mHealth Interventions Using the Beacon Mobile Phone App: Application Development and Validation Study. *JMIR mHealth uHealth,* **8**, e18413 (2020).